IMPACT OF TRANSCATHETER AORTIC VALVE REPLACEMENT ON CORONARY HEMODYNAMICS USING CLINICAL MEASUREMENTS AND AN IMAGE-BASED PATIENT-SPECIFIC LUMPED PARAMETER MODEL

IMPACT OF TRANSCATHETER AORTIC VALVE REPLACEMENT ON CORONARY HEMODYNAMICS USING CLINICAL MEASUREMENTS AND AN IMAGE-BASED PATIENT-SPECIFIC LUMPED PARAMETER MODEL

BY

LOUIS GARBER, B.A.Sc.

A Thesis Submitted to the School of Biomedical Engineering and the School of Graduate Studies in Partial Fulfilment of the Requirements for the Degree Master of Applied Science

December 2022

Master of Applied Science (2022). School of Biomedical Engineering, McMaster University, Hamilton, Ontario

TITLE: Impact of Transcatheter Aortic Valve Replacement on Coronary Hemodynamics using Clinical Measurements and an Image-Based Patient-Specific Lumped Parameter Model

AUTHOR: Louis Garber, B.A.Sc.

SUPERVISOR: Professor Zahra K. Motamed

PAGES: xii, 92

Lay Abstract

The heart is a vital part of the cardiovascular system, which helps deliver and regulate blood flow through the entire human body. The coronary arteries are a crucial part of this system since they deliver blood directly to heart muscles. For numerous reasons, the cardiovascular system can become diseased over time and require clinical treatment. Coronary artery disease and aortic valve stenosis are among the most prevalent cardiovascular diseases globally. While medical imaging on its own is a crucial part of the disease management and treatment process, advanced computational models can further enhance the process and provide clinics with data and predictions they might otherwise miss. In this thesis, a patient specific computational framework capable of simulating blood flow waveforms and cardiovascular data in the heart and coronary arteries using only non-invasive clinical data and images was developed and validated. The novel model was applied to a series of patients with aortic stenosis who underwent heart valve replacement with the aim of studying the impact on coronary blood flow and global cardiovascular metrics.

Abstract

Cardiovascular disease, including coronary artery disease and aortic valve stenosis, impacts tens of millions of people annually and carries a massive global economic burden. Advances in medical imaging, hardware and software are leading to an increased interest in the field of cardiovascular computational modelling to help combat the devastating impact of cardiovascular disease. Lumped parameter modelling (a branch of computational modelling) holds the potential of aiding in the early diagnosis of these diseases, assisting clinicians in determining personalized and optimal treatments and offering a unique *in-silico* setting to study cardiac and circulatory diseases due to its rapid computation time, ease of automation and relative simplicity.

In this thesis, cardiovascular lumped parameter modelling is presented in detail and a patient-specific framework capable of simulating blood flow waveforms and hemodynamic data in the heart and coronary arteries was developed. The framework used only non-invasive clinical data and images (Computed Tomography images, echocardiography data and cuff blood pressure) as inputs. The novel model was then applied to 19 patients with aortic stenosis who underwent transcatheter aortic valve replacement. The diastolic coronary flow waveforms in the left anterior descending artery, left circumflex artery and right coronary artery were validated against a

previously developed patient-specific 3D fluid-structure interaction model for all 19 subjects (pre and post intervention). There were strong qualitative and quantitative agreements between the two models.

After the procedure, aortic valve area and net pressure gradient across the aortic valve improved for almost all the subjects. As for the hemodynamic data, according to the model, there was substantial variability in terms of the increase or decrease post intervention. On average, left ventricle workload and maximum left ventricle pressure decreased by 4.5% and 13.0% while cardiac output, mean arterial pressure and resting heart rate increased by 9.9%, 6.9% and 1.9% respectively. There were also subject specific changes in coronary blood flow (37% had increased flow in all three coronary arteries, 32% had decreased flow in all coronary arteries, and 31% had both increased and decreased flow in different coronary arteries). All in all, a proof-of-concept cardiac and coronary lumped parameter framework was developed, validated, and applied in this thesis.

Acknowledgements

I would first like to start by acknowledging Professor Zahra K. Motamed for her continued support and great guidance over the past few years. She has challenged me in different academic areas and has helped me become a better researcher and engineer. I would also like to thank my academic committee, Dr. Quenneville and Dr. Srinivasan for the support and helpful feedback throughout this process.

Furthermore, I would like to extend my gratitude towards to the TAVR team at St. Joseph's Healthcare in Hamilton for providing us with crucial data for the studies and for helping to answer questions and provide support during my time at McMaster.

I would also like to acknowledge all my colleagues and lab mates who have helped me so much during my time in the Motamed lab. In particular, I would like to extend my thanks to Dr. Seyedvahid Khodaei for being both a great academic colleague, mentor and friend as well as Mason Kadem, Mohamed Abdelkhalek, Sydney Valentino, Massoud Ebrahimi-Dehshali, Mohammad Ali Daeian and Nikrouz Bahadormanesh. Additionally, I would like to extend a very large thank you to the staff in the School of Biomedical Engineering, especially Jane Mah whose continued support has helped me navigate the last few years.

Lastly, I would like to thank my incredible support system. Starting a new degree at a new school during COVID came with its own set of challenges and I could not have navigated them without all of you. I am forever grateful to my fiancé Molly, my parents (and Pepper of course) and all my close friends for their immeasurable and unwavering support over these last few years.

My work was supported by NSERC Discovery Grant (RGPIN-2017-05349) and NSERC CRD Grant (CRDPJ 537352 – 18) and the NSERC Ontario Graduate Scholarship.

Thank you again to everyone who has supported me during this journey.

Contents

List of Figures

List of Tables

Nomenclature

A_{Ao}	Ascending Aorta Cross-Sectional Area
$A_{LAD/LCX/RCA}$	Coronary Branch Cross Sectional Area
A_{sten}	Coronary Branch Cross Sectional Area w/ Stenosis
α	Area Reduction Factor
$\mathrm{C_{cor,p}}$	Proximal Coronary Compliance
$\mathrm{C_{cor,m}}$	Medial Coronary Compliance
EAO	Effective Orifice Area
E_{max}	Maximum Elastance
E_{min}	Minimum Elastance
$E_L Co$	Energy Loss Coefficient
m_1	Contraction Rate Constant
m_2	Relaxation Rate Constant
P_{im}	Intramyocardial pressure
$Q(t)$	Transvalvular Flow Rate
$Q_{cor,total}$	Total Coronary Blood Flow
$R_{cor,total}$	Total Coronary Resistance
$\mathrm{R_{cor,p}}$	Proximal Coronary Resistance
$\mathrm{R_{cor,m}}$	Medial Coronary Resistance
$\mathrm{R_{cor,d}}$	Distal Coronary Resistance
ρ	Blood Viscosity
τ_1	Systolic Time Constant
τ_2	Diastolic Time Constant
T	Duration of Cardiac Cycle

Abbreviations

AS	Aortic Stenosis
CABG	Coronary Artery Bypass Graft
CAD	Coronary Artery Disease
CCTA	Coronary Computed Tomography Angiography
CO	Cardiac Output
CT	Computed Tomography
CVD	Cardiovascular Disease
DE	Doppler Echocardiography

DBP	Diastolic Blood Pressure
Echo	Echocardiography
FSI	Fluid-Structure Interaction
HR	Heart Rate
LAD	Left Anterior Descending Artery
LCX	Left Circumflex Artery
LMCA	Left Main Coronary Artery
LPM	Lumped Parameter Modelling
LV	Left Ventricle
MAP	Mean Arterial Pressure
MRI	Magnetic Resonance Imaging
NYHA	New York Heart Association (heart failure classification)
PCI	Percutaneous Coronary Intervention
RCA	Right Coronary Artery
SAVR	Surgical Aortic Valve Replacement
SBP	Systolic Blood Pressure
TAVR	Transcatheter Aortic Valve Replacement

Declaration of Academic Achievement

Chapter 1, "Introduction and Background" was written by Louis Garber.

Chapter 2, "The Critical Role of Lumped Parameter Models in Patient-Specific Cardiovascular Simulations" Louis Garber (first author) conducted the literature analysis and investigation, wrote the original manuscript, and drafted all figures; Dr. Seyedvahid Khodaei reviewed and edited the paper and Dr. Zahra Keshavarz-Motamed aided with the conception, design of literature classification, critical revisions and final approval of the manuscript.

Chapter 3, "Impact of TAVR on coronary artery hemodynamics using clinical measurements and image-based patient-specific *in silico* modeling" Louis Garber (first author) conducted the data analysis, coronary LPM algorithm development, interpretation of data, and figure creation and manuscript writing. Dr. Seyedvahid Khodaei conducted the FSI modelling, FSI data analysis and critical revisions, Dr. Nima Maftoon was consulted on the LPM optimization development and Dr. Zahra Keshavarz-Motamed conducted the conception and project design, non-coronary LPM design, critical revisions and final approval of the manuscript.

Chapter 4, "Conclusions and Future Directions" was written by Louis Garber.

Chapter 1: Introduction and Background

1.1 Thesis Structure

Chapter 1 will set the stage for the research presented and provide the reader with the needed background to understand the chapters to come. The main aim of this section is to illustrate the global impact of cardiovascular disease and highlight two diseases in particular: aortic valve stenosis and coronary artery disease. Furthermore, this section aims to give a brief background of the medical imaging modalities commonly used to diagnose, plan, and treat cardiovascular diseases. Finally, the pairing of medical imaging and computational methods to enhance diagnosis, treatment and management will be presented.

Chapter 2 will provider the reader with an in-depth dive into the mathematical theory, motivations, recent innovations, and limitations of lumped parameter modelling (LPM) related to patient-specific cardiovascular modelling. Furthermore, it compares and contrasts LPM with other commonly used modelling methods. This chapter highlights the value of patient-specific LPMs in cardiovascular medicine.

Chapter 3 presents the development, validation, and application of a non-invasive, patient specific lumped parameter framework capable of simulating blood flow waveforms and global hemodynamic metrics in the major cardiac compartments and the coronary arteries. The novel model was applied to 19 subjects undergoing transcatheter aortic valve replacement (TAVR) to study the impact of the procedure on coronary blood flow and cardiac metrics. The model was validated against the results from a previously developed 3D fluid-structure interaction model for all the subjects and a sensitivity analysis was conducted. In-depth pre- and post-TAVR results are presented for the subjects.

Chapter 4 outlines the key findings from the previous chapters and brings all the presented ideas about cardiovascular disease, TAVR, coronary blood flow and LPMs together. Finally, future research ideas and directions are presented.

1.2 Introduction to the Heart

The heart is a muscular organ that pumps blood throughout the body and is the driving force for the cardiovascular system. It is divided into four chambers: the right atrium, which receives blood from the body; the left atrium, which receives blood from the lungs; the right ventricle, which

pumps blood to the lungs; and the left ventricle, which pumps blood to the rest of the body. The blood flow into these chambers is controlled by the heart valves (tricuspid, mitral, pulmonary, and aortic valves) which are constructed of either two or three leaflets [1].

The heart is surrounded by a network of blood vessels, including the coronary arteries, which supply oxygen and nutrients to the heart muscle (myocardium). These vessels branch off from the aorta, which is the main blood vessel that carries oxygenated blood from the left ventricle to the rest of the body. The right coronary artery (RCA) supplies blood to the right side of the heart, while the left main coronary artery (LMCA), which splits into the left anterior descending (LAD) artery and the left circumflex artery (LCX), supplies the left side [1]. The coronary arteries are critical to the heart's function, as they ensure that the heart receives the necessary blood flow to keep it functioning properly in all kinds of difference scenarios.

1.3 Cardiovascular Diseases

Cardiovascular diseases (CVDs) are a widespread issue that impacts the health and wellbeing of millions of people across the globe. Globally, CVDs are the leading cause of mortality and were responsible for an estimated 17.9 million deaths in 2019, three quarters of which took place in low and middle income countries [2]. CVDs are a grouping of diseases that impact the cardiovascular system including coronary artery disease (CAD), peripheral heart disease, stroke, heart failure, valvular disease and others [3]. Common risk factors for CVDs include high blood pressure (hypertension), high cholesterol levels, diabetes, smoking, obesity and physical inactivity [4]. Depending on the nature and severity of the disease, treatment and management options include medications (anticoagulants and angiotensin-converting-enzyme (ACE) inhibitors for example) and surgeries such as coronary angioplasty, coronary bypass grafting, transcatheter aortic valve replacement and more [5]. In particular, this thesis will focus on both aortic valve stenosis and coronary artery disease since they are common diseases and have a high rate of co-occurrence (roughly 40-80% of patients who underwent treatment for aortic stenosis had CAD) [6].

1.4 Aortic Valve Stenosis

Aortic valve stenosis (AS) is a heart disease that limits the opening of the aortic valve due to the long term build up of calcification on the valve leaflets (Figure 1). The impaired valve leads to an obstruction (or reduction) in blood flow from the left ventricle (LV) and causes the ventricle to work harder in an attempt to maintain the needed cardiac output. Not only does this impact the

systemic cardiovascular system, but the extended effort by the ventricle often leads to LV diastolic disfunction or various types of ventricle remodelling over time [7]. As with many cardiovascular diseases, AS diagnoses range from mild to severe depending on a variety of scoring criteria.

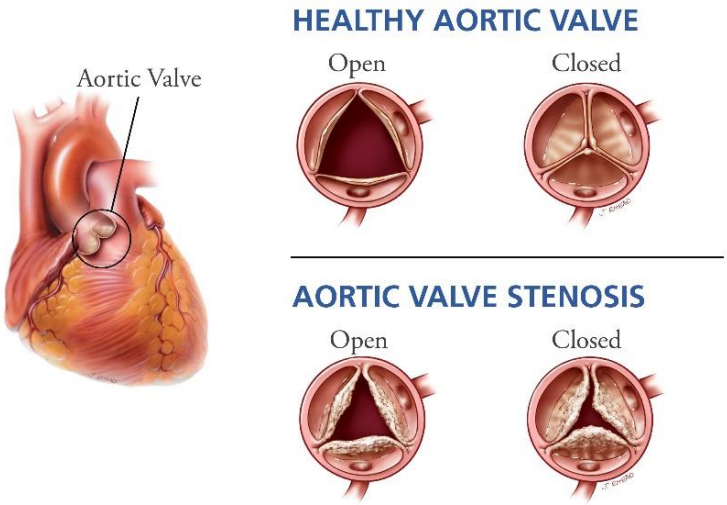

Figure 1: *Healthy and Diseased (Stenotic) Aortic Valve* [8]

AS is the third most common heart disease and primarily impacts the elderly population [9]. The prevalence of AS increases from ~1% in individuals less than 60 years old to greater than 10% after the age of 75 [9]. Unfortunately, AS has a bleak prognosis if left untreated (50% rate of morality after 2 years)[7] and currently the only treatment options for severe AS are minimally invasive transcatheter aortic valve replacement (TAVR) or open heart surgical aortic valve replacement (SAVR).

In recent years TAVR has become the more common treatment option due to the minimally invasive nature and rapid recovery time for patients [10]. Furthermore, TAVR is now being applied to younger and higher risk patients due to advancements in both the valve technology and surgical procedures. While TAVR has advanced significantly in the past decade and the overall risk has decreased considerably, some post procedure complications such as paravalvular leakage, vascular and bleeding complication, stroke, coronary obstruction, acute coronary syndrome and kidney injury still exist [11].

1.5 Coronary Artery Disease

CAD is caused by the build up of plaque in the coronary blood vessels, which supply blood to the myocardium (Figure 2). The narrowing of these crucial vessels leads to a reduction the blood flow to the heart muscles and can ultimately lead to a heart attack, heart failure or arrhythmias [12]. CAD is also the most common heart disease and is responsible for roughly 382,000 deaths in the United States in 2020 [13]. It is projected to result in over $215 billion USD in medical costs and $151 billion USD in indirect costs in the United States by 2035 (by far the most costly heart disease) [12]. While there are a variety of risk factors for CAD, the primary ones are similar to most heart diseases and include: high cholesterol consumption, hypertension, smoking, diabetes and obesity [4].

Depending on the severity of CAD, there exist a range of pharmaceutical management options and surgical procedures; primarily percutaneous coronary intervention (PCI) and coronary artery bypass graft surgery (CABG). PCI is a minimally invasive procedure in which a catheter is used to deploy a stent in the narrowed coronary vessel. Conversely, CABG is an open-heart procedure where a healthy blood vessel is harvested from another part of the patient (often their leg) and is attached to the aorta to bypass the narrowed or blocked section of the vessel. While PCI is less invasive and has a quicker recovery time for patients, some studies have shown that CABG resulted in fewer major adverse cardiac or cerebrovascular events post surgery [14].

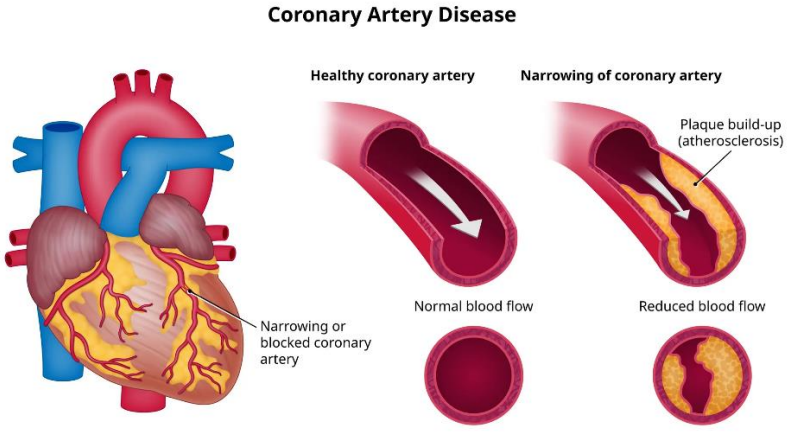

Figure 2: *Comparison between healthy coronary arteries and narrowed coronary arteries (the cause of CAD)* [15]

Currently, there is a debate about whether the coronary arteries or the aortic valve should be treated first (or simultaneously) when patients suffer from both severe CAD and AS. There are a few large-scale clinical studies underway at the moment to investigate the optimal treatment and management of both diseases [16, 17].

1.6 Cardiovascular Imaging Modalities

The aim of this section is to introduce a few of the medical imaging modalities used in the diagnosis and treatment of cardiovascular diseases. While this is not an all-encompassing list, it highlights the main modalities related to AS and CAD and focuses primarily on non-invasive modalities as that is one of the focuses of this thesis. Catheterization, although minimally invasive, was included since it currently plays an import role in the collection of hemodynamic data from the coronary arteries.

1.6.1 Echocardiography

Echocardiography (echo) is the most common cardiovascular imaging modality and is often used as the "first line of defense" when initially screening for possible CVDs due to its rapid results, portability and low cost [18]. Echo uses the reflection of sound waves emitted from an ultrasonic probe to construct images of different regions the cardiovascular systems. Doppler echo exploits the Doppler effect to estimate blood flow velocity in major cardiovascular structures (aorta, ventricle, valves, large arteries, etc.).

One of the major advantages of echo is that it is completely non-invasive and does not emit ionizing radiation, meaning it is very safe and patients can undergo multiple scans without any elevated risk. Additionally, it has high temporal resolution and the images from the scan can be visualized in almost real-time. The trade off thought, is that the resulting images have low spatial resolution and can only focus on a narrow region of the body. Additionally, it is difficult to reliably image smaller blood vessels including the coronary arteries.

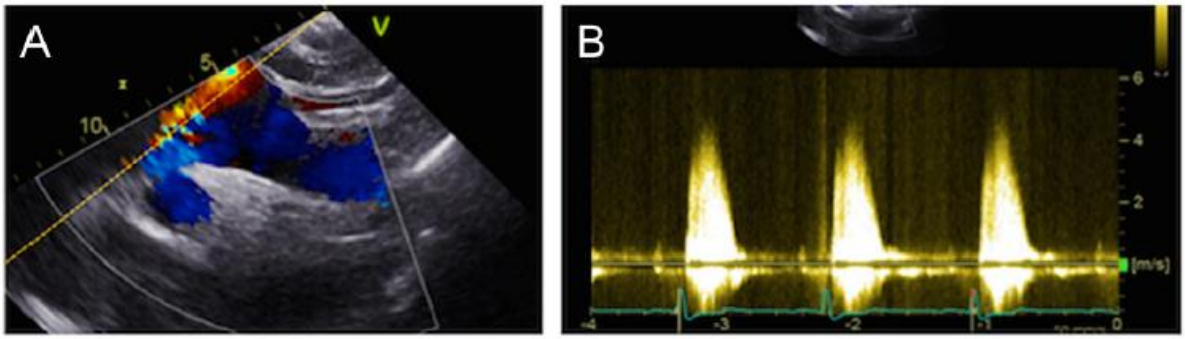

Figure 3: (A) *Doppler echo scan of a patient with aortic stenosis - suprasternal view;* ***(B)*** *corresponding Doppler waveform* [19]

In the case of patients with AS, echo is crucial in the diagnosis, assessment and management of the disease [19]. From continuous wave Doppler echo data (Figure 3 for example), clinicians can estimate the aortic valve area, maximal blood velocity and mean pressure gradient across the valve, which tend to increase as the valve progressively narrows [19]. These metrics are all crucial in the overall assessment of the severity of AS.

1.6.2 Computed Tomography

Alternatively, Computed Tomography (CT) imaging offers high spatial resolution that allows for high quality visualization of a variety of structures. It is based on a computerized x-ray imaging procedure in which x-ray tubes rotate quickly around a patient and produces a series of signals that are reconstructed into tomographic images (cross-sectional slices of the region of interest) [20]. The various images and then automatically stacked together to generate a 3D model from the scan. Depending on the scenario, a contrast dye is often administered (through IV or orally) to further enhance certain structures such as details of the heart valves [21].

While a limited number of CT scans is generally considered safe, the modality does produce ionizing radiation (from the x-rays) and repeat exposure may lead to elevated risk of diseases including cancer [20]. In recent years, advances in reconstruction algorithms and imaging procedures have led to a reduction in overall radiation doses for patients [22].

CT imaging is a crucial tool in the planning of TAVR for patients suffering from AS. During the TAVR planning stages, clinicians use CT images of the aortic valve and surrounding structures such as the sinus of Valsalva, sino-tubular junction, coronary ostia and ascending aorta (Figure 4) to determine parameters such as calcium score and distribution [23]. CT images are also critical in

access planning and implantation planning, allowing surgeons to improve valve placement and sizing and reduce post procedure complications [23].

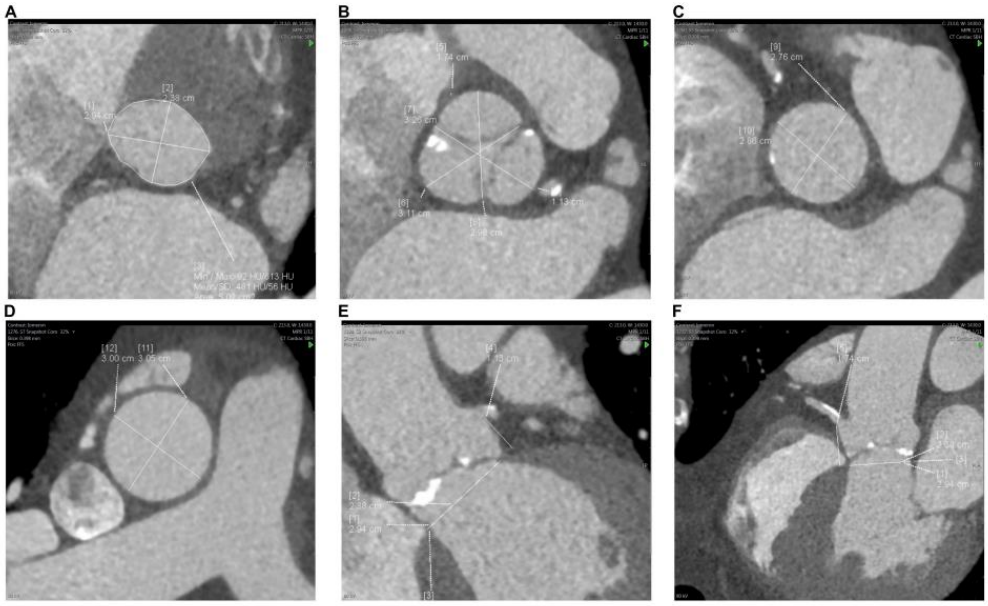

Figure 4: *CT images of* ***(A)*** *aortic valve annulus;* ***(B)*** *sinus of Valsalva;* ***(C)*** *sino-tubular junction;* ***(D)*** *ascending aorta;* ***(E)*** *left coronary ostial height;* ***(F)*** *right coronary ostial height* [23]

Coronary Computed Tomography Angiography (CCTA) is a specific type of contrast CT imaging applied to the coronary arteries to identify any plaque build up or stenosis. Similar to CT imaging of the valves, it produces a high-resolution 3D model of coronaries and surrounding structures and can be used in the diagnosis of CAD and the planning of surgeries such as PCI or CABG.

1.6.3 Magnetic Resonance Imaging

Magnetic resonance imaging (MRI) utilizes magnets and computer-generated radio-frequency waves to excite and detect changes of protons in water molecules in the body, which can be used to reconstruct a 3D image of the regions of interest [24]. Compared to CT, MRI is better suited to image soft tissue within the body (such as the brain, spinal cord and nerves) but is commonly used to diagnose various cardiovascular diseases [24]. A major upside to MRI is that it can generate images with high spatial resolution without emitting ionizing radiation. However, MRI is often more expensive than CT and echo and due to the strong magnetic field, patients with implants like pacemakers, stents, cochlear implants and insulin pumps are ineligible [24].

In recent years, advances in MRI technology, hardware, image reconstruction algorithms and data processing has led to clinically available four-dimensional (4D) flow MRI. This non-invasive modality allows clinicians to visualized 3D blood flow in the heart and great vessels during a short time window (Figure 5) [25]. Clinically useful metrics including forward flow, reverse flow, regurgitation fraction and peak velocity can be extracted and used to study, assess and diagnose cardiovascular diseases [25].

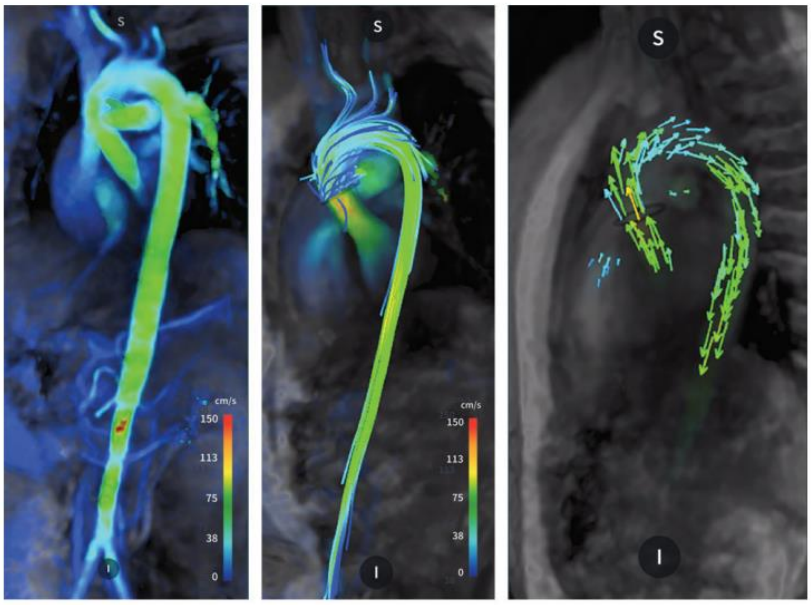

Figure 5: *Different imaging modes to visualize blood flow patterns in the aorta from 4D Flow MRI;* ***(A)*** *Colour-coded 3D rendering;* ***(B)*** *Colour-coded 3D rendering with streamlines;* ***(C)*** *Colour-coded 3D rendering with velocity vectors* [25]

1.6.4 Catheterization

Unlike the aforementioned modalities, cardiac catheterization is an invasive method to collect hemodynamic data from a patient. A thin catheter probe is inserted through a blood vessel (often near the groin, wrist, or neck) and guided into the heart, where pressure and blood velocity data can be collected [26]. Currently, it is the gold standard for obtaining local hemodynamic data from the coronary arteries. Often, a dye is injected through the catheter and into the coronary arteries and imaged using x-rays (coronary angiogram) to look for blockages or narrowed vessels [26]. Depending on the severity of the coronary blockages, clinicians may conduct a PCI directly (either through the placement of a metal/metal and drug eluting stent or by inflating a tiny balloon to

widen the arteries). While cardiac catheterization is generally safe, some risks include blood vessel injuries, kidney injuries, cerebral embolisms [26, 27].

1.7 Computational Modelling

While medical imaging on its own is a vital tool for clinicians, researcher and engineers are always looking to further enhance these modalities and combine them with the power of computation to create smarter tools. In recent years, the marriage between imaging and computational modelling has grown dramatically and lead to a variety of patient specific modelling techniques. These frameworks use medical images and data as inputs and provide clinicians with additional quantitative information and predictions about disease diagnoses, management, and procedure outcomes. While machine learning and deep learning have garnered most of the attention is this area [28], this thesis focuses on patient specific cardiovascular modelling (i.e. frameworks that use a series of equations to govern the behaviour of blood flow and are tuned for each patient based on the input data rather than learned from a large dataset). Within this area of patient specific cardiovascular computational modelling, the two main groups of models are (1) higher order models and (2) lower order models.

(1) Higher order models (such as computational fluid dynamics (CFD) models or fluid-structure interaction (FSI) models) allow for detailed 3D (or 2D) simulations of blood flow and pressure within a desired region of the cardiovascular system. Often medical imaging data from a patient is used to re-construct the area of focus (for instance the ventricle, valves, and ascending aorta) and generate input/output (boundary) conditions. Computational techniques are then applied to approximate blood flow and pressure in all 3 spatial coordinates within these structures using a variety of methods such as finite volume method [29, 30]. These models tend to provide highly detailed results with many possible metrics such as blood flow, pressure, wall shear stress, vortex structures and others but are computationally intensive and require a large amount of pre and post processing [29, 30].

(2) Alternatively, lower order models (such as LPM) offer a simpler but computationally more efficient method to simulate blood flow and pressure in the cardiovascular system. Like higher order models, patient specific input data is used but rather than simulating the flow in 3D, the outputs are time dependant waveforms for a certain cardiovascular region (such as the coronary

arteries, valves, or ventricles). These waveforms can be useful on their own or can be used to derive other metrics like ventricle workload [31].

In this thesis, the focus is on the development and application of a non-invasive, patient specific LPM aimed at the coronary arteries. A detailed review of LPM including the key equations, background, theory, optimization, impact, new developments, and important models is presented in Chapter 2.

1.8 Objectives of the Thesis

Aim 1: Highlight the importance of lumped parameter modelling in the future of patient specific cardiovascular medicine and provide a strong theoretical and applied background.

Aim 2: Develop a non-invasive, patient specific LPM framework aimed at simulating blood flow waveforms in the three main coronary arteries.

Aim 3: Validate the results from this novel framework against a patient specific 3D FSI framework and conduct a model sensitivity analysis to quantify how changes in input parameters will impact the model results.

Aim 4: Apply this developed framework to 19 patients who have undergone TAVR to non-invasively quantify the impact of the procedure (pre and post) on coronary blood flow and global hemodynamic metrics.

Chapter 2: The Critical Role of Lumped Parameter Models in Patient-Specific Cardiovascular Simulations

Louis Garber[1], Seyedvahid Khodaei[2], Zahra Keshavarz-Motamed[1,2,3]

1. School of Biomedical Engineering, McMaster University, Hamilton, ON, Canada
2. Department of Mechanical Engineering, McMaster University, Hamilton, ON, Canada
3. School of Computational Science and Engineering, McMaster University, Hamilton, ON, Canada

Published In:

Archives of Computational Methods in Engineering, 29, 2977-3000 (2022)

https://doi.org/10.1007/s11831-021-09685-5

2.1 Abstract

Cardiovascular (CV) disease impacts tens of millions of people annually and carries a massive global economic burden. Continued advances in medical imaging, hardware and computational efficiency are leading to an increased interest in the field of cardiovascular computational modelling to help combat the devastating impact of CV disease. This review article will focus on a computational modelling technique known as lumped parameter modelling (LPM). Due to its rapid computation time, ease of automation and relative simplicity, LPM holds the potential of aiding in the early diagnosis of CV disease, assisting clinicians in determining personalized and optimal treatments and offering a unique *in-silico* setting to study cardiac and circulatory diseases. In addition, it is one of the many tools that are needed in the eventual development of patient specific cardiovascular "digital twin" frameworks. This review focuses on how the personalization of cardiovascular lumped parameter models are beginning to impact the field of patient specific cardiovascular care. It presents an in-depth examination of the approaches used to develop current predictive LPM hemodynamic frameworks as well as their applications within the realm of cardiovascular disease. The roles of these models in higher order blood flow (1D/3D) simulations are also explored in addition to the different algorithms used to personalize the models. The article outlines the future directions of this field and the current challenges and opportunities related to the translation of this technology into clinical settings.

2.2 Introduction

Cardiovascular disease is a global epidemic that impacts millions of people annually and carries a massive global economic burden. In 2017, cardiovascular diseases were responsible for an estimated 17.8 million deaths, making it the number one cause of death globally and accounting for 37% of premature deaths from noncommunicable diseases [1, 2]. In Canada, one in every four deaths is from cardiovascular disease and it costs the Canadian economy more than $22 billion every year [3]. In the United States alone, it is projected that by 2035 annual medical costs and lost productivity due to cardiovascular disease will surpass USD$749 billion and USD$368 billion respectively, amounting to over USD$1 trillion in total costs [4]. Similarly, in 2017 the total estimated cost of cardiovascular diseases on the European union economy was €210 billion [5]. Given the enormous burden of this disease, researchers and clinicians are continually searching for ways to reduce its impact and improve outcomes for patients.

In the past two decades, breakthroughs in computation have driven substantial advances in technology and medicine [6]. Due to the increasing focus on personalized healthcare and the devastating impact of heart disease, there has been growing interest in the field of cardiovascular computational modelling. Cardiovascular *in-silico* models have assisted researchers in gaining a deeper and more complete understanding of heart and circulatory diseases and are beginning to aid clinicians in determining personalized and optimal treatments [7, 8]. Recent advances in medical imaging, computational efficiency and biological modelling have continued to propel this area of research [9, 10]. As the technology develops, researchers and physicians have envisioned the ultimate goal of a personalized whole heart computation model that incorporates personalized genomics, cellular behavior, tissue structure integrated with heart mechanics and fluid dynamics [6, 9, 11, 12]. Figure 6 Panel A and B illustrates the potential value of these models and certain proposed modelling pipelines (from Niederer et al. [9] and Kayvanpour et al. [13]). Uniting genomics, electrophysiology and hemodynamics into a single comprehensive simulation framework would mark a major milestone in the development of patient specific medicine. Despite many remarkable advances, there are still numerous challenges to be addressed in each of these respective fields.

"Cardiology is flow" [14] and indeed hemodynamic quantification can be immensely valuable for precise and early diagnosis, however, we still lack precise and early diagnostic tools for various

cardiovascular diseases because the hemodynamics analysis methods that can be used as engines of such diagnostic tools are not well developed yet [10]. The required quantities for these tools are local and global hemodynamics metrics [15-28]: **(1)** ***Metrics of circulatory function (local),*** e.g., detailed information of the dynamics of the circulatory system, and **(2)** ***Metrics of cardiac function (global)***, e.g., heart workload and its contribution breakdown of each component of the cardiovascular diseases. Assessments of hemodynamics, if available, would provide valuable information about the patient's state of cardiac deterioration as well as heart recovery and could be used for planning complex valvular-vascular-ventricular disease (C3VD) interventions and making critical clinical decisions with life-threatening risks. Although remarkable advances have been made in medical imaging, offering progressively detailed anatomy and flow information (in some cases), *there are no tools or imaging modalities available to invasively or noninvasively quantify local and global hemodynamics.* Phase-contrast magnetic resonance imaging (MRI) can provide velocity field, but it has a lower temporal resolution than Doppler echocardiography (DE) [29, 30]. It is important to note that magnetic resonance imaging (MRI) cannot be used for patients with most implanted medical devices except for MRI-conditional devices. Computed Tomography (CT) is often used for dimensional measurements of components having internal geometry and flexible structures [31], however, it has a low temporal resolution [32-34] and cannot measure any (local and global) hemodynamic parameters. Furthermore, CT uses ionizing radiation [35, 36] so receiving multiple scans increases the risk of developing cancer [37-40]. Cardiac catheterization is the gold standard for evaluating cardiac function, but it is invasive, carries significant risk [41], and is not feasible for diagnosis in daily clinical practice or serial follow-up examinations. Moreover, cardiac catheterization provides access to flow and pressure only in limited regions rather than comprehensive details of the physiological pulsatile flow and pressure throughout the heart and the circulatory system. Doppler echocardiography is risk-free, has high temporal resolution and can be used to investigate cardiac function in real time. Despite DE's potential advantages, there have been no DE methods to evaluate local hemodynamics precisely and to quantify global hemodynamics, and breakdown contributions of each component of the cardiovascular diseases.

In this paper, we seek for a method that can quantify global hemodynamics in addition to measures of local hemodynamics. Currently only lumped-parameter models have these capabilities to quantify both local and global hemodynamics due to the complexity of the cardiovascular system

and the unmanageable computational cost that 3-D models of hemodynamics in the entire cardiovascular system has. A clinical diagnostic lumped parameter model framework that can quantify both *local* and *global* hemodynamics in patients with cardiovascular diseases should satisfy the following 2 requirements:

1. The computational diagnostic framework should be developed based on the clinical patient-specific input parameters (e.g., hemodynamic metrics, clinical data and imaging). Upon development of a diagnostic lumped parameter model, its results should be validated against clinical data obtained using Doppler echocardiography, magnetic resonance imaging and especially cardiac catheterization (if available) as the clinical gold standard to evaluate pressure and flow through the heart and circulatory system.
2. The patient-specific input parameters for such development should be obtained *non-invasively* in each patient because obtaining them invasively (e.g., with catheterization) contradicts the whole purpose of the diagnostic computational framework.

Using personalized simulation tools to quantify cardiac function and blood flow characteristics also offers a unique avenue to examine the effects and patient-specific treatment options for a range of diseases [42-44]. Additionally, studying the cardiovascular system from an *in-silico* setting has allowed researchers to gain new insights and metrics into the characteristics of cardiovascular illnesses [15, 45-47]. This article reviews how the personalization of lumped parameter modelling is changing the field of patient-specific cardiovascular care. An overview of the modelling technique will be presented followed by a breakdown of different approaches to simulating the cardiac and circulatory system and cardiovascular diseases. Lumped parameter modelling in the context of higher order modelling will be reviewed and the personalization of these simulations through a range of optimization methods will also be discussed. Finally, the future directions and the current challenges and opportunities related to the translation of this technology into clinical settings will be reviewed.

2.3 Lumped Parameter Modelling

Lumped parameter modelling offers a basic approach in which the desired blood characteristics, such as pressure, flow rate and volume vary as a function of time. By relating the flow of fluids and the flow of electrons through the hydraulic-electrical analogy, one can simulate the desired

blood waveforms by using a series of electrical elements. By solving the associated equations that govern electronic circuits, a mathematical representation is formed which can be used to analyze and predict blood flow behaviour within the cardiovascular system [48, 49].

The concept of quantitatively modelling the arterial system was first proposed by German physician Otto Frank in 1899 who developed the early two element Windkessel model [50]. The simple model utilized a resistor and a capacitor in parallel to represent the arterial load faced by the heart and the hemodynamics in the aorta [50, 51]. Over time, more complex models were designed since the original model could not accurately account for high frequency components [52]. A three element Windkessel model was developed by adding a characteristic impedance to the original model, which better represented the oscillatory behaviour of the aortic input impedance at higher frequencies [53]. To account for the inaccuracies at lower frequencies in the three-element model, a four element Windkessel model was also proposed by adding an inductor element [54]. This component factored in the total inertance of the arterial system, which helped to reduce input impedance error over the entire frequency range but rendered parameter estimation more difficult due to the increased number of model elements [51].

Over the years, a series of different variations of these models have been proposed [55-57] with the goal of more accurately modelling different physiological phenomena such as microcirculation [58]. In the recent decades, this modelling technique has been used to test artificial heart devices [59-61], study hemodynamics related to surgical procedures [62-64] and is playing an important role in the development of personalized cardiovascular tools [15, 16, 18, 19, 42, 65-70]. A typical model includes heart chamber compartments acting as a blood pump (or simply an input pressure and flow waveform) and a series of vascular networks to transport the fluid throughout the body [48]. In the electrical domain, this configuration can be represented by using a combination of resistors, capacitors, and inductors to model the physical properties of the cardiovascular system. From a physiological perspective, the resistors represent the viscous resistance blood faces as it is pumped through the vessels. The capacitors are used to account for the energy stored by the vessel's compliance and the inductors factor in the inertia of the blood [49]. By adding or removing elements, models of different details and sophistications can be formed. Furthermore, different

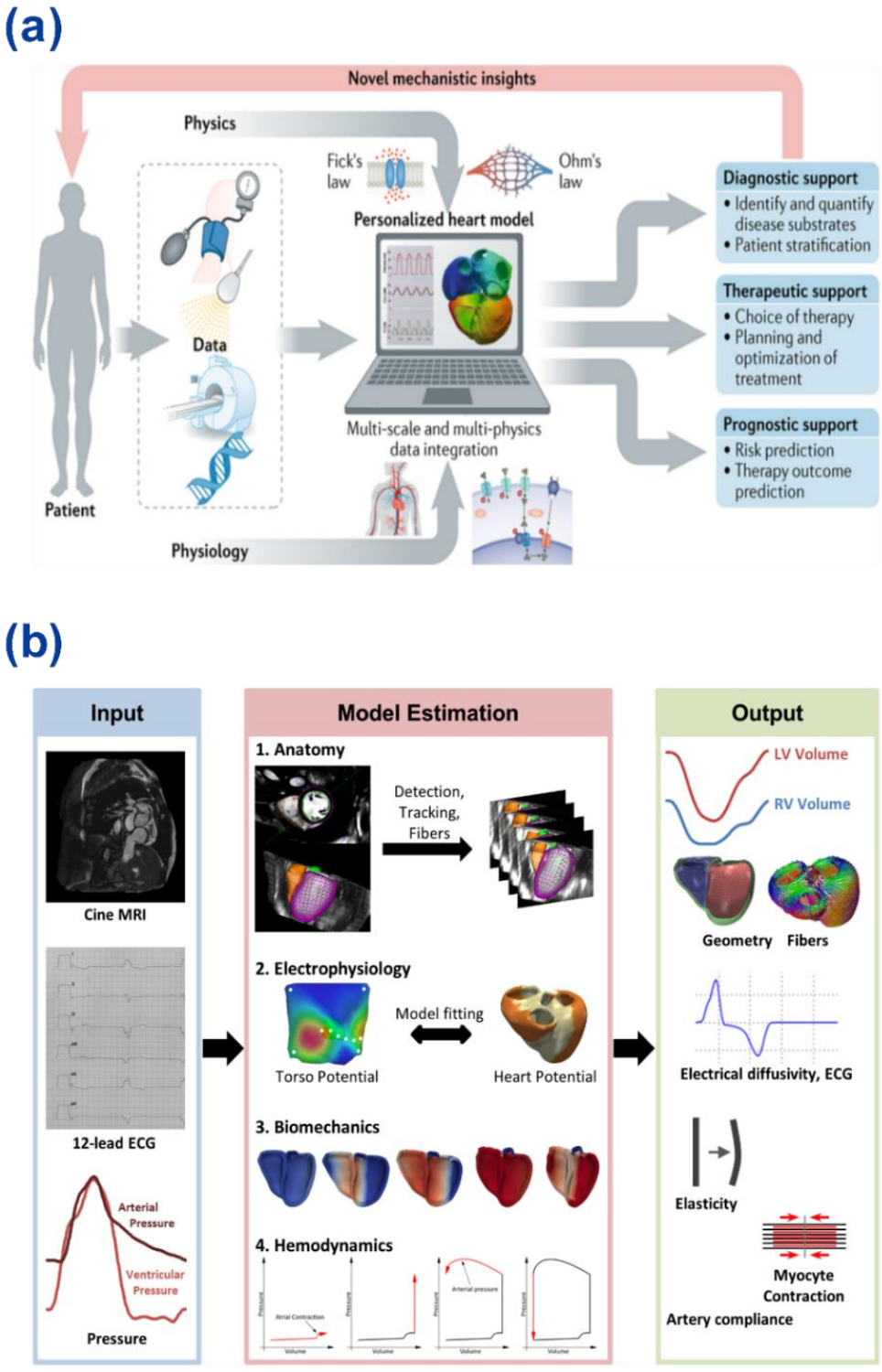

Figure 6: (a) *Overview of a general personalized computational cardiovascular framework that incorporates a variety of clinical data and outlines certain quantitative outputs that can add value to the clinical workflow from Niederer et al. [9];* ***(b)*** *Illustration of a patient-specific computational cardiology pipeline used in the multi-scale modelling of a failing heart from Kayvanpour et al. [13]*

cardiovascular diseases, including peripheral and vascular disease [46, 71-74], coronary artery disease [75, 76], valvular disease [15, 28, 72] and others can also be modelled using this approach.

In order for the system to behave in a realistic manner, physical governing equations are applied. In the hemodynamic domain, mass and momentum conservation are accounted for through the continuity equation, Poiseuille's Law and the Navier Stokes equations, which dictate the flow and pressure in the system [77]. Through the analogous relationship of fluid flow and electric current and fluid pressure and voltage, the concepts that govern fluid behaviour can be applied to the electrical model. These principles can be translated into the electrical domain by using Ohm's Law and Kirchhoff's laws, which govern the voltage and current behaviour in circuits [77, 78]. By combining these principles, each compartment is then mathematically represented by a series of ordinary differential equations and an algebraic equation to couple the pressure-volume relationship based on compliance [78]. Depending on the complexity of the design and the factors considered, these equations may be linear or non-linear in nature. The heart and valve compartments are also guided by relatively similar approaches. An examination of each of the main compartments will be explored in Section 2.4. Numerical methods can then be applied to solve these equations and the desired hemodynamic parameters including blood flow and pressure can be examined throughout the network at different points. Lumped parameter modelling derives one of its main strengths from the minimal computation time required to solve ODEs and algebraic equations. Furthermore, the relatively simple structure of the model allows most personalized simulations to be automated. These advantages may increase the ease of embedding this style of cardiovascular modelling into a high throughput clinical workflow [8, 79].

Within the realm of circulatory mechanics, lumped parameter modelling offers the unique ability to examine both cardiac function and global hemodynamics within the context of a single model. Due to the interconnected nature of the cardiovascular system, being able to quantify both is crucial for the effective prediction and diagnosis of CV diseases. Not only can the lumped parameter approach be an effective tool on its own, but its integration with higher order modelling can provide more realistic local phenomena [18, 19, 80]. However, one of the main challenges in lumped parameter modelling is determining appropriate values for each of the model elements. Since many of the model parameters do not directly represent measurable physiological quantities, they must be approximated or inferred. Additionally, even for the parameters that can be measured,

many require invasive and practically difficult measurements [77]. To account for this issue, many authors rely on a combination of values from literature sources, past studies, population averages and animal experiments [78, 81-85]. Another approach, which will be elaborated on in Section 2.6, is the individual tuning of some of these parameters based on non-invasive approaches [15, 16, 18, 19, 42, 65, 86-89]. Basing the model parameter on individual patient data leads to more personalized simulations, which is critical for developing patient-specific diagnostic and predictive tools. As one example, Figure 7, shows a schematic diagram (Panel A) and sample results (Panel B) of a fully Doppler-based patient-specific diagnostic, monitoring and predictive lumped parameter framework for complex and mixed valvular, vascular a ventricular disease that was validated against catheterization data in forty-nine patients (from Keshavarz-Motamed [42]).

While lumped parameter modelling is particularly advantageous for simulating global hemodynamics and cardiac function, there are other higher order modelling approaches such as 1-D propagation models and 3-D computational fluid dynamics (using conventional macroscopic numerical methods based on the discretization of Navier–Stokes equations; e.g., finite difference method, finite volume method, finite element method, etc.) that are suited to study local flow dynamics [90-94]. The major difference between lumped parameter modelling and higher order modelling is spatial detail. In a zero-dimensional model, the hemodynamic parameters only vary as a function of time, while in a 3-D model for example, they vary as a function of time as well as in all three spatial coordinates within the specified structure. In the mathematical sense, the variables of higher order models are represented by a series of non-linear partial differential equations (PDEs) as opposed to ordinary differential equations (ODEs). See Figure 8 (Panel A) for a sample using a 0-D lumped model and a 3-D Lattice Boltzmann model (LBM) [19]. Figure 8 (Panel B and C) outline samples of lumped models coupled with a 3-D model of the coronary arteries [95] and a finite element ventricular-vascular model coupled with a closed loop lumped parameter (0D) model [69] respectively.

Given the nature of lumped parameter modelling, it is a useful tool to simulate the heart and circulatory components as well as their associated diseases. By further improving and personalizing these models, the hope is that cardiovascular simulations may be one of the many avenues that helps combat the global impact of cardiovascular diseases.

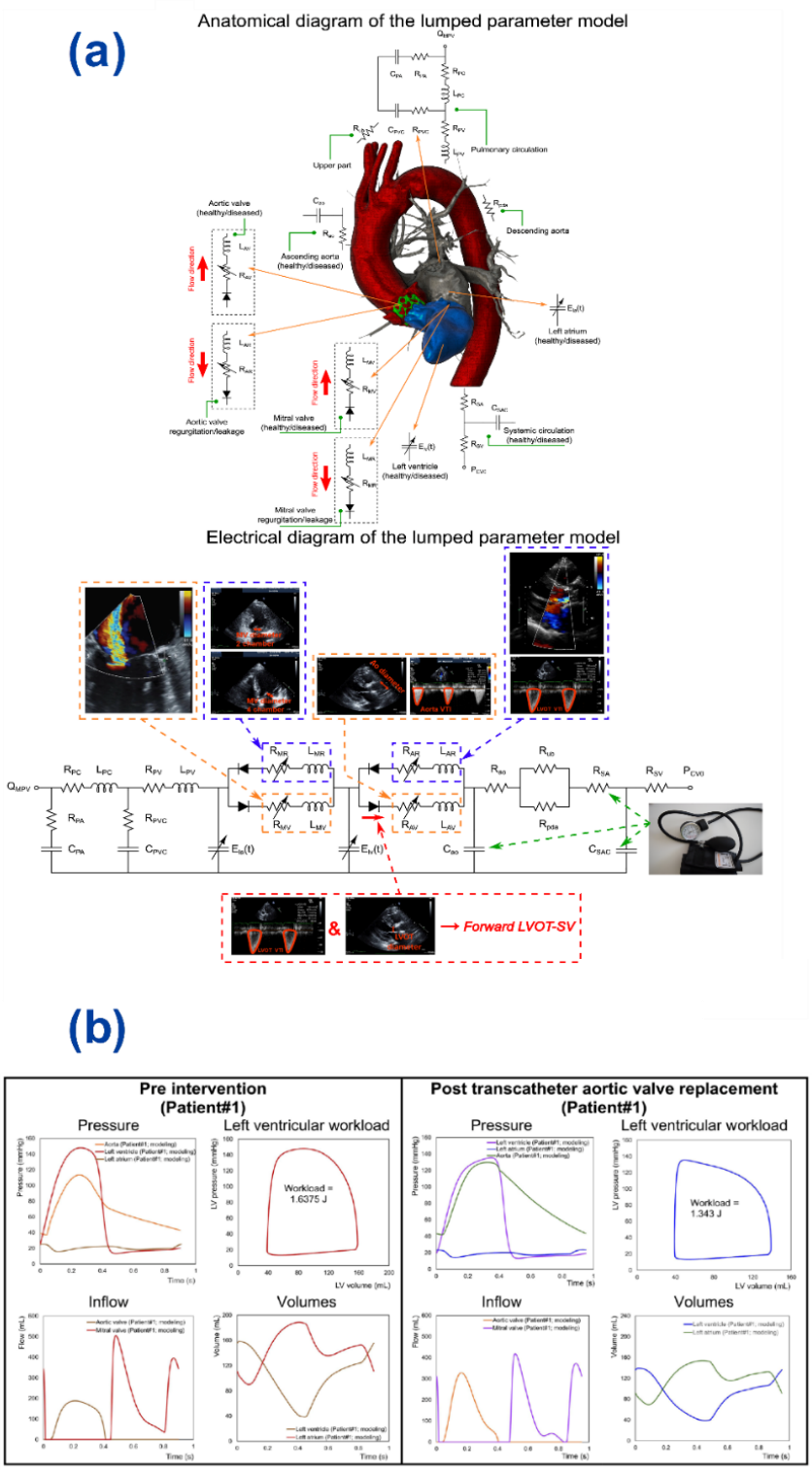

Figure 7: *(a) Schematic diagram of a diagnostic and predictive lumped parameter modelling framework to quantify local and global hemodynamics (a. Anatomical representation; b. Electrical representation) in patients with complex valvular, vascular, and ventricular diseases (from Keshavarz-Motamed [42]); (b) Example of predicted hemodynamics in a patient with complex valvular, ventricular and vascular diseases from baseline to 90 days post-transcatheter aortic valve replacement (TAVR) from Keshavarz-Motamed [42]*

2.4 Modelling of Heart Components and Cardiovascular Diseases

2.4.1 Cardiovascular Disease and the Implementation of Lumped Parameter Modelling

Cardiovascular disease is a broad group of diseases that encompass illnesses related to the heart and the blood vessels. It includes diseases associated with the narrowing of blood vessels such as coronary or peripheral artery disease, abnormal heart rhythms such as arrhythmia, diseases related to the heart valves and ventricles such as valvular stenosis and ventricular hypertrophy, heart failure and others [2, 96-98].

To aid in the diagnosis of these diseases, physicians often rely on blood flow and pressure information in addition to medical imaging, blood tests and physiological tests [97]. Currently, the gold standard technique for obtaining numerical hemodynamic data in the heart and coronary arteries is cardiac catheterization [42, 99]. Although it is a common and well-established technique, the process is also invasive, expensive, provides limited and semiquantitative data, and is not practical for a range of clinical scenarios [41, 97, 100].

The addition of personalized cardiovascular modelling into this process holds the potential to open a new chapter in non-invasive, quantitatively driven, cardiovascular disease diagnosis and predictive surgical planning [101, 102]. It offers a method to enhance current medical imaging and transform it into a comprehensive patient-centered predictive framework which can improve the availability of data in a range of scenarios such as post-operative follow-up examinations [10, 103]. Finally, it allows researchers and clinicians to study cardiovascular diseases in an in-silico setting, allowing for a unique method to study disease mechanisms and interactions with local and global hemodynamics as well as cardiac behaviour [15, 16, 45, 46, 104-107].

2.4.2 Heart Modelling and Ventricular Diseases

The heart is the central driving force for the cardiovascular system and is essential for transporting oxygen, carbon dioxide and nutrients to various portions of the body [49]. The four heart chambers (the left and right atriums and ventricles) act as the main pumping sources and are heavily intertwined with the entire cardiovascular system. Modelling the heart, and especially the chamber characteristics, is important for developing accurate and personalized cardiovascular models and is beginning to show promise in the areas related to cardiovascular diseases, treatment evaluation and medical device design [16, 18, 19, 42, 46, 48, 67, 68, 70, 108-111].

Modelling of the heart in lumped parameter models is based around developing a mathematical approach to generating pulsatile blood waveforms that are comparable to those achieved from the natural contractions of the human heart. A variety of different methodologies have been developed, but the majority can be classified based on a series of attributes.

Depending on the intent and required complexity of the model, authors tend to simulate either all four heart chambers or individual chambers. Certain authors [42, 65, 72, 112, 113], including Casas et al. [114] for example, focused predominantly on developing a model for the left portion of the heart since the goal was to study blood flow in the systemic circulation. Figure 9 (Panel D) displays a visualization of the 4D flow MRI data and analysis planes used in the study as well as a circuit schematic. Others, such as Broomé et al. [115] developed a four-chamber lumped parameter heart model since the experiment encompassed both hemodynamics and oxygen transport, which required both systemic and pulmonary circulation.

A commonly used method to simulate heart chamber contractions is based on the concept of time varying elastance [48, 116]. This approach was first proposed by Suga et al. [117] and centers around modelling myocardial mechanics through an instantaneous pressure volume ratio that represents the changing muscle stiffness during the heart contraction. In their experiment, they examined cardiac behaviour through pressure-volume (PV) loops and studied both ejecting and non-ejecting cardiac contractions [118]. They found that the pressure-volume data from these contractions, recorded at different points in the heart cycle, were all located on linear lines [117, 118]. These lines are described by their slopes, which represent elastance (E) since E = Pressure/Volume, and by their intercept, which has a quasi-constant volume (V_0) [118]. This led to the formulation of time varying elastance which was determined to be a load independent function. This concept is illustrated in Figure 9 (Panel A) and mathematically by the following equation.

$$E(t) = \frac{P(t)}{V(t) - V_0} \tag{1}$$

where P(t), V(t) and V_0 are ventricular time varying pressure, time varying volume and unstressed volume respectively [119, 120]. The time varying elastance heart model is often represented by using a periodic double-Hill function [25, 42, 65, 75, 112, 113, 115, 116, 120].

$$E(t) = \frac{E_{max} - E_{min}}{\max\left[\left(\frac{g_1}{1+g_1}\right)\left(\frac{1}{1+g_2}\right)\right]}\left(\frac{g_1}{1+g_1}\right)\left(\frac{1}{1+g_2}\right) + E_{min} \quad (2)$$

where

$$g_1 = \left(\frac{t}{\tau_1}\right)^{m_1} \; and \quad g_2 = \left(\frac{t}{\tau_2}\right)^{m_2}$$

where E_{max}, E_{min}, τ_1, τ_2, m_1 and m_2 are maximum elastance, minimum elastance, systolic time constant, diastolic time constant, contraction rate constant and relaxation rate constant respectively [113, 116] (see Figure 9 Panel B for a graphical representation). By combining the contraction and relaxation of the chambers, the double-Hill function can describe both systole and diastole since the function is comparable to the cooperative nature of myocyte recruitment during preload [42, 121]. Parameters for this function are often based on experimental data [119, 120, 122, 123] however certain authors have optimized a portion of these parameters by using patient specific cardiac measurements [25, 65, 112, 114]. While the double-Hill representation tends to be the more commonly used function, other authors have used different mathematical functions to model time varying elastance [66, 69, 81, 124-126]. Tang et al. [104] for instance, used a combination of Gaussian functions to simulate the heart chambers in a lumped parameter model aimed at studying the abnormal hemodynamic mechanisms related to pulmonary hypertension.

In the electrical analog model, the time varying elastance is typically simulated by a variable capacitor element [49] and is occasionally placed in series with a resistor [18, 81, 114, 116]. This allows for the generation of an analog signal that simulates the heart chamber contractions and thus the pulsatile behaviour of the blood flow and pressure over time.

Although the time varying elastance concept is one of the more popular approaches, certain authors have argued that some of the underlying assumptions, such as the load independence of E(t), may be flawed [127] and that the theory does not accurately characterize the atrial and ventricular behaviour [109, 125, 128]. Kim et al. [60] also argued that using the time varying elastance approach to model certain pathological conditions, such as irregular heart rhythms, was questionable. Instead, they proposed a synergistic model that incorporated the electrical, mechanical, and chemical activity of the heart tissues and macroscale heart properties to improve

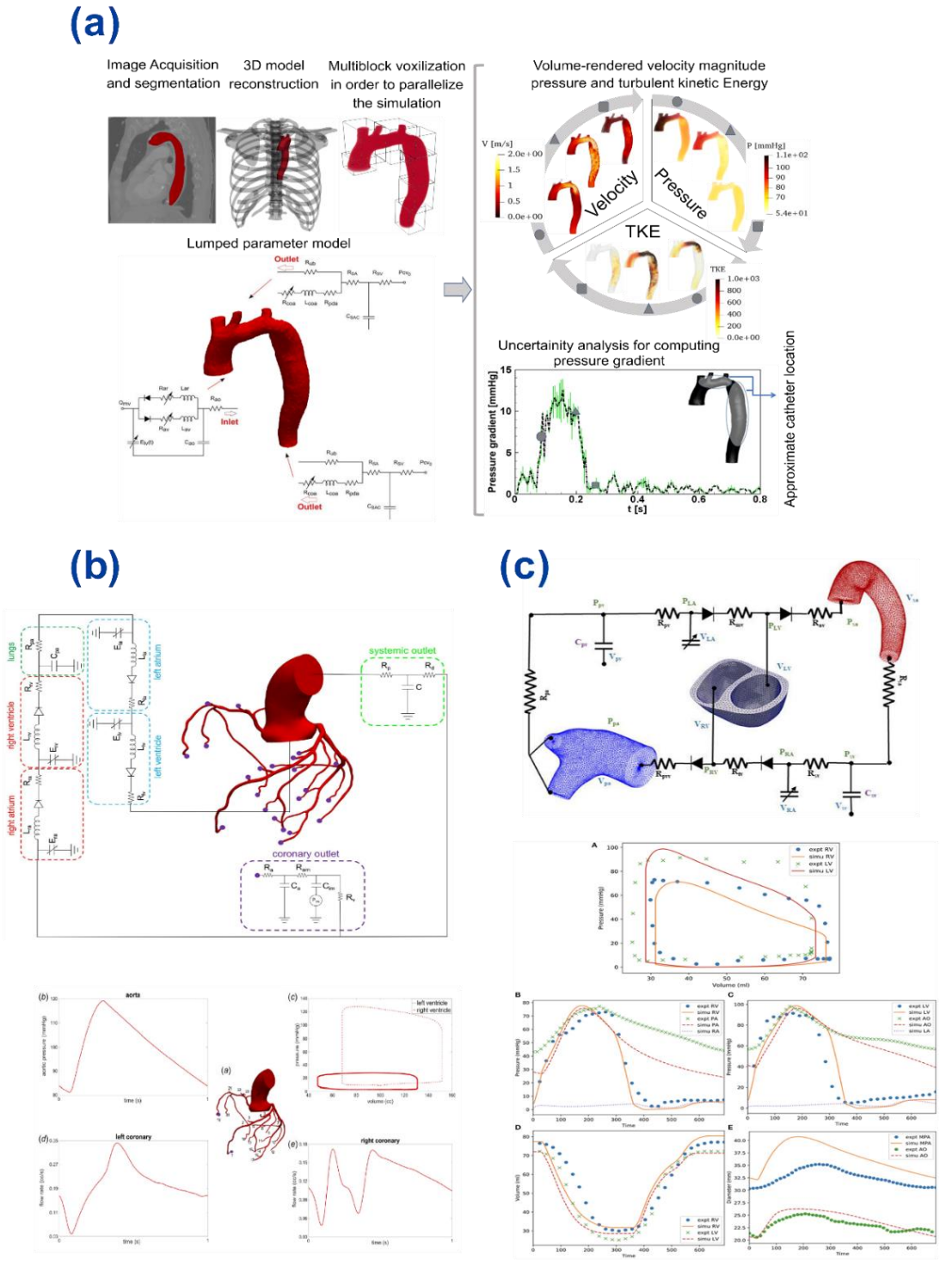

Figure 8*: (a) Sample results from a 0-D and 3-D Lattice Boltzmann method simulation (LBM) (from Sadeghi et al. [19]);* ***(b)*** *Schematic diagram of an image-based 3D model of a portion of the aorta and coronary arteries coupled with closed-loop lumped parameter models and sample of the pressure and flow results from the study by Mirramezani et al. [95];* ***(c)*** *Schematic diagram of a finite element ventricular-vascular model coupled with a closed loop lumped parameter (0D) model and sample simulation results from Shavik et al [69]*

the accuracy of the model for left ventricular assist device (LVAD)-heart interactions. Pironet et al. [129] also presented another mathematical multiscale model that factored in the cellular activity responsible for cardiac contraction to overcome the limitations of the time varying elastance theory. Regardless, the time varying elastance model continues to be used by many authors due to its ease of implementation, reliability, and acceptable accuracy for most experiments [48, 77, 115].

One of the major advantages of simulating the heart function, especially in personalized lumped parameter models, is that it yields quantitative data about the cardiac function. In cardiovascular medicine, pressure-volume loops offer crucial insight into different cardiac metrics [130]. These graphs are formed by plotting the ventricular pressure against ventricular volume throughout a cardiac cycle and they represent the relationship between the two parameters [98]. PV loops contain an abundance of information such as ejection fraction, contractility, stroke volume and stroke work which are important in evaluating the health of the heart [25, 105]. A variety of different cardiovascular diseases such as valvular stenosis, valvular regurgitation, hypertrophy and heart failure can impact the shape of a PV loop, making these graphs a useful tool in the diagnosis of these diseases [98, 112]. Although these PV loops contain large amounts of useful information, the needed data is typically obtained invasively using a catheter probe, limiting their overall availability in clinical settings, and reducing their application in routine examinations [25].

Lumped parameter models that incorporate non-invasive personalized cardiac parameters offer a unique way to generate these personalized PV loops in a rapid and non-invasive manner. Additionally, they can be used to study the impact of different treatment options and treatment priorities in a patient-specific manner [28, 72, 104, 105, 131]. In recent work, Motamed [42] used a personalized lumped parameter model with a time varying elastance heart model and non-invasive parameters to evaluate how different intervention options would impact the cardiac workload for a patient with multiple valvular diseases based on PV loops (Figure 9 Panel E). Itu et al. [112] also developed a non-invasive personalized automated lumped parameter framework that was able to accurately generate PV loops for patients with mild aortic valve regurgitation (Figure 9 Panel C).

2.4.3 Heart Modelling and Valvular Diseases

In addition to modelling the heart chambers, the heart valves are another crucial component for cardiovascular simulations. These four valves (mitral, aortic, tricuspid, and pulmonic) allow for

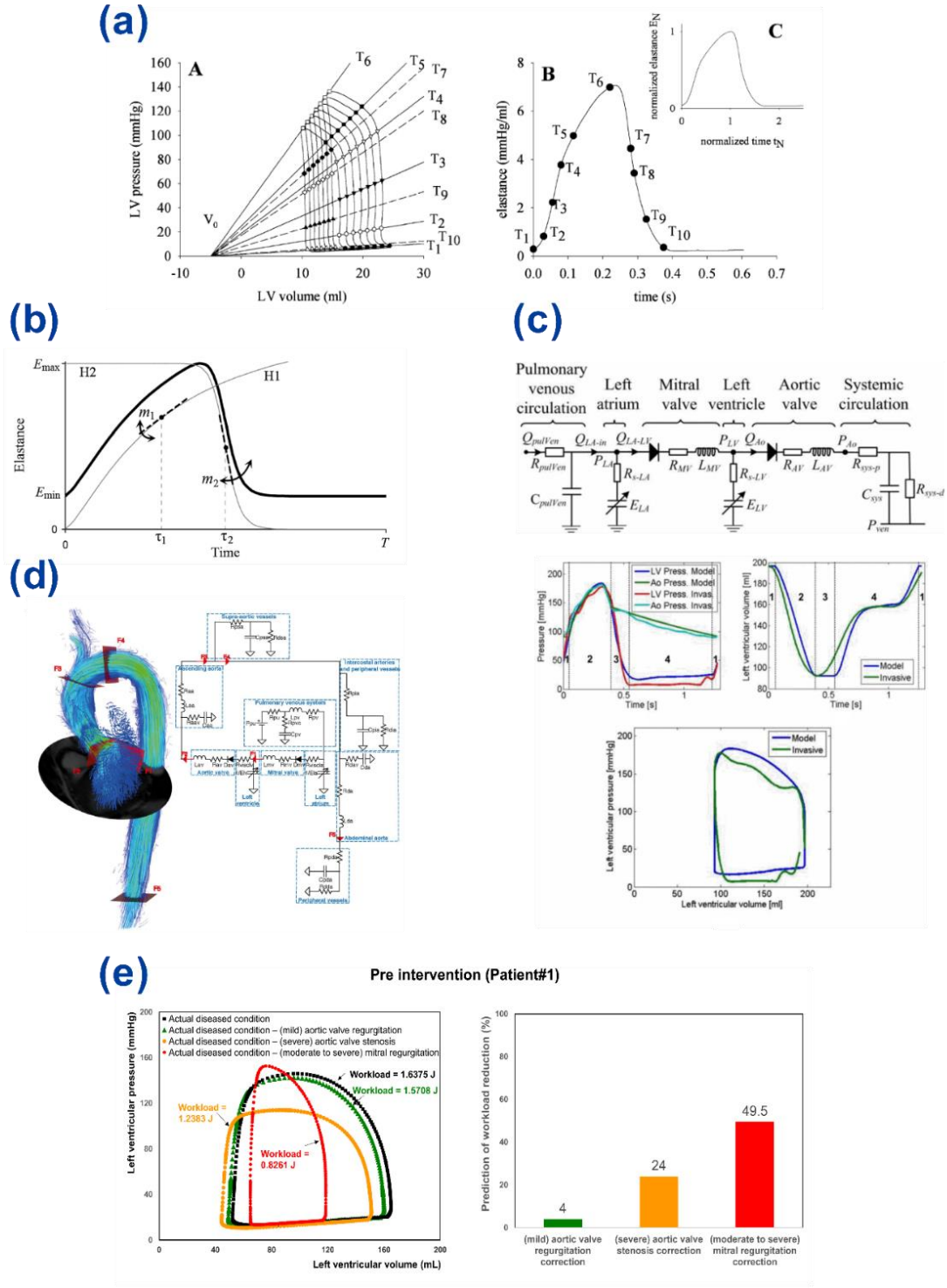

Figure 9: ***(a)*** *Illustration of time varying elastance curve (and normalized curve) derived from multiple PV loop from Segers et al. [118];* ***(b)*** *Time varying elastance curve based on a double-Hill function and data from the work of Mynard et al. [116];* ***(c)*** *Simulated and in-vivo pressure and volume results from a non-invasive automated echocardiography based 0-D model developed by Itu et al. [112];* ***(d)*** *Visualization of the 4D flow MRI data and analysis planes used in the study as well as the lumped parameter model schematic proposed by Casas et al. [65];* ***(e)*** *Pre intervention PV loop disease contributions based on a patient-specific non-invasive lumped parameter model from Motamed [42]*

the unidirectional flow of blood into and out of the ventricles during the cardiac cycle [98]. Since the opening and closing of heart valves is driven by the pressure gradient across these valves (as well as external fluid forces such as vortices and shear force) [132], a similar approach is often used to describe them in 0D models.

The net pressure gradient formulation (TPG_{net}) proposed by Garcia et al. [133] for example, is one of the mathematical functions that has been developed to model aortic valves and aortic stenosis. It is based around calculating the instantaneous net pressure gradient across the valve and characterizes the flow acceleration, deceleration, and energy losses [42, 65].

$$TPG_{net} = 2\pi\rho \frac{\partial Q(t)}{\partial t} \frac{1}{\sqrt{E_L Co}} + \frac{1}{2}\rho \frac{Q^2(t)}{E_L Co^2} \tag{3}$$

where

$$E_L Co = \frac{EAO\ A_{Ao}}{A_{Ao} - EOA} \tag{4}$$

where $Q(t), \rho, E_L Co, EAO, A_{Ao}$ are the transvalvular flow rate, blood viscosity, energy loss coefficient, effective orifice area and the ascending aorta cross-sectional area respectively [133]. The expression is highly time dependent over systole and incorporates instantaneous transvalvular flow rate and the energy loss coefficient to relate the left ventricular pressure and ascending aorta pressure [28, 133]. The energy loss coefficient is also included to account for the pressure recovery phenomenon which frequently occurs in patients with aortic stenosis [28, 65, 134]. This same formulation, with a few adjustments, can also be used to model the mitral valve [42, 45, 65].

This configuration, though commonly used, is a simplification of the valve mechanics and does not take into account the local hemodynamic factors such as the shear forces acting on the valve leaflets or the impact of vorticity generation [48, 77]. To account for these limitations, certain authors have developed more complex approaches to simulating heart valve dynamics [135-137]. Korakianitis et al. [138] proposed an advanced valve model to describe the blood-leaflet interactions by including parameters such as leaflet opening angle while Mynard et al. [116] also presented another model that incorporated the instantaneous pressure difference and the valve

position index. Both these models were designed to be implemented into a lumped parameter or 1D model.

Most zero-dimensional models use a diode in series with a resistor (and in certain cases an inductor) to model the heart valves [42, 44, 65, 66, 68-70, 75, 104, 112, 126, 139]. The diode, which allows for unidirectional current flow, switches states when the pressure or flow signal exceeds a certain threshold [112, 140, 141] or at a predefined time within the heart cycle [142].

Different valvular diseases, such as aortic stenosis and mitral regurgitation, can impact the opening and closing of the valve leaflets [143]. For the past few decades, lumped parameter models have been used to study a variety of different heart and valvular diseases and their impacts on local and global hemodynamics as well as aid in the design of mechanical heart valves [42, 45, 107, 109, 139, 144, 145]. Fiore et al. [146] for example, proposed a zero-dimensional model to study the hydraulic characteristics of three different clinically approved mechanical prosthetic heart valves. In a 2015 study, lumped parameter modelling also provided Scarsogli et al. [147] with a unique framework to examine the impact of atrial fibrillation on transvalvular flow dynamics without the presence of other valvular diseases, something that is difficult to study in clinical settings due to the concomitant nature of the pathologies. Furthermore, there have been a series of personalized non-invasive lumped models developed to evaluate the impact of valvular disease [16, 42, 112]. In a 2019 clinical study, Ben-Assa et al. [15] used a patient specific lumped parameter model, which utilized an arm cuff sphygmomanometer and echocardiography as inputs, to investigate the left ventricular stroke work and vascular impedance of seventy patients with severe aortic stenosis before and after a transcatheter aortic valve replacement (TAVR) (Figure 10 Panel A).

2.4.4 Coronary Arteries and Their Diseases

Given the substantial impact of coronary artery disease (CAD) [1, 2, 4], there has been a growing effort to develop personalized non-invasive cardiovascular simulation tools to model blood flow in the coronary arteries. The formulation of these simulations differs slightly from other vascular models due to the unique characteristics of blood flow in the coronary arteries. During the ventricular contraction of the myocardium, the blood flow in the large coronary arteries is briefly reversed due to the magnitude of the contractile force exerted on these arteries [148]. In contrast to the flow in the majority of blood vessels, maximum blood flow in the left coronary vessels occurs during early diastole as opposed to systole, since the ventricles have relaxed, and the

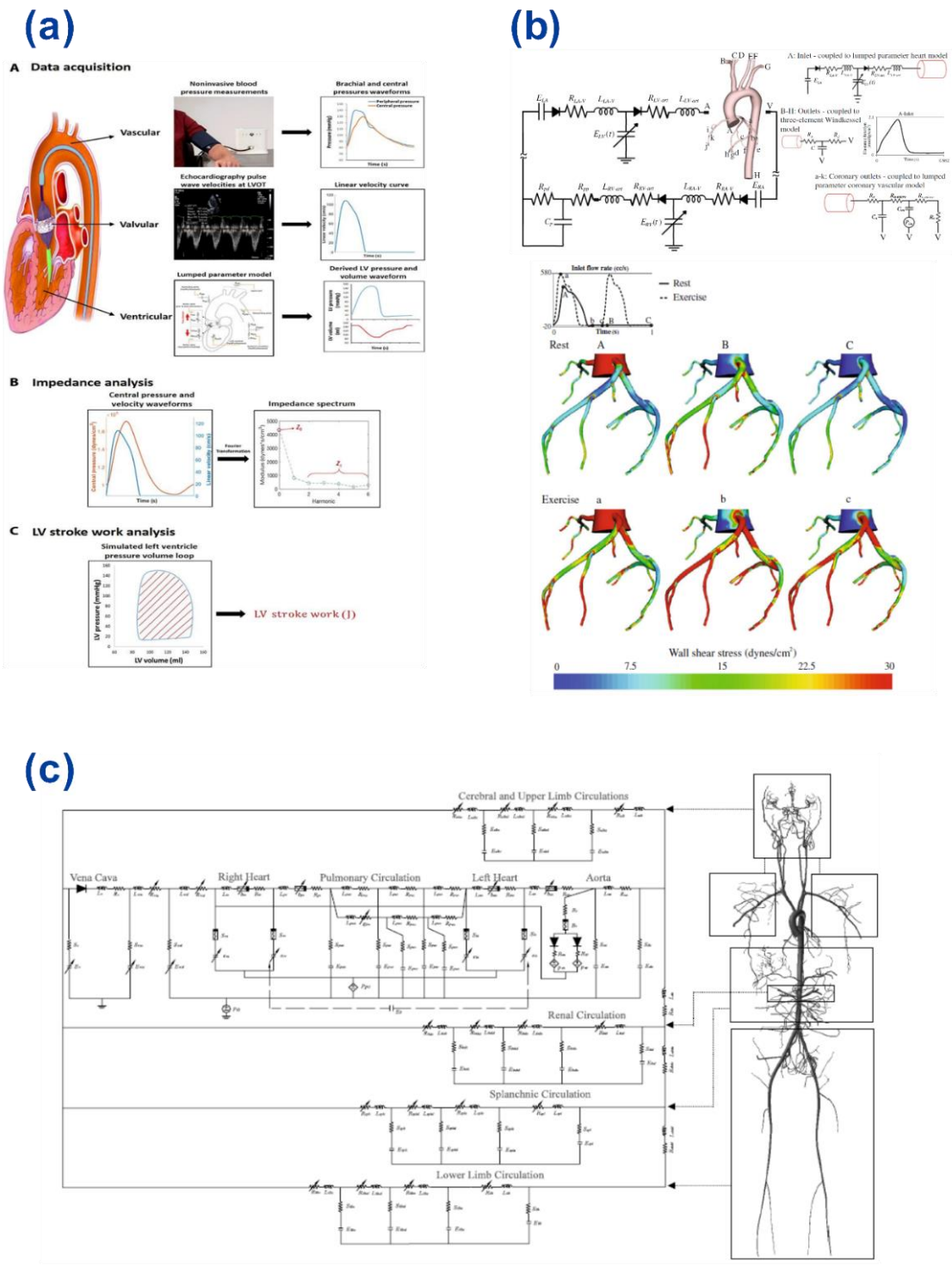

***Figure 10**: **(a)** Schematic of the data acquisition, impedance analysis and LV stroke work analysis used in the clinical study by Ben-Assa et al. [15]; **(b)** Lumped parameter model and multiscale model develop by Kim et al. [44] and the coronary artery wall shear stress results during rest and exercise simulations; **(c)** Comprehensive lumped parameter model used by Liang et al. [168] which included major branches of the cardiovascular system*

compression force is absent [148]. This phenomenon (known as extravascular compression) also occurs in the right coronary artery but is substantially less pronounced due to the lower force exerted by the right ventricle on the artery.

To simulate this behaviour, a pressure source is often embedded into the coronary vasculature model and is equated to a fraction of the left and right ventricular pressure [43, 44, 66, 68, 70, 75, 76] (a sample is shown in Figure 8 (Panel A) and Figure 10 (Panel B) – see Pim component in coronary outlet). These pressure values vary depending on the location in the coronary network since different positions will be impacted differently by the extravascular compression. The remainder of the coronary network is typically based around the same principles used to construct vessels and vasculature, which were outlined in Section 2.3. For further reading about the design of vasculature, readers are referred to reviews by Shi et al. [77] and Zhou et al. [52].

Most of the personalized coronary simulation tools developed to date are either 1D or 3D models, supplemented with lumped parameter portions. Higher order models are often used to simulate the coronary arteries since local spatial distribution of blood flow and pressure can be obtained. Other useful information, such as wall shear stress (WSS), wall shear stress gradient (WSSG) and flow disturbance data can also be generated, which can give additional insight into CAD and the formation of stenosis [14, 44, 149, 150]. These models tend to use 3D geometry obtained from an imaging modality (such as CT, CTA, IVUS or MRI) and existing software (ITK-SNAP, 3D slicer and Mimics for example) [151-153] to reconstruct the main vessel sections [48, 102]. The outlet boundary conditions are often formed by using lumped parameter circuits that are coupled to the outlet of each vessel [44, 68, 70, 76, 95, 110, 154]. In certain models, such as the ones proposed by Kim et al. [44] and Mirramezani et al. [95], a zero-dimensional heart model is also used to create the inlet pressure and flow waveforms. Lumped models can recreate realistic downstream conditions and can be tuned on a patient specific basis, making them useful boundary conditions [44, 77]. More details on the use and coupling of the lumped parameter models for higher order modelling will be discussed in Section 2.5.

These coronary models have been applied to a variety of clinical scenarios such as coronary artery surgery planning [70, 155-158]. Sankaran et al. [110] for example, developed a personalized model to study the hemodynamics in patients with multiple coronary artery bypass grafts (CABGs). Their simulation utilized Computed Tomography angiography (CTA) and non-invasive clinical

measurements in conjunction with CFD and lumped parameter boundary conditions to evaluate the impact of graft shape on local and global hemodynamics. Others have developed simulations for the management and diagnosis of coronary artery disease [76, 95, 159, 160]. Kim et al. [44] combined a 3D finite element coronary and aortic model, which included tunable lumped parameter boundary conditions, with cardiac-gated CT and brachial artery pulse pressure to study how different degrees of stenosis and exercise impacted the coronary blood flow, pressure and wall shear stress (Figure 10 Panel B). Similar work was also translated into the first FDA approved cardiovascular flow simulation tool (HeartFlow FFR_{CT} by HeartFlow Inc. ©) to conduct non-invasive coronary CTA-based fraction flow reserve (FFR) analysis [161].

In the past two decades, coronary lumped parameter models, without higher order components, have also been proposed based on generic or invasive physiological parameters. They have been used to simulate coronary artery related surgeries [84, 162], study coronary flow [106], and aid in the design of a physiologically representative in-vitro coronary model [163]. There have also been a limited, but growing, number of coronary focused lumped parameter models developed in recent years based on non-invasive patient specific parameters. Examples of these models include work by Duanmu et al. [66] and Li et al. [75] who both used CTA to obtain patient specific coronary artery geometry. Duanmu et al. [66] used the individual vessel diameters to determine the resistance, compliance, and inductance values for each section of the left and right coronary network and used their model to study the impact of different stenosis conditions on the simulated flow, pressure, and FFR. Li et al. [75] used CTA in addition to heart rate, non-invasive blood pressure, age and height paired with a genetic optimization algorithm [164] to personalize several of the heart and coronary model parameters. Mao et al. [43] also created a personalized lumped parameter framework for surgical planning of CABG. The model utilized CT imaging, Doppler ultrasound and non-invasive blood pressure in combination with various parameters from a model by Kim et al. [44] and the same optimization process used by Li et al. [75]. The final model was used to simulate different stenosis conditions and compared the bypass graft options (saphenous vein graft and left internal mammary artery graft).

As computational technology, medical imaging and predictive algorithms continue to progress, patient specific non-invasive coronary artery simulations will continue to be one of the main areas

of focus for clinical simulation tools in the coming years due to the severity and burden of coronary artery disease.

2.4.5 Multi-Compartment Models

In the lumped parameter domain, a series of researchers have also proposed more advanced and intricate closed loop models that attempt to simulate the major compartments of the human body all within a single model. These complex, multi-compartment lumped parameter models have been developed to study a variety of different physiological scenarios and examine the impact of regulatory systems on global hemodynamics. The underlying models are based around the same principles mentioned previously, but rather than focusing on one section, such as the coronary arteries or aortic arch, they encompass many different regions like the liver, kidney, brain, and others. Certain simulations include additional features such as neurological and auto regulatory control [102]. These multi-compartment models offer a framework to study the interconnected nature of the cardiovascular system in-silico, but often contain many unknown parameters and variables, which increases the difficulty of parameter personalization.

In a paper by Hassani et al. [82], an electronic circuit representation of the cardiovascular system was developed consisting of 42 segments representing the arterial system, which included the carotid, hepatic, and renal circulation. This model served as the basis to simulate the impacts of bradycardia, tachycardia as well as aortic aneurysms and renal stenosis on the cardiovascular system [47, 165]. Models such as these, although ideal and based on generic parameters, can be one of the effective tools for studying the pathogenesis of certain cardiovascular diseases [165].

Other authors have built upon advanced multi-compartment models and embedded regulatory mechanisms within them [49, 102, 166, 167]. Liang et al. [168] designed a comprehensive closed loop lumped model with an integrated autonomic nervous control system to study the cardiac characteristics of diastolic dysfunction. The model was capable of predicting global hemodynamics in seven main cardiovascular subsystems (upper limb, cerebral, pulmonary, renal, etc.) as well as hemodynamic regulation given system perturbations (Figure 10 Panel C). Similarly, Werner et al. [137] coupled a pulsatile model with the well-studied Guyton model [169], which consisted of hundreds of equations to model circulatory control and included control of the cardiovascular system via arterial baroreceptors, chemoreceptors, and ergoreceptors [137, 170]. This coupled model was then applied to study cardiac electrotherapy and the importance of a range

of factors such as the effect of impaired ventricular relaxation and the selection of appropriate cardiac pacemakers [137].

Due to the complexity of these models and the numerous unknown parameters, to the best of our knowledge, they currently have limited applications as personalized diagnostic tools for common cardiovascular diseases. As parameter optimization continues to advance, these large multi-compartment full body models may eventually play a role in the understanding and diagnosis of multiple CV diseases due to their ability to connect truly global hemodynamics with complex regulatory mechanisms.

2.5 Lumped Parameter Modelling in the Context of 3-D Modelling

Within the field of hemodynamic modelling, a large body of research is focused on multiscale modelling due to its powerful ability to simulate local dynamics with high spatial resolution. This modelling approach lends itself well to examining the local hemodynamic impacts of different cardiovascular diseases. Lumped parameter modelling often plays a role in the personalization of these models.

In these higher order simulations, the incompressible blood flow motion within the vasculature is governed by continuity and momentum equations, known as Navier-Stokes equations [171]. There is no analytical solution to these non-linear equations for complex geometries of the cardiovascular system. Computational fluid dynamics (CFD) is a method to calculate approximate numerical solutions by solving differential equations governing the fluid motion [171]. In addition to the conventional numerical methods based on discretization of macroscopic continuum equations in CFD, such as finite volume method (FVM) or finite element method (FEM), the lattice Boltzmann method (LBM) is an alternative method based on microscopic models and mesoscopic kinetic equations which is computationally faster thanks to its efficient parallel algorithms [19, 172-174]. If the vessel walls material property effects are also considered through the fluid structure interaction (FSI) method, the fluid domain will be coupled to the solid domain by adding an additional solid solver. While traditional FSI techniques are based around Arbitrary Lagrangian-Eulerian (ALE) method, more recent methods have been introduced as an alternative such as immersed boundary method (IBM) and coupled momentum method (CMM) [173].

Although CFD is a well-established computational tool for 3D flow analysis of local regions of vasculature, it is not possible to perform 3D simulations for the entire cardiovascular system due to its high computational cost [171, 173]. Therefore, CFD is usually used for a specific region of the cardiovascular system together with inlet and outlet boundary conditions [173]. These boundary conditions (in addition to patient geometry) are one of the main aspects that shape the personalization of simulations [175]. While for many CFD simulations, average patient data or literature data are used for boundary conditions, patient-specific tuned boundary conditions are essential to achieve a reliable, accurate, robust, and stable simulation [173, 176]. Lower-order models such as LPM can provide detailed non-invasive patient-specific pressure or flow boundary conditions efficiently, without wasting high temporal and spatial refinement on regions beyond the specific region of request [171]. Such LPM boundary conditions can be coupled to 3D CFD solvers explicitly or implicitly. In the case of implicit approach, LPM and 3D CFD models are coupled by adding an additional model to numerical algorithms to solve the governing equations [176].

Figure 11 (Panel A) depicts the typical modelling pipeline starting with image processing to result analysis for 3D CFD based simulations. This workflow is based on an open-source software (Sim Vascular) [177] which was developed to provide a complete environment for personalized cardiovascular blood flow simulations. Panel B in Figure 11 outlines certain open and closed loop 0D boundary conditions that can be applied to the 3D models from within the software [177].

Recently, Khodaei et al. [178] developed a patient-specific computational fluid dynamics framework formulated around a Doppler-based patient-specific lumped-parameter algorithm that allows for the analysis of any combination of complex valvular, vascular and ventricular diseases and a 3-D strongly-coupled fluid-solid interaction (FSI) (Figure 12, Panel A) to quantify: (1) metrics of circulatory function (global hemodynamics); (2) metrics of cardiac function (global hemodynamics) as well as (3) cardiac fluid dynamics (local hemodynamics) in patients with complex valvular, ventricular an vascular diseases who undergo transcatheter aortic valve replacement (TAVR) in both pre and post intervention states (Figure 12, Panel B).

2.6 Personalization Algorithms for Lumped Parameter Models

One of the major challenges in designing 0-D models to represent the cardiovascular system or represent boundary conditions for higher order models, is accurately determining the values of each of the required elements. Many models developed to date rely on literature data, population

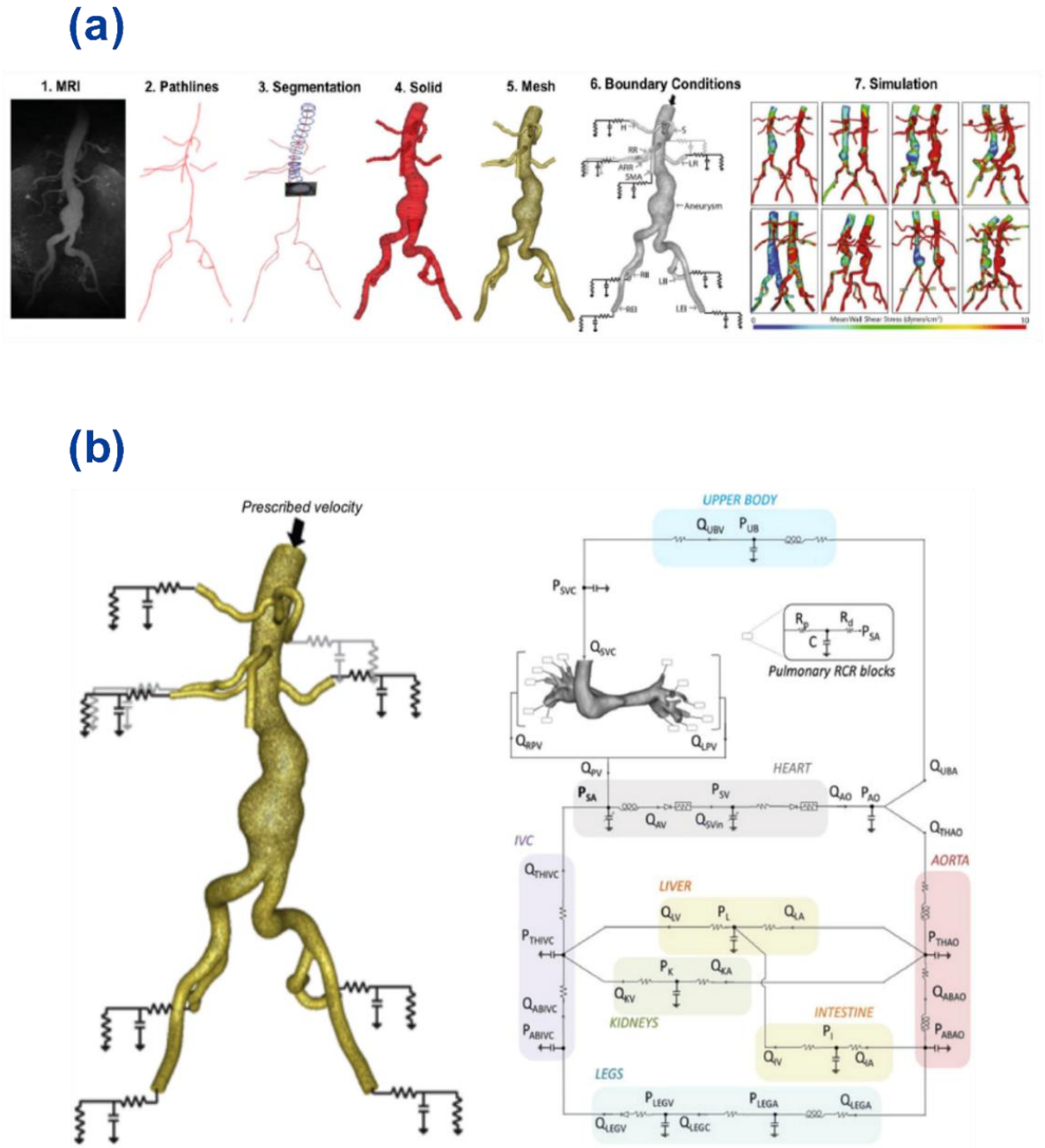

Figure 11: (a) *Typical patient-specific image-based 3D cardiovascular modelling pipeline based on the open source software Sim Vascular [177];* ***(b)*** *Open and closed loop 0D boundary conditions applied to 3D models from within the Sim Vascular software [177]*

averages and animal models in an attempt to create a generic patient model [78, 81-85]. A key limitation of relying on generic values is that they do not consider the unique characteristics of an individual. A wide variety of factors including age, sex, and lifestyle choices such as diet and exercise have been shown to influence the compliance of blood vessels for instance [51, 52, 71, 179], which are important cardiovascular model parameters. As the focus in medicine and patient care slowly shift towards patient-specific medicine, so has the field of cardiovascular simulation tools. In recent years, there has been an increased focus on the development of patient-specific models that use non-invasive measurements to tune model parameters [42-44, 65, 75, 87-89, 102, 112, 180, 181]. To accurately tune these values, a variety of methods have been employed, drawing knowledge from the areas of control systems [182] to statistical stochastic modelling [87].

Many of the developed personalized hemodynamic models lay on the intersection between forward modelling and inverse modelling [182, 183]. Broadly, these models are developed to mimic the behaviour of the cardiovascular system and then are used to derive predictions about that system. Often physiological data (in the form of blood pressure, blood flow rate, geometrical details, and other measurements) is also fed into the framework to further personalize these models. Most patient-centered cardiovascular simulation tools use a combination of these modelling approaches where a portion of the parameters are derived from physical principles while others are tuned based on patient specific data [42, 48, 102, 181, 182].

The general technique for parameter identification and estimation of lumped 0-D models is to tune model parameters so that the difference between the resulting output data and the measured patient specific data is minimized. To accomplish this, a variety of algorithms have been developed and deployed based on a series of different approaches. Additionally, sensitivity analyses and uncertainty quantification can be conducted on the identified parameters to examine their overall impact on the simulation results. One of the classical approaches to parameter identification and tuning is based on manual tuning. This approach will not be discussed as it is often time consuming

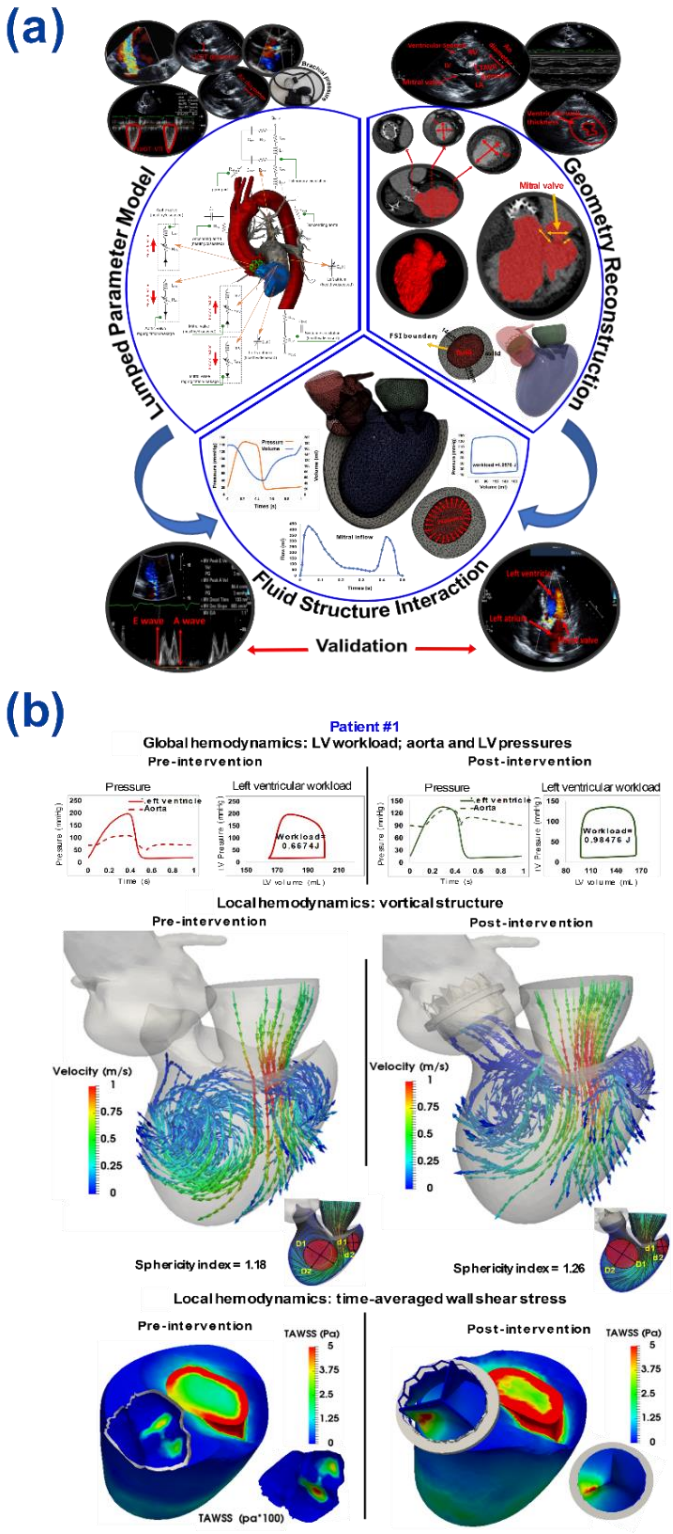

Figure 12: (a) *Illustration of a patient-specific lumped parameter modelling and fluid solid interaction modelling developed by Khodaei et al. [178];* ***(b)*** *Changes in local and global hemodynamics in a sample patient between baseline and 90-day post-TAVR by Khodaei et al. [178]*

and prone to inconsistencies [87-89]. Instead, this section will be focusing on more advanced tuning algorithms.

In recent work, Huang and Ying [86] develop an on-line parameter identification framework for a patient specific 5-element 0-D arterial model. The process involved applying a genetic and iterative optimization algorithm to minimize the squared error between the predicted state space model output and the cardiovascular model output by adjusting the values of the circuit elements. Figure 13 (Panel A) outlines the general process flow in addition to the simulated and predicted aortic pressure. Similarly, Casas et al. [65] combined a series of approaches including non-linear optimization based on the Levenberg-Marquardt algorithm [184] to minimize the error between the measured 4D flow MRI waveforms and the predicted model flow waveforms (Figure 13 Panel C). Zhang et al. [181] also used the same Levenberg-Marquardt algorithm to personalize a 1D/0D model of the major cardiovascular vessels using only non-invasive ultrasound and brachial blood pressure measurements from 62 volunteers. Figure 13 (Panel B) illustrates the general patient specific data collection and blood pressure tuning approach. Others including Spilker et al. [185], Ismail et al. [186] and Itu et al. [102] have also employed similar strategies for parameter identification. Figure 13 (Panel D) outlines an approach used by Itu et al. [102] in which a model is initially reduced to an LPM to obtain initial solutions for the parameters (described as a “warm start” to the optimization algorithm). This improves the initial guess for the boundary condition element values used in the model algorithm and reduces the number of iterations required. For more details regarding different optimization methods, readers are referred to a review by Marsden [175] which examines optimization in cardiovascular modelling.

Another method is based around the implementation of Kalman filters to determine optimal model parameters. Arthurs and colleagues [89] for instance, proposed a computational framework which utilizes a Reduced Order Unscented Kalman Filter (ROUKF) or a constrained least squares version (ROUKF-CLS), depending on the model complexity, in conjunction with non-invasive patient data to estimate 0-D model parameters. These low-order models were used as boundary conditions in a 3D FSI patient specific hemodynamic simulation. Likewise, Pant et al. [180] applied an unscented Kalman filter (UKF) paired with clinical measurements to estimate model parameters and developed a set of sensitivity analysis tools to examine possible identifiability problems. The scheme was then applied to a patient specific aortic coarctation simulation. Huang et al. [187] also

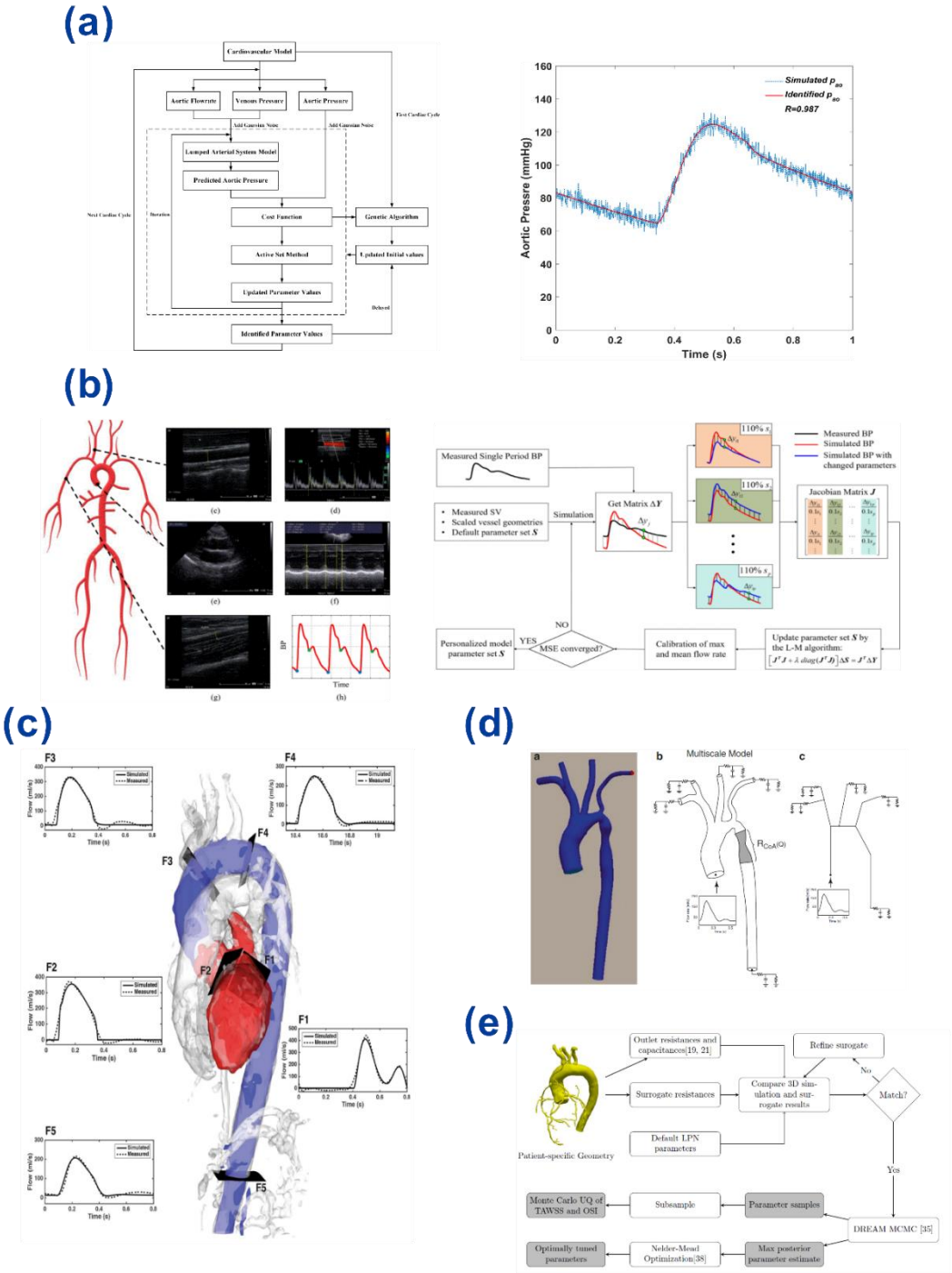

Figure 13: ***(a)*** *Illustration of the on-line parameter estimation algorithm developed by Huang and Ying [86] as well as the simulated and identified aortic pressure based on the proposed framework;* ***(b)*** *Patient specific non-invasive data acquisition process and blood pressure tuning algorithm used in personalized hemodynamic model by Zhang et al. [181];* ***(c)*** *Simulated and measured flow waveforms at five locations in the heart and aorta post parameter optimization from work by Casas et al. [65];* ***(d)*** *Outline of the transformation from patient specific aorta geometry with coarctation to multiscale model to LPM, which is used in the warm start portion of the optimization algorithm developed by Itu et al. [102];* ***(e)*** *The workflow for the automated parameter tuning and uncertainty quantification framework developed by Tran et al. [87]*

used an Iterated Unscented Kalman Filter (IUKF) algorithm to identify optimal model parameters and element layout for a 4-element systemic arterial system used in mock circulatory loops to test left ventricular assist devices.

One of the difficulties faced in this process is accurately accounting for the uncertainty that arises from the acquisition of patient specific clinical data and understanding how this may impact the estimation process and ultimately the model results. A proposed method to deal with these uncertainties was recently developed by Tran et al. [87] in which an automatic parameter tuning framework that quantified the estimation uncertainty and indicated the resulting confidence in the predicted hemodynamic results was designed. The approach paired Bayesian estimation with parameter computation as well as a Monte Carlo method to propagate the calculated uncertainties into a coronary artery model. Figure 13 (Panel E) outlines the general workflow of the proposed framework. A similar algorithm was also proposed by Schiavazzi et al. [88] which focused on single-ventricle simulation.

2.7 Conclusions and Future Directions

The future of personalized cardiovascular simulations appears to be promising. Continued advances in computational capabilities, together with the exponential growth of digital cardiology data, is driving simulation tools closer to successful integration into clinical workflows. Within these computational frameworks, lumped parameter modelling is playing a crucial role in the personalization of both stand alone 0D models and models used to examine global and local hemodynamics and the impacts of cardiovascular diseases. These tools are being used to predict and manage diseases, plan interventions, quantify the outcomes and study disease mechanisms through a novel lens.

To truly appreciate the progress made in the field of mathematical and computational hemodynamics over the last 20 years, we refer readers to *Modeling the Cardiovascular System—A Mathematical Adventure: Part I & II* [188, 189] where author Alfio Quarteroni discusses the possibilities and challenges that lay ahead in this area of research in early 2001. In Part II [189], Quarteroni acknowledges that “the mathematical adventure of developing models for the numerical simulation of the cardiovascular system of a real patient is in the very early stages. Its evolution will require the tackling of several central issues in applied mathematics and numerical modeling”. It is incredible to observe the considerable advances made over the last 2 decades and

makes one ponder about the computational cardiology tools that may be available 20 years from now.

With the exciting advances in artificial intelligence (AI) being applied to cardiology, this marks one of the next chapters for cardiovascular simulation tools. The integration of these advanced methods has the potential to render LPM and frameworks even more personalized, reduce the needed computation time and provide clinicians and scientists with previously inaccessible data and trends [190-194].

Moving forward, one of the major challenges in cardiovascular modelling, spanning not only hemodynamics but also electrophysiological modelling is long term patient specific predictions. The vast majority of current models are capable of predicting outcomes in the short term, such as directly following interventions, but as is the case with most predictive models, the further into the future predictions are estimated, the more uncertainty there is. The eventual integration of complex factors such as tissue remodeling and growth into cardiovascular models for example, will help improve the long-term accuracy of these simulations [9, 195, 196].

In order for these modelling tools to become part of a clinical routine, it is paramount that the results obtained from the computational frameworks can be presented in a simple yet informative manner. As Niederer and colleagues [9] point out in a recent publication, the model development requires a deep knowledge of a variety of fields such as numerical analysis, computer science and mechanics. For the technology to translate into a clinical setting, the results and inferences must be user-friendly for cardiologists and medical experts [9, 197].

This will become increasingly important as the cardiovascular models become more complex and AI algorithms are integrated. Simple conclusion driven results are needed while allowing the operators to understand how the algorithm determined its predictions. In the field of AI, there has been a focus on developing algorithms that can explain how they arrive at their conclusions (explainable artificial intelligence), with the goal of increasing trust and clarity in the process [198, 199]. This same principle needs to be applied to cardiovascular modelling frameworks to help clinicians develop trust in the models and not view them simply as a black box.

Another key front that needs to be further examined is the value added from these modelling technologies. An interesting consideration is discussed by Fernando DiCarli and colleagues [10]

where they note that in recent years, there has been a dramatic growth in multimodal cardiovascular imaging technologies which are leading to extraordinary progress in the areas of disease diagnosis, risk assessment and disease management. The substantial cost increase associated with this growth in imaging though, has prompted discussions regarding the impact of the technologies on the patient specific decision making process and if they are indeed better than the current alternatives. Further comparative effectiveness studies need to be conducted to examine how the imaging technologies are impacting clinical factors such as improved patient quality of life and long-term outcomes [10].

This same argument can be made for cardiovascular simulation tools which will also require further larger scale clinical studies to truly evaluate the benefits and value added in comparison with traditional techniques and tools [131, 200]. In certain cases for example, simpler solutions, such as a fully lumped parameter model may be sufficient as opposed to a 3-D CFD model due to the lower computational cost and ease of automation [8, 79].

Regardless, these are all obstacles that can be overcome through continued collaboration between researchers, engineers, clinicians, and computer scientists. As these computational tools continue to advance, it appears they will play a substantial role in the field of patient specific cardiovascular care and may be one of the many channels to help combat the global burden of cardiovascular disease.

Acknowledgments

This work was supported by NSERC Discovery Grant (RGPIN-2017-05349) and NSERC CRD Grant (CRDPJ 537352 – 18). NSERC (https://www.nserc-crsng.gc.ca/index_eng.asp) as the funders had no role in study design, data collection and analysis, decision to publish, or preparation of the manuscript.

Competing interests

The authors declare that they have no competing interests.

2.8 References

1. Virani, S. S. et al (2020) Heart Disease and Stroke Statistics—2020 Update: A Report From the American Heart Association. Circulation 141:e139-e596
2. World Health Organization (2017) Cardiovascular diseases (CVDs). https://www.who.int/news-room/fact-sheets/detail/cardiovascular-diseases-(cvds)
3. Public Health Agency of Canada (2009) Tracking Heart Disease and Stroke in Canada
4. American Heart Association (2017) Cardiovascular Disease: A Costly Burden for America, Projections Through 2035
5. Wilkins, E. et al (2017) European Cardiovascular Disease Statistics 2017 edition
6. Trayanova, N. A. (2011) Whole-Heart Modeling: Applications to Cardiac Electrophysiology and Electromechanics. Circ Res 108:113–128
7. Gray, R. A. & Pathmanathan, P. (2018) Patient-Specific Cardiovascular Computational Modeling: Diversity of Personalization and Challenges. J Cardiovasc Transl Res 11:80–88
8. Niederer, S. A. & Smith, N. P. (2016) Using physiologically based models for clinical translation: predictive modelling, data interpretation or something in-between? J Physiol 594:6849–6863
9. Niederer, S. A., Lumens, J. & Trayanova, N. A. (2019) Computational models in cardiology. Nat Rev Cardiol 16:100–111
10. Carli, M. F. D., Geva, T. & Davidoff, R. (2016) The Future of Cardiovascular Imaging. Circulation 133:2640–2661
11. Bassingthwaighte, J., Hunter, P. & Noble, D. (2009) The Cardiac Physiome: perspectives for the future. Exp Physiol 94:597–605
12. Corral-Acero, J. et al (2020) The 'Digital Twin' to enable the vision of precision cardiology. Eur Heart J 41:4556–4564
13. Kayvanpour, E. et al (2015) Towards Personalized Cardiology: Multi-Scale Modeling of the Failing Heart. PLOS ONE 10:e0134869
14. Richter, Y. & Edelman, E. R. (2006) Cardiology Is Flow. Circulation 113:2679–2682
15. Ben-Assa, E. et al (2019) Ventricular stroke work and vascular impedance refine the characterization of patients with aortic stenosis. Sci. Transl. Med. 11:eaaw0181
16. Keshavarz-Motamed, Z. et al (2016) Elimination of Transcoarctation Pressure Gradients Has No Impact on Left Ventricular Function or Aortic Shear Stress After Intervention in Patients With Mild Coarctation. JACC Cardiovasc Interv 9:1953–1965
17. Taylor, C. A. & Steinman, D. A. (2010) Image-Based Modeling of Blood Flow and Vessel Wall Dynamics: Applications, Methods and Future Directions. Ann Biomed Eng 38:1188–1203
18. Keshavarz-Motamed, Z. et al (2020) Mixed Valvular Disease Following Transcatheter Aortic Valve Replacement: Quantification and Systematic Differentiation Using Clinical Measurements and Image-Based Patient-Specific In Silico Modeling. J Am Heart Assoc 9: e015063
19. Sadeghi, R., Khodaei, S., Ganame, J. & Keshavarz-Motamed, Z. (2020) Towards non-invasive computational-mechanics and imaging-based diagnostic framework for personalized cardiology for coarctation. Sci Rep 10:9048
20. Dweck, M. R., Boon, N. A. & Newby, D. E. (2012) Calcific Aortic Stenosis. J Am Coll Cardiol 60:1854–1863

21. Antonini-Canterin, F. et al (2013) The ventricular-arterial coupling: From basic pathophysiology to clinical application in the echocardiography laboratory. J Cardiovasc Echography 23:91-95
22. Borlaug, B. A. & Kass, D. A. (2008) Ventricular–Vascular Interaction in Heart Failure. Heart Fail Clin 4:23–36
23. Yin, F. (1987) Ventricular/Vascular Coupling: Clinical, Physiological, and Engineering Aspects. Springer-Verlag, New York
24. Ikonomidis, I. et al (2019) The role of ventricular–arterial coupling in cardiac disease and heart failure: assessment, clinical implications and therapeutic interventions. A consensus document of the European Society of Cardiology Working Group on Aorta & Peripheral Vascular Diseases, European Association of Cardiovascular Imaging, and Heart Failure Association. Eur J Heart Fail 21:402–424
25. Seemann, F. et al (2019) Noninvasive Quantification of Pressure-Volume Loops From Brachial Pressure and Cardiovascular Magnetic Resonance. Circ Cardiovasc Imaging 12: e008493
26. Burkhoff, D., Mirsky, I. & Suga, H. (2005) Assessment of systolic and diastolic ventricular properties via pressure-volume analysis: a guide for clinical, translational, and basic researchers. Am J Physiol Heart Circ Physiol 289, H501–H512
27. Ky, B. et al (2013) Ventricular-Arterial Coupling, Remodeling, and Prognosis in Chronic Heart Failure J Am Coll Cardiol 62:1165–1172
28. Keshavarz-Motamed, Z. et al (2014) Non-Invasive Determination of Left Ventricular Workload in Patients with Aortic Stenosis Using Magnetic Resonance Imaging and Doppler Echocardiography. PLoS ONE 9:e86793
29. Elkins, C. J. & Alley, M. T. (2007) Magnetic resonance velocimetry: applications of magnetic resonance imaging in the measurement of fluid motion. Exp Fluids 43:823–858
30. Kilner, P. J., Gatehouse, P. D. & Firmin, D. N. (2007) Flow Measurement by Magnetic Resonance: A Unique Asset Worth Optimising. J Cardiovasc Magn Reson 9:723–728
31. Villarraga-Gómez, H., Lee, C. & Smith, S. T. (2018) Dimensional metrology with X-ray CT: A comparison with CMM measurements on internal features and compliant structures. Precis Eng 51:291–307
32. Watson, S. R., Dormer, J. D. & Fei, B. (2018) Imaging technologies for cardiac fiber and heart failure: a review. Heart Fail Rev 23:273–289
33. Rehman, R., Yelamanchili, V. S. & Makaryus, A. N. (2020) Cardiac Imaging. In: StatPearls [Internet]. StatPearls Publishing, Treasure Island
34. Maleki, M. & Esmaeilzadeh, M. (2012) The Evolutionary Development of Echocardiography. Iran J Med Sci 37:222–232
35. Fleischmann, D., Liang, D. H. & Herfkens, R. J. (2008) Technical Advances in Cardiovascular Imaging. Semin Thorac Cardiovasc Surg 20:333–339
36. Burgstahler, C. & Schroeder, S. (2007) Magnetic resonance imaging versus computed tomography for the detection of coronary stenosis: do we really have to focus on ‘stenoses’? Heart 93:1322–1324
37. Edwards, A. D. & Arthurs, O. J. (2011) Paediatric MRI under sedation: is it necessary? What is the evidence for the alternatives? Pediat Radiol 41:1353–1364
38. Pearce, M. S. et al (2012) Radiation exposure from CT scans in childhood and subsequent risk of leukaemia and brain tumours: a retrospective cohort study. The Lancet 380:499–505

39. Rigsby, C. K. et al (2018) Radiation dose management for pediatric cardiac computed tomography: a report from the Image Gently 'Have-A-Heart' campaign. Pediatr Radiol 48:5–20
40. Power, S. P. et al (2016) Computed tomography and patient risk: Facts, perceptions and uncertainties. World J Radiol 8, 902-915
41. Omran, H. et al (2003) Silent and apparent cerebral embolism after retrograde catheterisation of the aortic valve in valvular stenosis: a prospective, randomised study. The Lancet 361:1241–1246
42. Keshavarz-Motamed, Z. (2020) A diagnostic, monitoring, and predictive tool for patients with complex valvular, vascular and ventricular diseases. Sci Rep 10:6905
43. Mao, B. et al (2019) Lumped parameter model based surgical planning for CABG. Med Nov Technol Devices 2:100014
44. Kim, H. J. et al (2010) Patient-Specific Modeling of Blood Flow and Pressure in Human Coronary Arteries. Ann Biomed Eng 38:3195–3209
45. Tanné, D., Kadem, L., Rieu, R. & Pibarot, P. (2008) Hemodynamic impact of mitral prosthesis-patient mismatch on pulmonary hypertension: an in silico study. J Appl Physiol 295:1916–1926
46. Keshavarz-Motamed, Z., Edelman, E. R., Garcia, J., Dahdah, N. & Kadem, L. (2015) The role of aortic compliance in determination of coarctation severity: lumped parameter modeling, in vitro study and clinical evaluation. J Biomech 48:4229–4237
47. Abdi, M., Karimi, A., Navidbakhsh, M., Jahromi, G. P. & Hassani, K. (2014) A lumped parameter mathematical model to analyze the effects of tachycardia and bradycardia on the cardiovascular system. Int J Numer Model 28:346–357
48. Vassilevski, Y., Olshanskii, M., Simakov, S., Kolobov, A. & Danilov, A. (2020) Personalized Computational Hemodynamics. Academic Press, Cambridge
49. Ottesen, J. T., Olufsen, M. S. & Larsen, J. K. (2004) Applied Mathematical Models in Human Physiology. Society for Industrial and Applied Mathematics
50. Li, J. K.-J. (2000) The Arterial Circulation - Physical Principles and Clinical Applications. Humana Press Inc., New York
51. Westerhof, N., Lankhaar, J-W. & Westerhof, B. E. (2009) The arterial Windkessel. Med Biol Eng Comput 47:131–141
52. Zhou, S. et al (2019) A review on low-dimensional physics-based models of systemic arteries: application to estimation of central aortic pressure. Biomed Eng OnLine 18:41
53. Westerhof, N., Bosman, F., De Vries, C. J. & Noordergraaf, A. (1969) Analog studies of the human systemic arterial tree. J Biomech 2:121–143
54. Stergiopulos, N., Westerhof, B. E. & Westerhof, N. (1999) Total arterial inertance as the fourth element of the windkessel model. Am J Physiol 276:H81–H88
55. Deswysen, B., Charlier, A. A. & Gevers, M. (1980) Quantitative evaluation of the systemic arterial bed by parameter estimation of a simple model. Med Biol Eng Comput 18:153–166
56. Goldwyn, R. M. & Watt, T. B. (1967) Arterial Pressure Pulse Contour Analysis Via a Mathematical Model for the Clinical Quantifcation of Human Vascular Properties. IEEE Trans Biomed Eng BME 14:11–17
57. Rose, W. C. & Shoukas, A. A. (1993) Two-port analysis of systemic venous and arterial impedances. Am J Physiol 265:H1577–H1587
58. Frasch, H. F., Kresh, J. Y. & Noordergraaf, A. (1996) Two-port analysis of microcirculation: an extension of windkessel. Am J Physiol 270:H376–H385

59. Nestler, F. et al (2014) A Hybrid Mock Circulation Loop for a Total Artificial Heart: Hybrid Mock Circulation Loop. Artif Organs 38:775–782
60. Kim, E. & Capoccia, M. (2019) Synergistic Model of Cardiac Function with a Heart Assist Device. Bioengineering 7:1
61. Molfetta, A. D. et al (2017) Application of a Lumped Parameter Model to Study the Feasibility of Simultaneous Implantation of a Continuous Flow Ventricular Assist Device (VAD) and a Pulsatile Flow VAD in BIVAD Patients. Artif Organs 41:242–252
62. Benevento, E., Djebbari, A., Keshavarz-Motamed, Z., Cecere, R. & Kadem, L. (2015) Hemodynamic Changes following Aortic Valve Bypass: A Mathematical Approach. PLOS ONE 10:e0123000
63. Kresh, J. Y., Brockman, S. K. & Noordergraaf, A. (1990) Theoretical and experimental analysis of right ventricular bypass and univentricular circulatory support. IEEE Trans Biomed Eng 37:121–127
64. Migliavacca, F. et al (2001) Modeling of the Norwood circulation: effects of shunt size, vascular resistances, and heart rate. Am J Physiol Heart Circ Physiol 280:H2076–H2086
65. Casas, B. et al (2017) Bridging the gap between measurements and modelling: a cardiovascular functional avatar. Sci Rep 7:6214
66. Duanmu, Z., Yin, M., Fan, X., Yang, X. & Luo, X. (2018) A patient-specific lumped-parameter model of coronary circulation. Sci Rep 8:874
67. Arthurs, C. J. et al (2017) Reproducing Patient-Specific Hemodynamics in the Blalock–Taussig Circulation Using a Flexible Multi-Domain Simulation Framework: Applications for Optimal Shunt Design. Front Pediatr 5:78
68. Vieira, M. S., Arthurs, C. J., Hussain, T., Razavi, R. & Figueroa, C. A. (2018) Patient-specific modeling of right coronary circulation vulnerability post-liver transplant in Alagille's syndrome. PLOS ONE 13:e0205829
69. Shavik, S. M., Tossas-Betancourt, C., Figueroa, C. A., Baek, S. & Lee, L. C. (2020) Multiscale Modeling Framework of Ventricular-Arterial Bi-directional Interactions in the Cardiopulmonary Circulation. Front Physiol 11:1–13
70. Sengupta, D. et al (2012) Image-based modeling of hemodynamics in coronary artery aneurysms caused by Kawasaki disease. Biomech Model Mechanobiol 11:915–932
71. Marone, A. et al (2019) Modeling of the hemodynamics in the feet of patients with peripheral artery disease. Biomed Opt Express 10:657–669
72. Keshavarz-Motamed, Z., Garcia, J., Pibarot, P., Larose, E. & Kadem, L. (2011) Modeling the impact of concomitant aortic stenosis and coarctation of the aorta on left ventricular workload. J Biomech 44:2817–2825
73. Saitta, S. et al (2019) Evaluation of 4D flow MRI-based non-invasive pressure assessment in aortic coarctations. J Biomech 94:13–21
74. van Bakel, T. M. J. et al (2019) Cardiac remodelling following thoracic endovascular aortic repair for descending aortic aneurysms. Eur J Cardiothorac Surg 55:1061–1070
75. Li, B., Wang, W., Mao, B. & Liu, Y. (2019) A Method to Personalize the Lumped Parameter Model of Coronary Artery. Int J Comput Methods 16:1842004
76. Itu, L. et al (2012) A patient-specific reduced-order model for coronary circulation. 2012 9th IEEE International Symposium on Biomedical Imaging:832–835
77. Shi, Y., Lawford, P. & Hose, R. (2011) Review of Zero-D and 1-D Models of Blood Flow in the Cardiovascular System. Biomed Eng OnLine 10:33

78. Jung, E.-O. & Lee, W-H. (2006) Lumped parameter models of cardiovascular circulation in normal and arrhythmia cases. J Korean Math Soc 43:885–897
79. Holmes, J. W. & Lumens, J. (2018) Clinical Applications of Patient-Specific Models: The Case for a Simple Approach. J Cardiovasc Transl Res 11:71–79
80. Mirramezani, M. & Shadden, S. C. (2020) A Distributed Lumped Parameter Model of Blood Flow. Ann Biomed Eng 48:2870-2886
81. de Canete, J. F. (2013) Object-oriented modeling and simulation of the closed loop cardiovascular system by using SIMSCAPE. Comput Biol Med 43:323-333
82. Hassani, K., Navidbakhsh, M. & Rostami, M. (2006) Simulation of the cardiovascular system using equivalent electronic system. Biomed Pap 150:105–112
83. Vennin, S. et al (2017) Identifying Hemodynamic Determinants of Pulse Pressure: A Combined Numerical and Physiological Approach. Hypertension 70:1176–1182
84. Pietrabissa, R., Mantero, S., Marotta, T. & Menicanti, L. (1996) A lumped parameter model to evaluate the fluid dynamics of different coronary bypasses. Med Eng Phys 18:477–484
85. Mynard, J. P., Penny, D. J. & Smolich, J. J. (2014) Scalability and in vivo validation of a multiscale numerical model of the left coronary circulation. Am J Physiol Heart Circ Physiol 306:H517–H528
86. Huang, F. & Ying, S. (2020) On-line parameter identification of the lumped arterial system model: A simulation study. PLOS ONE 15:e0236012
87. Tran, J. S., Schiavazzi, D. E., Ramachandra, A. B., Kahn, A. M. & Marsden, A. L. (2017) Automated tuning for parameter identification and uncertainty quantification in multi-scale coronary simulations. Comput Fluids 142:128–138
88. Schiavazzi, D. E., Baretta, A., Pennati, G., Hsia, T.-Y. & Marsden, A. L. (2017) Patient-specific parameter estimation in single-ventricle lumped circulation models under uncertainty. Int J Numer Method Biomed Eng 33:1–59
89. Arthurs, C. J. et al (2020) A flexible framework for sequential estimation of model parameters in computational hemodynamics. Adv Model Simul Eng Sci 7:48
90. Parker, K. H. & Jones, C. J. H. (1990) Forward and Backward Running Waves in the Arteries: Analysis Using the Method of Characteristics. J Biomech Eng 112:322–326
91. Sherwin, S. J., Formaggia, L., Peiró, J. & Franke, V. (2003) Computational modelling of 1D blood flow with variable mechanical properties and its application to the simulation of wave propagation in the human arterial system. Int J Numer Methods Fluids 43:673–700
92. Wan, J. et al (2002) A One-dimensional Finite Element Method for Simulation-based Medical Planning for Cardiovascular Disease. Comput Methods Biomech Biomed Engin 5: 195–206
93. Taylor, C. A. et al (1999) Predictive Medicine: Computational Techniques in Therapeutic Decision-Making. Comput Aided Surg 4:231–247
94. Xie, X., Zheng, M., Wen, D., Li, Y. & Xie, S. (2018) A new CFD based non-invasive method for functional diagnosis of coronary stenosis. Biomed Eng OnLine 17:36
95. Mirramezani, M., Diamond, S. L., Litt, H. I. & Shadden, S. C. (2019) Reduced Order Models for Transstenotic Pressure Drop in the Coronary Arteries. J Biomech Eng 141:031005
96. American Heart Association (2017) What is Cardiovascular Disease? https://www.heart.org/en/health-topics/consumer-healthcare/what-is-cardiovascular-disease
97. Zipes, D. P. et al (2019) Braunwald's Heart Disease: A Textbook of Cardiovascular Medicine Eleventh Edition. Elsevier, Philadelphia

98. Klabunde, R. E. (2012) Cardiovascular Physiology Concepts Second Edition. Lippincott Williams & Wilkins, Baltimore
99. Pijls, N. H. J. et al (1996) Measurement of Fractional Flow Reserve to Assess the Functional Severity of Coronary-Artery Stenoses. N Engl J Med 334:1703–1708
100. Taylor, C. A., Fonte, T. A. & Min, J. K. (2013) Computational Fluid Dynamics Applied to Cardiac Computed Tomography for Noninvasive Quantification of Fractional Flow Reserve. J Am Coll Cardiol 61:2233–2241
101. Ricotta, J. J. et al (2008) Cardiovascular disease management: The need for better diagnostics. Med Biol Eng Comput 46:1059–1068
102. Itu, L. M., Sharma, P. & Suciu, C. (2017) Patient-specific Hemodynamic Computations: Application to Personalized Diagnosis of Cardiovascular Pathologies. Springer International Publishing, Cham
103. Lamata, P. et al (2014) Images as drivers of progress in cardiac computational modelling. Prog Biophys Mol Biol 115:198–212
104. Tang, H. et al (2020) Lumped-Parameter Circuit Platform for Simulating Typical Cases of Pulmonary Hypertensions from Point of Hemodynamics. J Cardiovasc Transl Res 13:826–852
105. Warriner, D. R. et al (2014) Closing the Loop: Modelling of Heart Failure Progression from Health to End-Stage Using a Meta-Analysis of Left Ventricular Pressure-Volume Loops. PLoS ONE 9:e114153
106. Garcia, D. et al (2009) Impairment of coronary flow reserve in aortic stenosis. J Appl Physiol 106:113–121
107. Pant, S. et al (2018) A Lumped Parameter Model to Study Atrioventricular Valve Regurgitation in Stage 1 and Changes Across Stage 2 Surgery in Single Ventricle Patients. IEEE Trans Biomed Eng 65:2450–2458
108. Quarteroni, A., Manzoni, A. & Vergara, C. (2017) The cardiovascular system: Mathematical modelling, numerical algorithms and clinical applications. Acta Numer 26:365–590
109. Frolov, S. V. et al (2017) A Lumped Parameter Model of Cardiovascular System with Pulsating Heart for Diagnostic Studies. J Mech Med Biol 17:1750056
110. Sankaran, S. et al (2012) Patient-Specific Multiscale Modeling of Blood Flow for Coronary Artery Bypass Graft Surgery. Ann Biomed Eng 40:2228–2242
111. Ryu, J., Hu, X. & Shadden, S. C. (2015) A Coupled Lumped-Parameter and Distributed Network Model for Cerebral Pulse-Wave Hemodynamics. J Biomech Eng 137:101009
112. Itu, L. et al (2014) Model based non-invasive estimation of PV loop from echocardiography. 2014 36th Annual International Conference of the IEEE Engineering in Medicine and Biology Society:6774–6777
113. Zhu, S., Luo, L., Yang, B., Li, X. & Wang, X. (2017) Improving hemodynamics of cardiovascular system under a novel intraventricular assist device support via modeling and simulations. Comput Assist Surg 22:221–231
114. Casas, B. et al (2018) Non-invasive Assessment of Systolic and Diastolic Cardiac Function During Rest and Stress Conditions Using an Integrated Image-Modeling Approach. Front Physiol 9:1515
115. Broomé, M., Maksuti, E., Bjällmark, A., Frenckner, B. & Janerot-Sjöberg, B. (2013) Closed-loop real-time simulation model of hemodynamics and oxygen transport in the cardiovascular system. Biomed Eng OnLine 12:69

116. Mynard, J. P., Davidson, M. R., Penny, D. J. & Smolich, J. J. (2012) A simple, versatile valve model for use in lumped parameter and one-dimensional cardiovascular models. Int J Numer Methods Biomed Eng 28:626–641
117. Suga, H., Sagawa, K. & Shoukas, A. A. (1973) Load Independence of the Instantaneous Pressure-Volume Ratio of the Canine Left Ventricle and Effects of Epinephrine and Heart Rate on the Ratio. Circ Res 32:314–322
118. Segers, P. et al (2003) Systemic and pulmonary hemodynamics assessed with a lumped-parameter heart-arterial interaction model. J Eng Math 47:185–199
119. Senzaki Hideaki, Chen Chen-Huan, & Kass David A. (1996) Single-Beat Estimation of End-Systolic Pressure-Volume Relation in Humans. Circulation 94:2497–2506
120. Stergiopulos, N., Meister, J. J. & Westerhof, N. (1996) Determinants of stroke volume and systolic and diastolic aortic pressure. Am J Physiol Heart Circ Physiol 270:H2050–H2059
121. Moss, R. L., Razumova, M. & Fitzsimons, D. P. (2004) Myosin Crossbridge Activation of Cardiac Thin Filaments: Implications for Myocardial Function in Health and Disease. Circ Res 94:1290–1300
122. Gleason, W. L. & Braunwald, E. (1962) Studies on the first derivative of the ventricular pressure pulse in man. J Clin Invest 41:80–91
123. Dell'Italia, L. J. & Walsh, R. A. (1988) Application of a time varying elastance model to right ventricular performance in man. Cardiovasc Res 22:864–874
124. Shimizu, S. et al (2018) Lumped parameter model for hemodynamic simulation of congenital heart diseases. J Physiol Sci 68:103–111
125. Pironet, A. et al (2013) Simulation of Left Atrial Function Using a Multi-Scale Model of the Cardiovascular System. PLoS ONE 8e65146
126. Heldt, T., Shim, E. B., Kamm, R. D. & Mark, R. G. (2002) Computational modeling of cardiovascular response to orthostatic stress. J Appl Physiol 92:1239–1254
127. Burkhoff, D., de Tombe, P. P., Hunter, W. C. & Kass, D. A. Contractile strength and mechanical efficiency of left ventricle are enhanced by physiological afterload. Am. J. Physiol.-Heart Circ. Physiol. 260, H569–H578 (1991).
128. Claessens, T. E. et al (2006) Nonlinear isochrones in murine left ventricular pressure-volume loops: how well does the time-varying elastance concept hold? Am J Physiol Heart Circ Physiol 290:H1474–H1483
129. Pironet, A. et al (2013) A multi-scale cardiovascular system model can account for the load-dependence of the end-systolic pressure-volume relationship. Biomed Eng OnLine 12:8
130. Borlaug, B. A. & Kass, D. A. (2009) Invasive Hemodynamic Assessment in Heart Failure. Heart Fail Clin 5:217–228
131. Capoccia, M., Marconi, S., Singh, S. A., Pisanelli, D. M. & De Lazzari, C. (2018) Simulation as a preoperative planning approach in advanced heart failure patients. A retrospective clinical analysis. Biomed Eng OnLine 17:52
132. Bellhouse, B. J. (1972) The Fluid Mechanics of Heart Valves. In: Cardiovascular Fluid Dynamics. Elsevier, Philadelphia, pp 261–285
133. Garcia, D., Pibarot, P. & Durand, L.-G. (2005) Analytical modeling of the instantaneous pressure gradient across the aortic valve. J Biomech 38:1303–1311
134. Baumgartner, H., Stefenelli, T., Niederberger, J., Schima, H. & Maurer, G. (1999) "Overestimation" of Catheter Gradients by Doppler Ultrasound in Patients With Aortic Stenosis: A Predictable Manifestation of Pressure Recovery. J Am Coll Cardiol 33:1655–1661

135. Korakianitis, T. & Shi, Y. (2006) Numerical simulation of cardiovascular dynamics with healthy and diseased heart valves. J Biomech 39:1964–1982
136. Shi, Y., Yeo, T. J. H. & Zhao, Y. (2004) Numerical Simulation of a Systemic Flow Test Rig. ASAIO J 50:54–64
137. Werner, J., Bohringer, D. & Hexamer, M. (2002) Simulation and prediction of cardiotherapeutical phenomena from a pulsatile model coupled to the Guyton circulatory model. IEEE Trans Biomed Eng 49:430–439
138. Korakianitis, T. & Shi, Y. (2006) A concentrated parameter model for the human cardiovascular system including heart valve dynamics and atrioventricular interaction. Med Eng Phys 28:613–628
139. Pennati, G., Migliavacca, F., Dubini, G., Pietrabissa, R. & de Leval, M. R. (1997) A mathematical model of circulation in the presence of the bidirectional cavopulmonary anastomosis in children with a univentricular heart. Med Eng Phys 19:223–234
140. Sun, Y., Sjoberg, B. J., Ask, P., Loyd, D. & Wranne, B. (1995) Mathematical model that characterizes transmitral and pulmonary venous flow velocity patterns. Am J Physiol Heart Circ Physiol 268:H476–H489
141. Trenhago, P. R., Fernandes, L. G., Müller, L. O., Blanco, P. J. & Feijóo, R. A. (2016) An integrated mathematical model of the cardiovascular and respiratory systems. Int J Numer Methods Biomed Eng 32:e02736
142. Simakov, S. S. (2019) Lumped parameter heart model with valve dynamics. Russ J Numer Anal Math Model 34:289–300
143. Maganti, K., Rigolin, V. H., Sarano, M. E. & Bonow, R. O. (2010) Valvular Heart Disease: Diagnosis and Management. Mayo Clin Pro. 85:483–500
144. Waite, L., Fine, J., Veres, G. & Szabó, G. (2009) A Lumped-Parameter Model of Mitral Valve Blood Flow for Assessment of Diastolic Left Ventricular Filling. IFMBE Proc 25:1984–1985
145. Garcia, D. et al (2005) A ventricular-vascular coupling model in presence of aortic stenosis. Am J Physiol Heart Circ Physiol 288:H1874–H1884
146. Fiore, G. B. et al (2002) Hydraulic functional characterisation of aortic mechanical heart valve prostheses through lumped-parameter modelling. J Biomech 35:1427–1432
147. Scarsoglio, S., Camporeale, C., Guala, A. & Ridolfi, L. (2015) Fluid dynamics of heart valves during atrial fibrillation: a lumped parameter-based approach. Comput Methods Biomech Biomed Engin 19:1060–1068
148. Pappano, A. J. & Gil Wier, W. (2019) Cardiovascular Physiology, 11th Edition. Elsevier, Philadelphia
149. Ojha, M. (1994) Wall shear stress temporal gradient and anastomotic intimal hyperplasia. Circ Res 74:1227–1231
150. Zarins, C. K. & Ku, D. N. (1987) Shear stress regulation of artery lumen diameter in experimental atherogenesis. J Vasc Surg 5:413–420
151. Yushkevich, P. A. et al (2006) User-guided 3D active contour segmentation of anatomical structures: Significantly improved efficiency and reliability. NeuroImage 31:1116–1128
152. Kikinis, R., Pieper, S. D. & Vosburgh, K. G. (2014) 3D Slicer: A Platform for Subject-Specific Image Analysis, Visualization, and Clinical Support. In: Jolesz, F. A. (ed) Intraoperative Imaging and Image-Guided Therapy. Springer, New York, pp 277–289
153. Materialise Mimics. Materialise https://www.materialise.com/en/medical/mimics-innovation-suite/mimics

154. Reymond, P., Merenda, F., Perren, F., Rüfenacht, D. & Stergiopulos, N. (2009) Validation of a one-dimensional model of the systemic arterial tree. Am J Physiol Heart Circ Physiol 297:H208–H222
155. Agoshkov, V., Quarteroni, A. & Rozza, G. (2006) A Mathematical Approach in the Design of Arterial Bypass Using Unsteady Stokes Equations. J Sci Comput 28:139–165
156. Sankaran, S. & Marsden, A. L. (2010) The impact of uncertainty on shape optimization of idealized bypass graft models in unsteady flow. Phys Fluids 22:121902
157. Dur, O. et al (2011) Computer-Aided Patient-Specific Coronary Artery Graft Design Improvements Using CFD Coupled Shape Optimizer. Cardiovasc Eng Technol 2:35–47
158. Hajati, O., Zarrabi, K., Karimi, R. & Hajati, A. (2012) CFD simulation of hemodynamics in sequential and individual coronary bypass grafts based on multislice CT scan datasets. 2012 Annual International Conference of the IEEE Engineering in Medicine and Biology Society:641–644
159. Schrauwen, J. T. C. et al (2015) Fast and Accurate Pressure-Drop Prediction in Straightened Atherosclerotic Coronary Arteries. Ann Biomed Eng 43:59–67
160. Taylor, C. A. & Figueroa, C. A. (2009) Patient-Specific Modeling of Cardiovascular Mechanics Annu Rev Biomed Eng 11:109–134
161. HeartFlow (2016) https://www.accessdata.fda.gov/cdrh_docs/pdf15/K152733.pdf
162. Maasrani, M. et al (2010) Simulations of fluxes in diseased coronary network using an electrical model. The XIX International Conference on Electrical Machines - ICEM 2010:1–6
163. Geven, M. C. F., Bohte, V. N. & Aarnoudse, W. H. (2004) A physiologically representative in vitro model of the coronary circulation. Physio Meas 25:891–904
164. Goldberg, D. E. (1989) Genetic algorithms in search, optimization, and machine learning. Addison-Wesley Longman Publishing Co, Boston
165. Hassani, K., Navidbakhsh, M. & Rostami, (2007) M. Modeling of the aorta artery aneurysms and renal artery stenosis using cardiovascular electronic system. Biomed Eng OnLine 6:22
166. Ursino, M. (1998) Interaction between carotid baroregulation and the pulsating heart: a mathematical model. Am J Physiol Heart Circ Physiol 275:H1733–H1747
167. Kim, H. J., Jansen, K. E. & Taylor, C. A. (2010) Incorporating Autoregulatory Mechanisms of the Cardiovascular System in Three-Dimensional Finite Element Models of Arterial Blood Flow Ann Biomed Eng 38:2314–2330
168. Liang, F. & Liu, H. (2005) A Closed-Loop Lumped Parameter Computational Model for Human Cardiovascular System. JSME Int J Ser C 48:484–493
169. Guyton, A. C., Coleman, T. G. & Granger, H. J. (1972) Circulation: Overall Regulation. Annu Rev Physiol 34:13–44
170. Montani, J. & Van Vliet, B. N. (2009) Understanding the contribution of Guyton's large circulatory model to long-term control of arterial pressure. Exp Physiol 94:382–388
171. Morris, P. D. et al (2016) Computational fluid dynamics modelling in cardiovascular medicine. Heart 102:18–28
172. Chen, S. & Doolen, G. D. (1998) Lattice Boltzmann method for fluid flows. Annu Rev Fluid Mech 30:329–364
173. Randles, A., Frakes, D. H. & Leopold, J. A. (2017) Computational Fluid Dynamics and Additive Manufacturing to Diagnose and Treat Cardiovascular Disease. Trends Biotechnol 35:1049–1061

174. Pandey, R., Kumar, M., Majdoubi, J., Rahimi-Gorji, M. & Srivastav, V. K. (2020) A review study on blood in human coronary artery: Numerical approach. Comput Methods Programs Biomed 187:105243
175. Marsden, A. L. (2014) Optimization in Cardiovascular Modeling. Annu Rev Fluid Mech 46:519–546
176. Zhong, L. et al (2018) Application of Patient-Specific Computational Fluid Dynamics in Coronary and Intra-Cardiac Flow Simulations: Challenges and Opportunities. Front Physiol 9:742
177. Updegrove, A. et al (2017) SimVascular: An Open Source Pipeline for Cardiovascular Simulation. Ann Biomed Eng 45:525–541
178. Khodaei, S. et al (2021) Personalized intervention cardiology with transcatheter aortic valve replacement made possible with a non-invasive monitoring and diagnostic framework. Nat Sci Rep In-Press
179. Sacre, J. W., Jennings, G. L. R. & Kingwell, B. A. (2014) Exercise and Dietary Influences on Arterial Stiffness in Cardiometabolic Disease. Hypertension 63:888–893
180. Pant, S., Fabrèges, B., Gerbeau, J.-F. & Vignon-Clementel, I. E. (2014) A methodological paradigm for patient-specific multi-scale CFD simulations: from clinical measurements to parameter estimates for individual analysis. Int J Numer Methods Biomed Eng 30:1614–1648
181. Zhang, X., Wu, D., Miao, F., Liu, H. & Li, Y. (2020) Personalized Hemodynamic Modeling of the Human Cardiovascular System: A Reduced-Order Computing Model. IEEE Trans Biomed Eng 67:2754–2764
182. Mukkamala, R. & Cohen, R. J. (2001) A forward model-based validation of cardiovascular system identification. Am J Physiol Heart Circ Physiol 281:H2714–H2730
183. Nakamura, G. & Potthast, R. (2015) Inverse Modeling An introduction to the theory and methods of inverse problems and data assimilation. IOP Publishing, Bristol
184. Moré, J. J. (1978) The Levenberg-Marquardt algorithm: Implementation and theory. In: Watson, G. A. (ed) Numerical Analysis: Proceedings of the Biennial Conference Held at Dundee, June 28–July 1, 1977. Springer, Berlin, pp 105–116
185. Spilker, R. L. & Taylor, C. A. (2010) Tuning Multidomain Hemodynamic Simulations to Match Physiological Measurements. Ann Biomed Eng 38:2635–2648
186. Ismail, M., Wall, W. A. & Gee, M. W. (2013) Adjoint-based inverse analysis of windkessel parameters for patient-specific vascular models. J Comput Phys 244:113–130
187. Huan Huang, Ming Yang, Wangfu Zang, Shunjie Wu, & Yafei Pang. (2011) In Vitro Identification of Four-Element Windkessel Models Based on Iterated Unscented Kalman Filter. IEEE Trans Biomed Eng 58:2672–2680
188. Quarteroni, A. (2001) Modeling the Cardiovascular System - A Mathematical Adventure-Part I. SIAM News 34(5):1-3
189. Quarteroni, A. (2001) Modeling the Cardiovascular System - A Mathematical Adventure-Part II. SIAM News 34(6):1-3
190. Athanasiou, L., Nezami, F. R. & Edelman, E. R. (2019) Computational Cardiology. IEEE J Biomed Health Inform 23:4–11
191. Mansi, T., Passerini, T. & Comaniciu, D. (2020) Artificial Intelligence for Computational Modeling of the Heart. Elsevier, Philadelphia
192. Lopez-Jimenez, F. et al (2020) Artificial Intelligence in Cardiology: Present and Future. Mayo Clin Proc 95:1015–1039

193. Feiger, B. et al (2020) Accelerating massively parallel hemodynamic models of coarctation of the aorta using neural networks. Sci Rep 10:9508
194. Bikia, V. et al (2020) Noninvasive estimation of aortic hemodynamics and cardiac contractility using machine learning. Sci Rep 10:15015
195. Witzenburg, C. M. & Holmes, J. W. A (2017) Comparison of Phenomenologic Growth Laws for Myocardial Hypertrophy. J Elast 129:257–281
196. Maksuti, E. et al (2019) Cardiac remodeling in aortic and mitral valve disease: a simulation study with clinical validation. J Appl Physiol 126:1377–1389
197. Lopez-Perez, A., Sebastian, R. & Ferrero, J. M. (2015) Three-dimensional cardiac computational modelling: methods, features and applications. Biomed Eng OnLine 14:35
198. Amann, J., Blasimme, A., Vayena, E., Frey, D. & Madai, V. I. (2020) Explainability for artificial intelligence in healthcare: a multidisciplinary perspective. BMC Med Inform Decis Mak 20:310
199. Hosanagar, K. (2019) A Human's Guide to Machine Intelligence: How Algorithms Are Shaping Our Lives and How We Can Stay in Control. Viking, New York
200. Winslow, R. L., Trayanova, N., Geman, D. & Miller, M. I. (2012) Computational Medicine: Translating Models to Clinical Care. Sci Transl Med 4:158rv11

Chapter 3: Impact of TAVR on Coronary Hemodynamics using Clinical Measurements and Image-Based Patient-Specific *in-silico* Modeling

Louis Garber[1], Seyedvahid Khodaei[2], PhD; Nima Maftoon[3,4], PhD; Zahra Keshavarz-Motamed[1,2,5], PhD

1. School of Biomedical Engineering, McMaster University, Hamilton, ON, Canada
2. Department of Mechanical Engineering, McMaster University, Hamilton, ON, Canada
3. Department of Systems Design Engineering, University of Waterloo, Waterloo, ON, Canada
4. Centre for Bioengineering and Biotechnology, University of Waterloo, Waterloo, ON, Canada
5. School of Computational Science and Engineering, McMaster University, Hamilton, ON, Canada

Submitted to:

Nature Scientific Reports (November 2022)

3.1 Abstract

In recent years, transcatheter aortic valve replacement (TAVR) has become the leading method for treating aortic stenosis. While the procedure has improved dramatically in the past decade, there are still uncertainties about the impact of TAVR on coronary blood flow. Recent research has indicated that negative coronary events after TAVR may be partially driven by impaired coronary blood flow dynamics. Furthermore, the current technologies to rapidly obtain non-invasive coronary blood flow data are relatively limited. Herein, we present a lumped parameter framework to simulate coronary blood flow in the main arteries as well as a series of cardiovascular hemodynamic metrics. The model was designed to only use a few inputs parameters from echocardiography, Computed Tomography and a sphygmomanometer. The novel framework was then validated and applied to 19 patients undergoing TAVR to examine the impact of the procedure on coronary blood flow in the left anterior descending (LAD) artery, left circumflex (LCX) artery and right coronary artery (RCA*)* and various global hemodynamics metrics. Based on our findings, the changes in coronary blood flow after TAVR varied and were subject specific (37% had increased flow in all three coronary arteries, 32% had decreased flow in all coronary arteries, and 31% had both increased and decreased flow in different coronary arteries). Additionally, valvular pressure gradient, left ventricle (LV) workload and maximum LV pressure decreased by 61.5%, 4.5% and 13.0% respectively, while mean arterial pressure and cardiac output increased by 6.9% and 9.9% after TAVR. By applying this proof-of-concept framework, a series of hemodynamic metrics were generated non-invasively which can help to better understand the individual relationships between TAVR and mean and peak coronary flow rates. In the future, tools such as these may play a vital role by providing clinicians with rapid insight into various cardiac and coronary metrics, rending the planning for TAVR and other cardiovascular procedures more personalized.

3.2 Introduction

Since the first procedure in 2002, transcatheter aortic valve replacement (TAVR) has revolutionized the landscape of interventional cardiology [1]. It has made heart valve replacement accessible to a wider spectrum of patients with aortic stenosis (AS), especially previously inoperable or high-risk populations [1]. Since the initial Food and Drug Administration approval, the number of TAVR surgeries has increased each year and in 2019, TAVR surpassed conventional surgical aortic valve replacement in the United States (72,900 procedures vs. 57,600 respectively) [2]. Similar trends are present globally, with over 450,000 patients in 65 countries undergoing TAVR [3]. However, as is the case with most medical developments, TAVR is associated with some complications and drawbacks. Although the procedure has improved considerably in the past decade, patients still suffer from post-intervention complications such as vascular complications [4], coronary obstruction [5], acute coronary syndrome [6], cerebrovascular events [7], paravalvular leakage [8] and others.

Furthermore, a large fraction of patients undergoing TAVR also have comorbid diseases such as coronary artery disease (CAD) [9, 10]. Given the high prevalence of concomitant CAD in patients undergoing TAVR (40-70% [10]) and the widespread impact of heart disease and CAD (leading cause of death globally) [11, 12], additional insight into how the procedure would impact coronary blood flow is crucial. Being able to understand, quantify and predict how TAVR would impact coronary blood flow and global hemodynamics on a patient specific basis during the procedure planning may help to prevent adverse coronary related incidences post-TAVR. Acute coronary syndrome for instance, which is caused by a significant reduction in blood flow to the myocardium, has been reported in roughly 5% of patients who underwent TAVR and is associated with a high 30-day morality rate [6]. With rapidly available and quantitative data about coronary hemodynamics, clinicians may be able to better personalize and optimize TAVR planning.

Moreover, as younger and lower risk patients receive TAVR, it is increasingly likely that they will need a follow up valve replacement in their lifetime (valve in valve TAVR for example) [13, 14]. Recently though, it has become clear that in a substantial number of these cases, invasive coronary catheter access becomes unfeasible due to the leaflet re-location from the first valve implantation [13, 14]. Having a tool that could non-invasively simulate coronary blood flow behaviour would allow

clinicians to better plan the follow up procedure and screen for possible coronary related complications when invasive access is not possible.

While medical imaging has allowed clinicians to visualize parts of the cardiovascular system, modalities to capture hemodynamics are relatively limited and are usually restricted to larger arteries and ventricles. Furthermore, they are typically limited to imaging velocity instead of blood flow rate and pressure. Angiography (invasive) and CT-angiography (minimally/non-invasive) are the primary imaging methods used to evaluate coronary arteries but are limited to capturing the structure of the vessels [15]. Echocardiography has shown promise in visualize and quantify hemodynamics in the coronary arteries but is often limited to just the left main or left anterior descend branch and has seen limited clinical adoption in this domain [16]. Furthermore, it is not possible in all patients and requires extensive technician training to obtain reliable measurements [16]. Recently 4D flow MRI has been applied to capture coronary flow but was limited to only the left main coronary artery and required long scan times [17]. Functional coronary hemodynamic data is predominantly obtained from invasive catheterization to evaluate the severity of CAD and guide coronary interventions, but it is not always collected in the pre/post-TAVR settings [18].

In the past decade, researchers have paired medical imaging and routine clinical data with the power of computing to generate non-invasive personalized cardiovascular hemodynamics models. The marriage of computational science and cardiology has yielded tools capable of simulating possible interventions [19, 20, 21, 22] studying cardiovascular diseases in-silico [23, 24, 25, 26] and generating patient specific metrics [27, 28, 29, 30]. While many of these models are aimed at the coronary arteries and compute clinically relevant parameters (such as fractional flow reserve [31, 32]) few are designed to simulate or predict the patient-specific impact of TAVR or other non-coronary interventions on coronary hemodynamics. Furthermore, many of these advanced 3D simulation tools require pre-processing and computation time in the order of days for each patient, making the automation and implementation into a clinical workflow challenging [33]. Alternatively, lumped parameter modelling (LPM) offers a simpler, but computationally quicker method to simulate patient specific cardiology models. It relies on using electronic circuits (and the hydraulic-electrical analogy) to simulated waveforms such as blood flow or pressure over time in different regions of the heart [34]. By combining a variety of medical imaging techniques, circuit layouts, element tuning, and optimization techniques, patient-specific waveforms can be obtained [34]. While

there exist a series of pure LPMs designed to estimate coronary blood flow [34], none of them are highly patient specific and utilize multiple clinical modalities to rapidly estimate both cardiac, circulatory and coronary parameters simultaneously. Moreover, none have been directly applied to study patients undergoing TAVR.

In this paper, we developed a novel lumped parameter framework to simulate blood flow waveforms in the main proximal coronary branches: LAD, LCX and RCA as well as other global cardiovascular hemodynamic parameters. The model was designed to only utilizes limited, non-invasive clinical inputs. The framework was then applied to 19 patients with AS who underwent TAVR to examine the impact of the procedure on coronary blood flow rate and various cardiovascular metrics. The coronary flow results from the model were compared with those from a patient specific 3D fluid structure interaction (FSI) model (n=19) along with a model sensitivity analysis.

3.3 Methods

A novel, proof-of-concept patient-specific, image-based LPM framework was developed, validated, and tested in this study (Figure 14, Schematic Diagram; Table 2). The model was aimed at: 1) quantifying metrics of circulatory function **(global hemodynamics)**; 2) quantifying metrics of cardiac function **(global hemodynamics)**; 3) providing non-invasive insight into coronary blood flow patterns in the pre-intervention and in the post-intervention states **(local hemodynamics)**. The computational framework used Doppler echocardiography (DE), Computed Tomography (CT) and sphygmomanometer data to generate patient-specific cardiovascular models. The developed framework was tested on a retrospective dataset of 19 patients who underwent transcatheter aortic valve replacement (TAVR). The aim was to quantify the impact of the procedure on circulatory, cardiac and coronary artery blood flow metrics without the use of invasive catheters.

Our lab previously developed a non-invasive diagnostic computational-mechanics framework for complex valvular, vascular and ventricular disease (called C3V-LPM for simplicity) [35]. The method was described in detail elsewhere [35]. In this study, we further developed C3V-LPM to enable the quantification of local and global hemodynamics in patients with mixed and complex valvular, vascular, mini-vascular and ventricular diseases (known as C3VM-LPM) (Figure 14, Table 2). The developed framework uses limited input parameters that can all be reliably measured

non-invasively using DE, CT and a sphygmomanometer. Currently, none of the above metrics (global and local hemodynamics) can be obtained noninvasively in patients and when invasive procedures are performed, the gathered metrics cannot be by any means as complete as the results that C3VM-LPM provides. The previously created model, C3V-LPM, was validated against clinical catheterization data in forty-nine AS patients with a substantial inter- and intra-patient variability with a wide range of disease [35]. In addition, some of the sub-models of the patient-specific LPM algorithm have been used previously [27, 28, 36, 37, 38, 39, 40], with validation against in vivo cardiac catheterization (N=34) [41, 42] in patients with vascular diseases, in vivo MRI data (N=57) [43] in patients with AS, and in vivo MRI data (N=23) [44] in patients with coarctation and mixed valvular diseases.

The major development with the new C3VM-LPM framework is the additional capability to non-invasively capture and quantify patient-specific hemodynamics in the following left and right coronary artery branches: 1) LAD 2) LCX 3) RCA. The following sections outline the different compartments and tuning approaches developed for this patient specific model (see Figure 14 for the complete electrical representation).

3.3.1 Study population and data acquisition

19 patients who underwent TAVR in 2020 at St. Joseph's Healthcare and Hamilton Health Science (Hamilton, Canada) were considered in this study. The study protocols were reviewed and approved by the Hamilton Integrated Research Ethics Board (HiREB) for Hamilton Health Science and St. Joseph's Healthcare. Informed consents were obtained from all human participants. All methods and measurements were performed in accordance with all relevant guidelines and regulations including guidelines from the American College of Cardiology and American Heart Association. Data was collected at 2 time points: pre-procedure and post-procedure. Table 1 outlines the demographic and procedural data of the patients. All data and results are expressed as mean ± standard deviations (SD).

3.3.2 Coronary arteries

Each of coronary branches is modeled using a circuit comprised of 3 resistors ($\mathrm{R_{cor,p}}, \mathrm{R_{cor,m}}, \mathrm{R_{cor,d}}$), 2 capacitors ($\mathrm{C_{cor,p}}, \mathrm{C_{cor,m}}$) and an embedded pressure (voltage) source (P_{im}). This circuit representation was initially proposed by Mantero et al. [45] and further advanced and popularized by Kim et al. [46]. It has been used in numerous LPMs [31, 47, 48, 49, 50] and has been

Table 1: *Baseline and post-TAVR patient characteristics*

	Pre-TAVR (n=19, mean ± SD)	**90-day post-TAVR (n=19, mean ± SD)**
Patient Characteristics		
Age (year)	77.8 ± 6.0	N/A
Female subjects	10 (53%)	N/A
Mean weight (kg)	85.2 ± 33.3	N/A
Mean height (cm)	168.5 ± 9.6	N/A
Body mass index (kg/m^2)	2.0 ± 0.4	N/A
NYHA – Class I	0	11 (58%)
NYHA – Class II	10 (53%)	3 (16%)
NYHA – Class III	9 (47%)	5 (26%)
NYHA – Class IV	0	0
Arterial Characteristics		
Brachial systolic BP (mmHg)	133.0 ± 18.9	142.0 ± 22.3
Brachial diastolic BP (mmHg)	70.5 ± 9.2	72.0 ± 15.4
Hypertension	15 (79%)	N/A
Coronary artery disease	5 (26%)	N/A
Echocardiography Findings		
Heart rate (bpm)	71 ± 14	73 ± 13
Ejection fraction (%)	59.9 ± 8.4	62.3 ± 7.0
Stenotic aortic valve EOA (cm^2)	0.84 ± 0.19	N/A
Stenotic aortic valve type	Tricuspid: 11 (58%) Bicuspid: 5 (26%) Unknown: 3 (16%)	N/A
Max aortic valve flow velocity (m/s)	4.45 ± 0.56	2.75 ± 0.65
Mean aortic valve pressure gradient (mmHg)	47.2 ± 13.1	18.2 ± 8.3
Paravalvular leakage	N/A	Trace: 0 Mild: 1 Moderate-to-Severe: 1 Severe: 0

shown to capture the bi-phasic nature of coronary flow, in which peak blood flow occurs during the diastole phase rather than during systole [45, 46]. While inductors are including in the ventricle

and valvular portion of the model, they were not included in the coronary branches since the inertial phenomena is not significant in the coronary arteries [45]. The following ODEs are obtained from the circuit layout to model each of the coronary branches [49]:

$$q_{in} = \frac{P_{in} - P_p}{R_{cor,p}} \tag{1}$$

$$q_{in} = C_{cor,p}\frac{dP_p}{dt} + q_m \tag{2}$$

$$P_p = q_m R_{cor,m} + P_m \tag{3}$$

$$q_m = q_{out} + C_{cor,m}\frac{dP_{im}}{dt} \tag{4}$$

$$P_m = q_{out} R_{cor,d} + P_{out} \tag{5}$$

where q_{in}, P_{in}, q_{out} and P_{out} are the blood flow and pressure into and out of the coronary branch. $R_{cor,p}, R_{cor,m}, R_{cor,d}$ are the proximal, medial, and distal resistors while $C_{cor,p}, C_{cor,m}$ are the proximal and medial capacitors. P_p, P_m and P_{im} are the proximal, medial and intramyocardial pressures.

P_{im} is set to be either the left ventricle (LV) or right ventricle (RV) pressure, depending on the coronary artery that it is coupled to. In this study, we used the LV pressure for the left branches (LAD and LCX) and $0.5P_{LV}$ [51] to create the RV pressure for the right branch (RCA).

Determining arterial resistance and compliance in coronaries

Total coronary resistance

The mean flow rate to the coronary arteries was assumed to be 4.0% of the cardiac output (CO) [46]. The total coronary resistance was then estimated based on a relationship between pressure and flow [31]:

$$R_{cor,total} = \frac{MAP}{Q_{cor,total}} = \frac{MAP}{(0.04) * CO} \tag{6}$$

where $R_{cor,total}$ is the total coronary resistance and mean arterial pressure (MAP) is calculated based on systolic blood pressure (SBP), diastolic blood pressure (DBP) and heart rate (HR) [52]:

$$MAP = DBP + [\frac{1}{3} + (HR * 0.0012)](SBP - DBP) \tag{7}$$

Coronary vessel resistance and compliance

The total coronary resistance was divided between each of the branches based on a variation of Murray's law [53], which relates resistance to vessel diameter:

$$R_{cor,j} = \frac{\sum_{i=1}^{n} \sqrt{A_i}^{2.6}}{\sqrt{A_j}^{2.6}} R_{cor,total} \qquad where\ j = \{LAD, LCX\ or\ RCA\} \tag{8}$$

where $R_{cor,j}$ is the total coronary resistance in the desired branch and A_i is the cross-sectional area of each of the coronary vessels [46]. Further division of the total vessel resistance into the 3 resistive elements in the circuit was based on the work of Sankaran et al. [54]:

$$R_{cor,j,p} = (0.32)R_{cor,j} \quad R_{cor,j,m} = (0.52)R_{cor,j} \quad R_{cor,j,d} = (0.16)R_{cor,j} \tag{9}$$

where $R_{cor,j,p}$, $R_{cor,j,m}$, $R_{cor,j,d}$ are the proximal, medial, and distal resistors.

To account for the cases with coronary vessel stenoses or vessels with considerable reductions in diameters, the following approach was used [55]:

$$\alpha = \frac{A_{sten}}{A_0} \tag{10}$$

$$R_{cor,red,j} = R_{cor,j}(\alpha^{-2}) \tag{11}$$

where A_{sten} represents the cross-sectional area of the stenosis/diameter reduction and A_0 represents the normal cross-sectional area (non-stenotic area). The original resistance for the vessel ($R_{cor,j}$), assuming no stenosis, is then multiplied with an area reduction factor (α) to yield the new branch resistance ($R_{cor,red,j}$), which can then be further divided into the sub resistors.

The left coronary compliance was computed by dividing up the total left coronary compliance based on vessel diameter:

$$C_{cor,j} = \frac{A_j}{\sum_{i=1}^{n} A_i} C_{cor,total}^{L} \quad (12)$$

where $C_{cor,j}$ is the left coronary vessel compliance, $C_{cor,total}^{L}$ is the total left coronary compliance and A_i is the cross-sectional area of each of the left coronary branches [46]. A manual tuning process was utilized to determine total left coronary compliance value that led to physiological coronary flow waveforms [56, 57, 58].

The compliances were then divided across the 2 capacitors based on the following relationship, developed by Sankaran et al. [54]:

$$C_{cor,j,p} = (0.11)C_{cor,j} \qquad C_{cor,j,m} = (0.89)C_{cor,j} \quad (13)$$

where $C_{cor,j,p}$ and $C_{cor,j,m}$ are the proximal and medial capacitors. The same process was applied for the right coronary vessels.

3.3.3 Input parameters and geometry reconstruction

The C3VM-LPM used the following patient specific measurements as inputs: forward left ventricle outflow tract stroke volume (Forward LVOT-SV), cardiac cycle time (T), ejection time (T_{EJ}), effective orifice area of the aortic valve (EOA_{AV}), effective orifice area of the mitral valve (EOA_{MV}), area of left ventricle outflow tract (A_{LVOT}), aortic regurgitant effective orifice area (EOA_{AR}), mitral regurgitant effective orifice area (EOA_{MR}) and paravalvular leakage volume (V_{leak}) measured by DE. Branchial systolic and diastolic blood pressure were measured by a sphygmomanometer.

ITK-SNAP (version 3.8.0-BETA) [59] and the collected CT data were used to re-construct the 3D geometries of the main coronary arteries (left main coronary artery (LMCA), proximal LAD, LCX

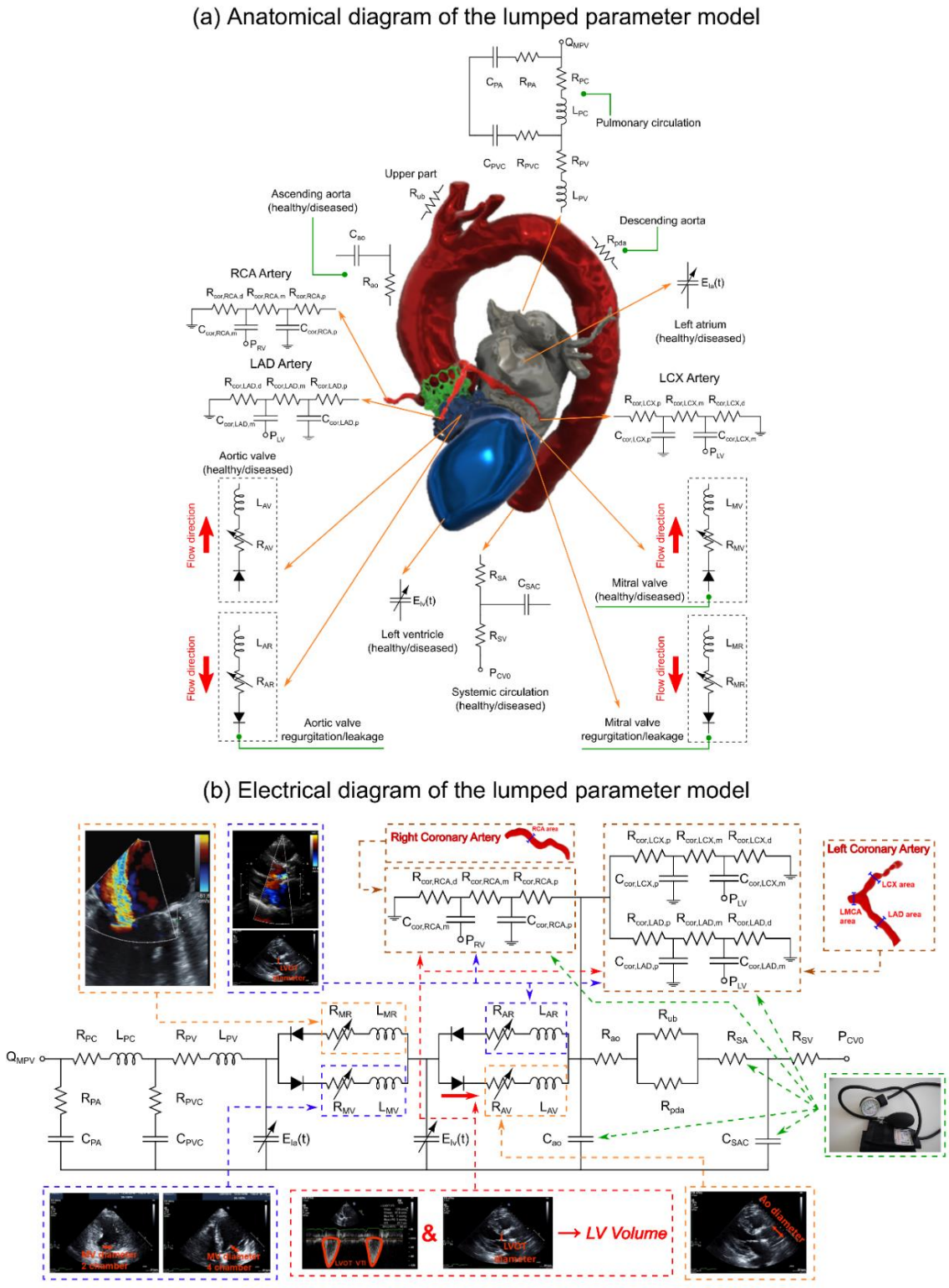

Figure 14: *Electrical and anatomical schematic diagrams of the LPM.* ***(a)*** *Anatomical illustration showing the different circuit meshes and their relationship to the cardiovascular system;* ***(b)*** *Electrical diagram with data inputs. The model includes the following sub-models: LAD, LCX and RCA, left ventricle, aortic valve, left atrium, mitral valve, aortic valve regurgitation, mitral valve regurgitation, systemic circulation, pulmonary circulation. Abbreviations in the schematic are the same as in Table 2.*

and RCA) in both the pre-TAVR and post-TAVR cases. Figure 14 Panel B outlines how the inputs parameters are related to the lumped parameter sub-models.

Table 2: *Parameter summary for patient specific LPM*

Parameter Description	Abbreviation	Value
Valve Parameters		
Effective orifice area	EOA	Measured using DE
Energy loss coefficient	$E_L CO$	$\frac{(EAO)A}{A-EOA}$; A measured using DE
Mitral valve inertance	M_{MV}	Constant value: 0.53 g/cm^2 [32]
Systemic Circulation Parameters		
Aortic resistance	R_{ao}	Constant value: 0.05 mmHg·s/mL [31]
Aortic compliance	C_{ao}	Initial value: 0.5 mL/mmHg Optimized based on branchial pressure
Systemic vein resistance	R_{SV}	Constant value: 0.05 mmHg·s/mL [31]
Systemic arteries and veins compliance	C_{SAC}	Initial value: 2 mL/mmHg Optimized based on branchial pressure
Systemic arteries resistance	R_{SA}	Initial value: 0.8 mmHg·s/mL Optimized based on branchial pressure
Upper body resistance	R_{ub}	Adjusted to direct 15% of total flow rate in healthy cases [33]
Proximal descending aorta resistance	R_{pda}	Constant value: 0.05 mmHg·s/mL [31]
Elastance Function Parameters		
Maximum elastance	E_{max}	2.1 (LV) | 0.17 (LA) [34, 35]
Minimum elastance	E_{min}	0.06 (LV & LA) [34, 35]
Elastance ascending gradient	m_1	1.32 (LV & LA) [34, 35]
Elastance descending gradient	m_2	27.4 (LV) | 13.1 (LA) [34, 35]
Elastance ascending time translation	τ_1	0.269T (LV) | 0.110T (LA) [34, 35]
Elastance descending time translation	τ_2	0.452T (LV) | 0.18T (LA) [34, 35]
Coronary Parameters		
Proximal coronary resistance	$R_{cor,p}$	Adjusted based on CO, MAP, and coronary branch cross sectional area
Medial coronary resistance	$R_{cor,m}$	Adjusted based on CO, MAP, and coronary branch cross sectional area
Distal coronary resistance	$R_{cor,d}$	Adjusted based on CO, MAP, and coronary branch cross sectional area
Proximal coronary compliance	$C_{cor,p}$	Adjusted based on total coronary compliance and branch cross sectional area

Medial coronary compliance	$C_{cor,m}$	Adjusted based on total coronary compliance and branch cross sectional area
Pulmonary Circulation Parameters		
Pulmonary vein inertance	L_{PV}	Constant Value: 0.0005 mmHg·s^2/mL [32]
Pulmonary vein resistance	R_{PV}	Constant Value: 0.002 mmHg·s/mL [32]
Pulmonary vein and capillary resistance	R_{PVC}	Constant Value: 0.001 mmHg·s/mL [32]
Pulmonary vein and capillary compliance	C_{PVC}	Constant Value: 40 mL/mmHg [32]
Pulmonary capillary inertance	L_{PC}	Constant Value: 0.0003 mmHg·s^2/mL [32]
Pulmonary capillary resistance	R_{PC}	Constant Value: 0.21 mmHg·s/mL [32]
Pulmonary arterial resistance	R_{PA}	Constant Value: 0.01 mmHg·s/mL [32]
Pulmonary arterial compliance	C_{PA}	Constant Value: 4 mL/mmHg [32]
Mean flow rate of pulmonary valve	Q_{MPV}	Optimized flow parameter s.t the model could reproduce the Forward LVOT-SV seen in DE
Input and Output Conditions		
Forward left ventricular outflow tract stroke volume	Forward LVOT-SV	Measured using DE
Central venous pressure	P_{CV0}	Constant value: 4 mmHg [31]
Additional Parameters		
Heart rate	HR	Measured using DE
Duration of cardiac cycle	T	Measured using DE
Density of blood	ρ	Constant value: 1050 kg/m^3 [31]
Systolic end ejection time	T_{EJ}	Measured using DE
End diastolic volume	EDV	Measured using DE
End systolic volume	ESV	Measured using DE

3.3.4 Computational algorithm

The ordinary differential equations which govern the LPM circuit were formulated and solved in Matlab Simscape (MathWorks Inc, Natick USA). Addition functions were written in Matlab and Simulink to enhance the Simscape code. The Matlab Optimization Toolbox and Simulink Design Optimization Toolbox were also used to implement part of the parameter tuning algorithms based on in-house code. The trapezoid rule variable step solver (ode23t) was used with an initial step time of 0.1 milliseconds. The initial voltages and currents of the capacitors and inductors in the circuit were set to zero and the convergence residual criterion was set to 10^{-6}. On average, the model had a computation time in the order of 10-15s (on a workstation with the configurations of

Intel Core™ i7-10700 CPU @2.90 GHz and 64 GB Ram). Table 4 outlines all the model parameters and their values or formulas.

3.4 Results

3.4.1 Model verification

In many cases, during the pre-TAVR workup, invasive flow and pressure data in the coronary arteries are not collected and angiography images are often used to decide if the coronary arteries should be re-vascularized before, during or after TAVR [60]. Since this invasive coronary data in the pre- and post-TAVR cases is limited and not routinely collected, we used our patient-specific 3-D FSI model results to validate our newly developed LPM. While this approach is not true gold-standard validation, using a complex FSI model offers a strong proof-of-concept verification method to examine the performance of the LPM. This full 3D modelling technique was applied to the 19 patients and the mean and peak flows for the LAD, LCX and RCA were computed.

The 3D FSI model used individual CT images to reconstruct the geometry of the coronary arteries, proximal ascending aorta, and aortic valve leaflets. The boundary conditions were based on patient specific DE and blood pressure data. The 3D coronary arteries flow was simulated using FSI method [61, 62] using finite volume method - the details of FSI algorithm can be found elsewhere [19, 20]. Due to the complexity of heart valve motions during full cardiac cycle, the FSI model simulated blood flow in the structure during the diastole phase (main filling phase for coronaries) assuming rigidly closed aortic valve. As the majority of coronary blood flow occurs in diastole (due to the impact of extravascular ventricle compression in systole [63]), this allows for a relatively complete validation of the total blood flow during the cardiac cycle.

Figures 15 and 16 outline the blood flow waveforms in the pre- and post-TAVR settings for all 3 coronary branches for two samples patients according to the LPM developed in this paper (C3VM-LPM) along with the 3D FSI model results. Overall, there is a strong agreement in the waveforms between the modelled coronary blood flow rates from the CV3M-LPM (lumped) and the FSI (3D) model. Table 3 outlines the average mean and peak flow rate error between the two models in pre- and post-TAVR (n=19).

Table 3: *Mean and peak blood flow rate error % (± std) between the LPM and the FSI models in the three main coronary artery branches (n=19)*

	Mean Flow Rate Error			**Peak Flow Rate Error**		
	LAD	LCX	RCA	LAD	LCX	RCA
Pre-TAVR	13.2 ± 17%	11.7 ± 11%	16.1 ± 29%	15.3 ± 14%	18.1 ± 18%	22.7 ± 28%
Post- TAVR	17.3 ± 17%	11.0 ± 15%	13.3 ± 10%	15.9 ± 19%	15.2 ± 24%	19.9 ± 18%

To better understand how the C3VM-LPM responded to possible independent variations in parameters and inputs, a sensitivity analysis was conducted. The focus of this analysis was on the coronary branches as previous parameter analyses have been conducted on the values in the cardiac and circulatory regions; see [36, 37] and [64] for more details. Table 4 outlines the parameters that control the mean flow rate and shape of the coronary flow curves in the model (see equations 6-12). Each parameter was independently varied by ± 20% and the maximum relative error percentage in the computed mean flow rate for the LAD, LCX and RCA was tabulated (Table 2). Following the approach of Tran et al. [65], the heart rate was assumed to a deterministic parameter.

Table 4 outlines the results from the coronary branch sensitivity analysis. The mean coronary flow rates estimated from the model are relatively sensitive to changes in MAP (27.4% max relative error averaged across all 3 branches), CO (22.0%) and branch cross sectional area (LAD – 14.2%, LCX – 12.6% and RCA – 11.5%). Conversely, the mean coronary flow rate is not significantly impacted by changes in the left and right coronary compliance (5.1% and 0.7% respectively). Vessel compliance tends to impact the shape the waveform rather than the mean flow rate directly [65]. When the left and right coronary compliances were varied by ± 20%, the max relative error in the peak flow rates were only 7.1% and 7.4% respectively.

3.4.2 Cardiac and circulatory function and hemodynamics (global hemodynamics)

Using the lumped model, pre- and post-TAVR cardiac and ventricular indices were calculated for the patients (Figure 17). All the patients who underwent the procedure had aortic stenosis and the severity was assessed by senior cardiologists based on aortic valve flow dynamics according to the European Association of Cardiovascular Imaging and American Society of Echocardiography guidelines [66].

The reduction in valve area caused by aortic stenosis led to the formation of high velocity jets driven by the pressure gradient across the valve. In all but 1 patient, valve pressure gradient

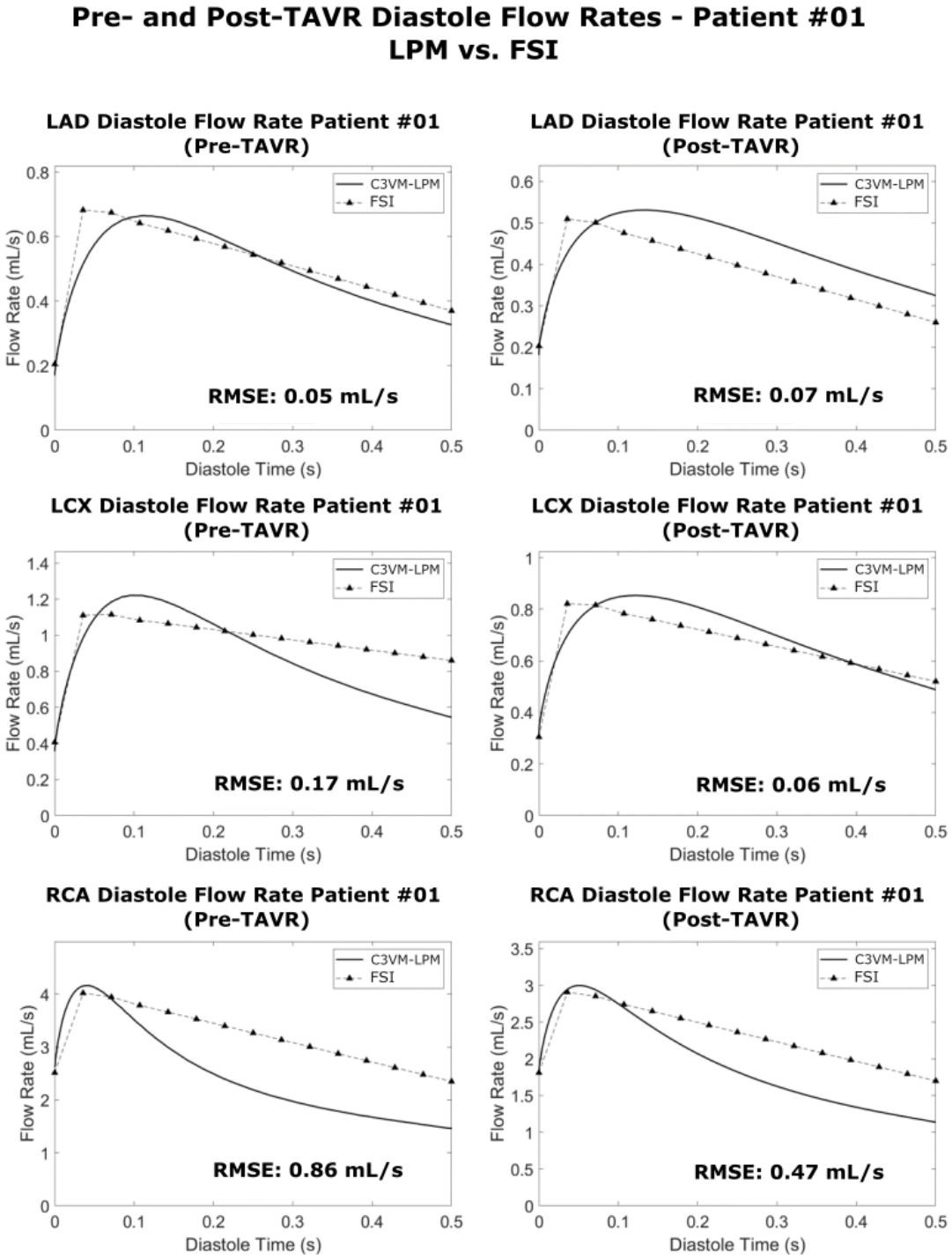

Figure 15: *Coronary Blood Flow Waveform Validation – Patient #01. The pre- and post-TAVR diastole blood flow waveforms in all 3 branches (LAD, LCX and RCA) from the LPM and the 3D FSI model for patient #01. The time has been normalized to 0.5s. RMSE – root mean squared error between the waveforms.*

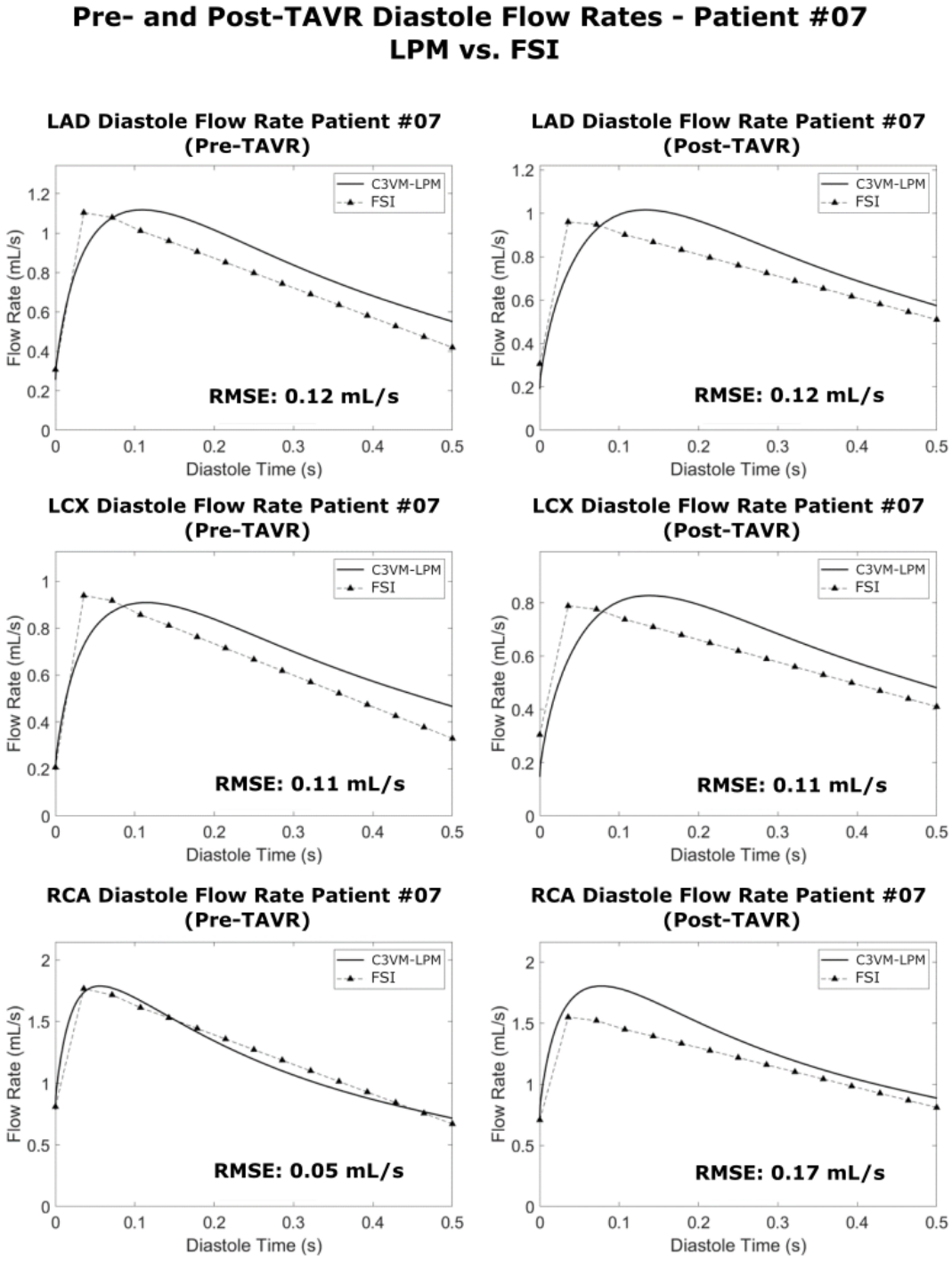

***Figure 16**: Coronary Blood Flow Waveform Validation – Patient #07. The pre- and post-TAVR diastole blood flow waveforms in all 3 branches (LAD, LCX and RCA) from the LPM and the 3D FSI model for patient #07 The time has been normalized to 0.5s. RMSE – root mean squared error between the waveforms.*

decreased (61.5% on average) after TAVR. While the valvular pressure reduced for almost all patients, this reduction is not always associated with improved global hemodynamics and better prognosis [27].

Table 4: *Maximum relative error (%) in the computed mean coronary branch flow rates from the sensitivity analysis in response to independent variation in model parameters and inputs*

Description	**Parameter**	**Range**	**Max Relative Error – LAD** (%)	**Max Relative Error – LCX** (%)	**Max Relative Error – RCA** (%)	**Mean across LAD/LCX/RCA** (%)
Mean Arterial Pressure	MAP	± 20%	28.4	27.9	25.7	27.4
Cardiac Output	CO	± 20%	22.9	22.4	20.8	22.0
LAD Area	A_{LAD}	± 20%	16.0	13.5	13.0	14.2
LCX Area	A_{LCX}	± 20%	7.3	21.1	9.3	12.6
RCA Area	A_{RCA}	± 20%	7.1	7.2	20.2	11.5
Total left coronary compliance	$C^{L}_{cor,total}$	± 20%	5.2	5.0	-	5.1
Total right coronary compliance	$C^{R}_{cor,total}$	± 20%	-	-	0.7	0.7

LV workload is a measure of the required work by the left ventricle to eject blood and overcome the opposing cardiovascular systemic load [19, 43]. The workload was computed through the integral of the left ventricle pressure-volume loop generated by the lumped model. On average, the workload decreased by 4.5% after TAVR (but increased in 9 of the 19 subjects). Similarly, the presence of aortic stenosis pre-TAVR led to elevated LV pressure and impaired LV function for the patients. By surgically implanting the valve, TAVR led to the reduction in LV pressure for 16 of the 19 patients and decreased the pressure by 13.0% on average.

SBP increased in 13 patients (7.3% average increase across all patients) and DBP increased in 13 patients (5.5% average increase). Mean atrial pressure, which represents a weighted average between SBP and DBP, increased by 6.9% on average after TAVR, while increasing for 13 of the patients. Sustained increase in blood pressure after TAVR is often associated with better prognosis while decreased BP may be linked to less favourable prognoses [67, 68]. Similarly, cardiac output

increased by 9.9% on average (increased in 12 patients) and a 1.9% increase in resting heart rate was observed (increase in 12 patients - not shown in Figure 17).

3.4.3 Coronary blood flow dynamics (local hemodynamics)

Coronary blood flow is crucial for delivering oxygen to the myocardium and is heavily governed by numerous physiological factors including cardiac output, heart rate, ventricular pressure, coronary perfusion pressure, vessel diameter, aortic valve area, disease status (such as AS or CAD) as well as other biological regulation factors [57, 69, 70].

As there was patient-specific variation in many of these parameters (Figure 17), there was also large individual variations in the impact of TAVR on coronary artery blood flow across the 3 branches (Figure 18). Of the 19 patients, 7 had increases in coronary blood flow in all branches, 6 patients had decreases in all branches, while the remainder had increases and decreases in difference branches. Across all the patients, mean flow increased by 2.8% on average post-TAVR (5.4%, -3.0% and -0.1% for the LAD, LCX and RCA branches, respectively; N=19). When broken down into the cardiac phases, the coronary blood flow increased by 17.5% post-TAVR during systole (15.7%, 22.6% and 14.3% for the LAD, LCX and RCA branches, respectively; N=19) while decreasing by 7.1% during diastole (-1.2%, -7.6% and -12.4% for LAD, LCX and RCA branches; N=19).

Similar trends were observed for the peak coronary flow rate. After TAVR, there was an 8.4% increase during systole (3.8%, 6.8% and 14.5% LAD, LCX and RCA branches; N=19) but a 11.1% decrease during diastole (-5.1%, -11.8% and -16.3% LAD, LCX and RCA branches; N=19). Overall, the coronary blood flow rate during systole was impacted more than the blood flow rate during diastole.

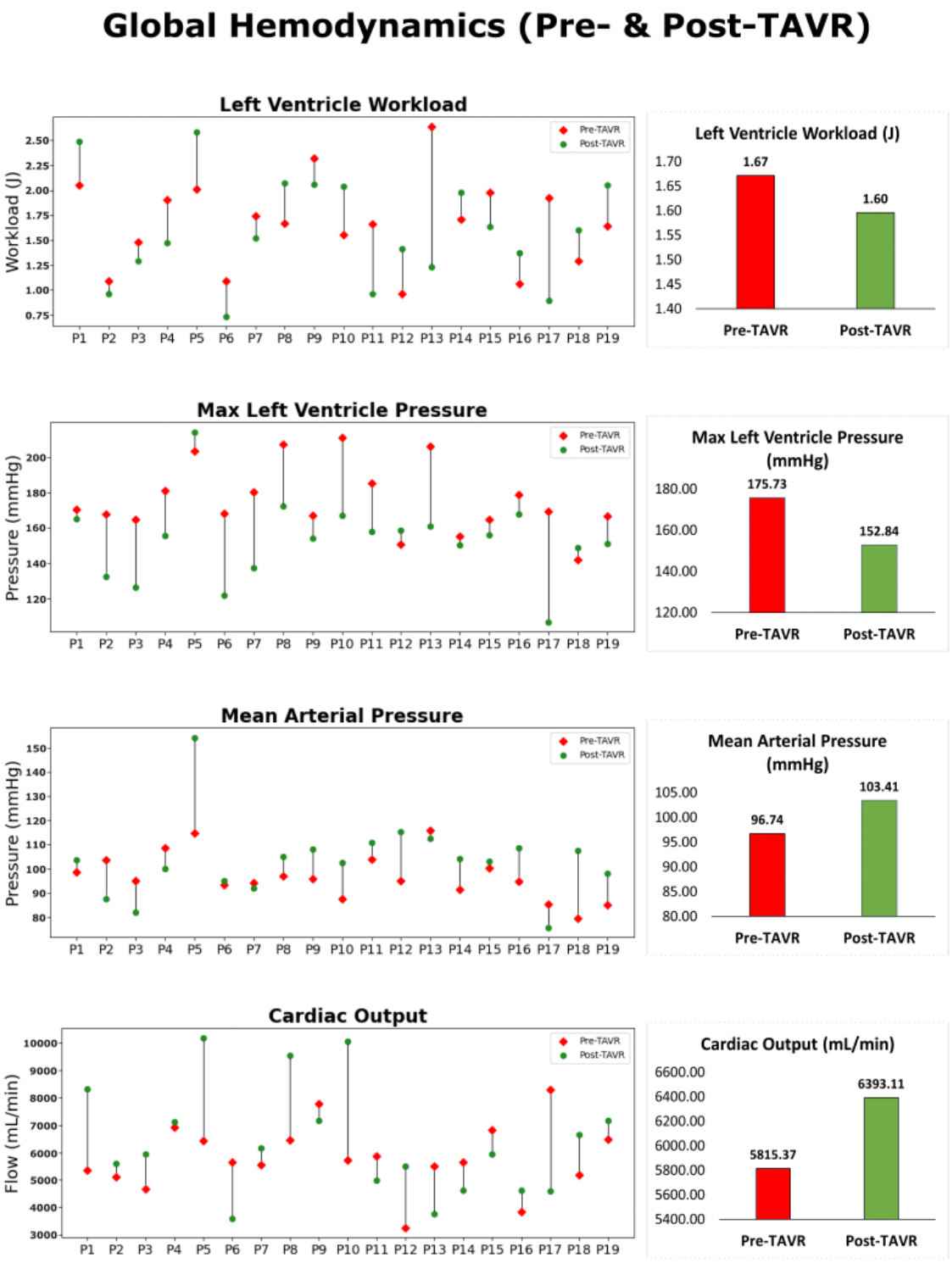

***Figure 17**: Global Hemodynamic Metrics Pre- and Post-TAVR. The changes in individual and mean global hemodynamic metrics from pre-TAVR to post-TAVR (n=19) for **(a)** left ventricle workload (J); **(b)** max left ventricle pressure (mmHg); **(c)** mean arterial pressure (mmHg); **(d)** cardiac output (mL/min)*

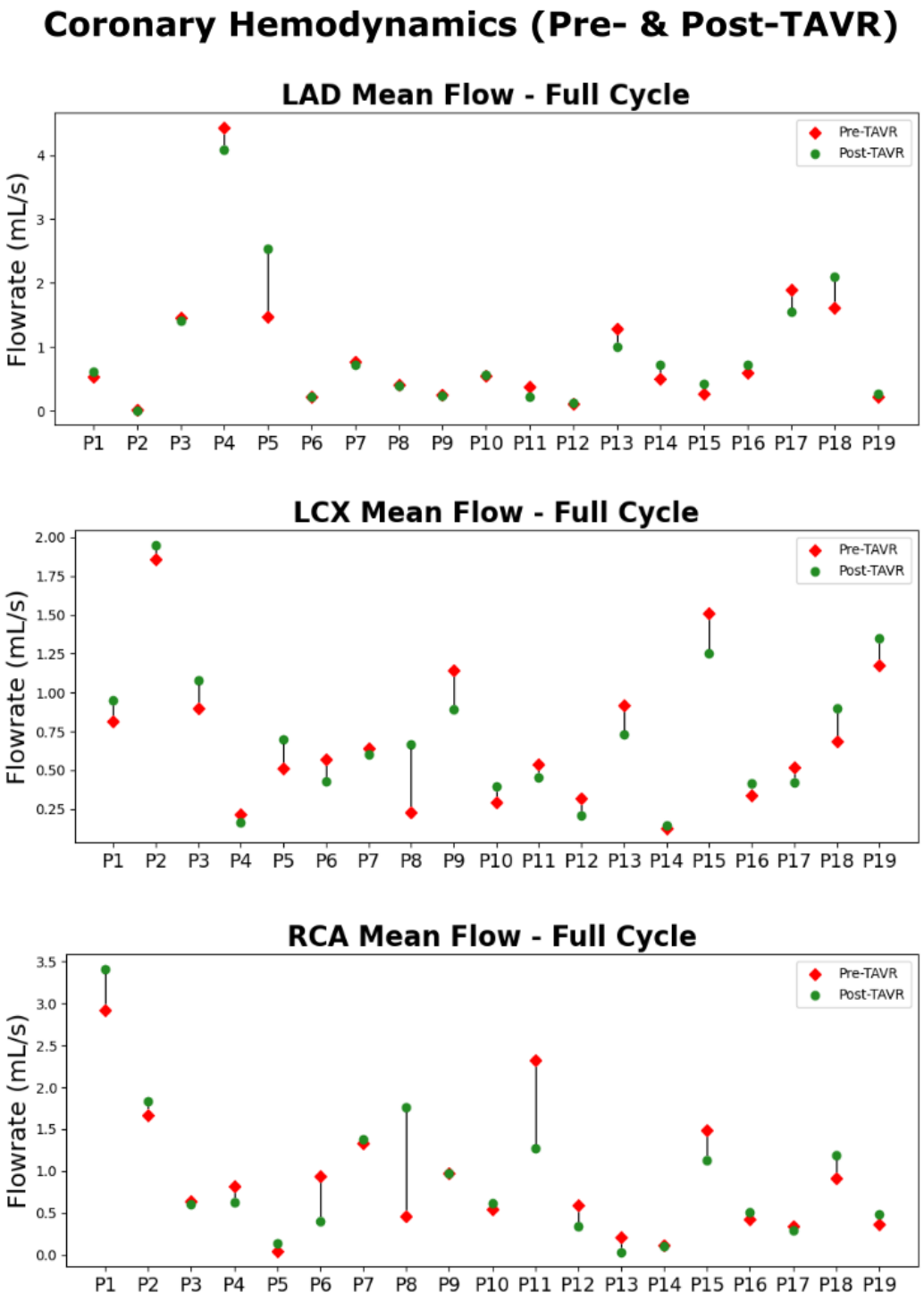

Figure 18: *Coronary Blood Flow Rate Pre- and Post-TAVR. The changes in individual coronary blood flow rate (mL/s) from pre-TAVR to post-TAVR (n=19)* ***(a)*** *LAD;* ***(b)*** *LCX;* ***(c)*** *RCA*

3.4.4 Patient Specific Coronary Hemodynamics

Coronary artery blood flow dynamics are impacted by various physiological factors and diseases [71]. For a computational tool to appropriately predict these waveforms, it must be able to capture the patient specific impacts between the various cardiac and circulatory interactions. Since the C3VM-LPM is designed to include not only the coronary arteries but also the pulmonary circulation, left atrium, mitral valve, aortic valve, ascending aorta and systemics circulation, it can simulate a portion of the cardiovascular system. Furthermore, it can provide a window to examine various aspects of the system in both the pre- and post-intervention setting for individual patients.

Figures 19, 20 and 21 illustrate patient specific cardiovascular data for various regions of the heart and coronary arteries in both the pre- and post-TAVR cases. Patients #18, #13 and #16 were selected to illustrate cases in which the procedure led to varying outcomes in coronary flow rates and cardiac dynamics.

Patient #18 was suffering from severe aortic stenosis prior to receiving a TAVR procedure, which had led to an increased burden on the left ventricle. Following TAVR, the aortic valve area increased from 0.80 to 2.30 cm^2 and the ejection fraction increased from 69% to 71%. Based on the model, the intervention led to an increase in peak LV pressure (+4.7%), an increase in the MAP (+35.2%), an increase in LV workload (+24.0%), an increase in cardiac output (+28.3%), and an increase in resting heart rate (+2.9 %). Overall, an increase in the LAD (+31.1%), LCX (+32.4%) and RCA (+30.8%) flow rates were observed post-TAVR. Additionally, the total estimated myocardial blood flow (coronary blood flow per gram of cardiac mass) increased from 2.36 to 4.06 mL/min/g.

Patient #13 was also suffering from severe aortic stenosis prior to receiving TAVR. Similar to patient #18, the intervention increased the aortic valve area from 0.90 to 1.04 cm^2 and the ejection fraction increased from 60% to 64%. According to the model, the intervention led to a decrease in the peak LV pressure (-21.8%), a decrease in LV workload (-53.4%), a decrease in MAP (-2.9%), an increase in resting heart rate (+9.1%) and a decrease in cardiac output (-31.4%). The coronary

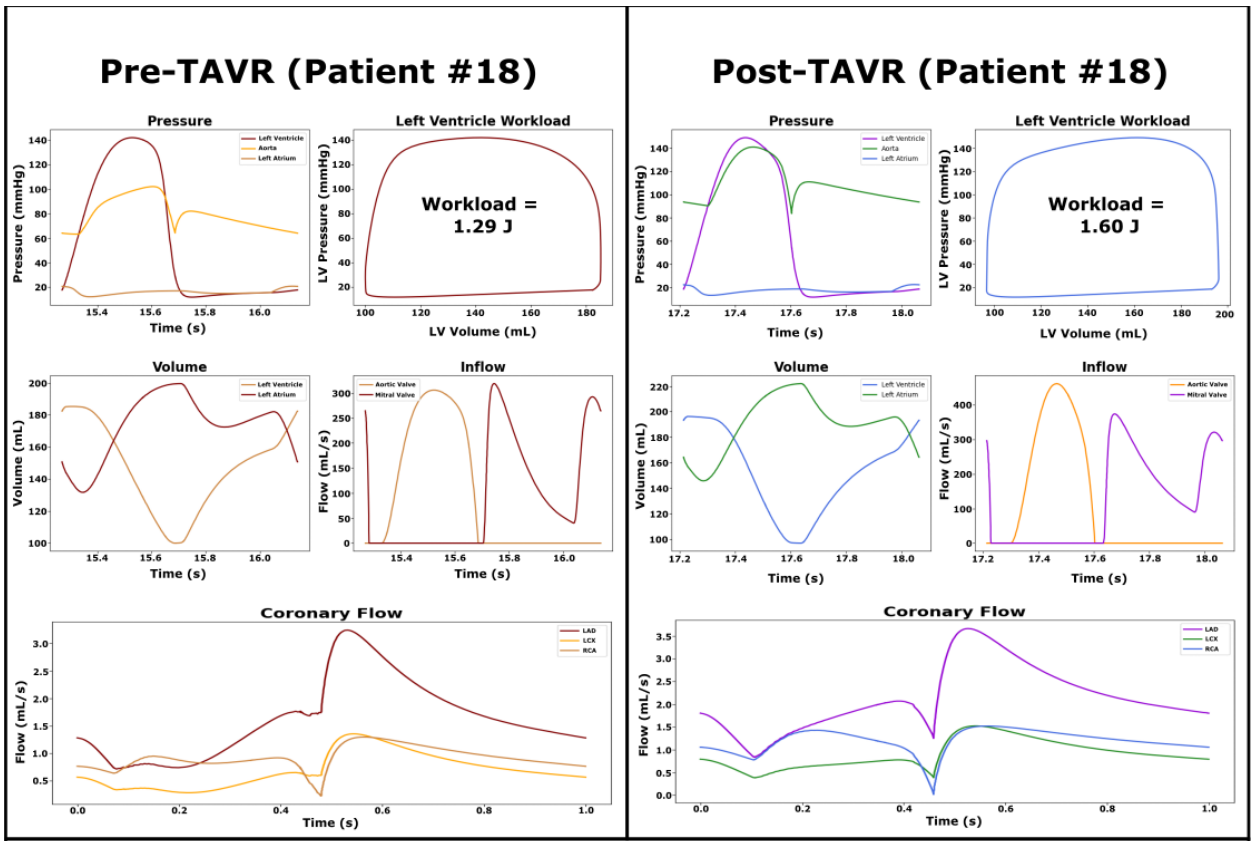

	Aortic Stenosis Severity	Aortic Valve Area (cm^2)	Max AV Velocity (m/s)	Ejection Fraction (%)	Cardiac Output (mL/s)	Resting Heart Rate (beats/min)	Mean Arterial Pressure (mmHg)	Maximum LV Pressure (mmHg)	Mean LAD Flowrate (mL/s)	Mean LCX Flowrate (mL/s)	Mean RCA Flowrate (mL/s)	Myocardial Blood Flow (mL/min/g)
Pre-TAVR	Severe	0.8	4.19	38	5186	69	79.5	142.1	1.61	0.68	0.91	2.36
Post-TAVR	-	2.3	2.25	41	6653	71	107.5	148.8	2.11	0.90	1.19	4.06

Figure 19: *Predicted cardiac and coronary hemodynamics (Patient #18). The plots on the left and right illustrate the pre-TAVR and post-TAVR data respectively. Before the intervention, this patient suffered from severe aortic stenosis. After TAVR, the mean pressure gradient and max aortic valve velocity decreased and all the other predicted hemodynamic metrics increased, including myocardial blood flow.*

flow in the LAD, LCX and RCA decreased by 22.5%, 20.7% and 85.7% after surgery, respectively. The total estimated myocardial blood flow also decreased from 2.42 to 2.39 mL/min/g.

Patient #16 suffered from the same condition and severity as the other subjects. As with the other subjects, the aortic valve area increased after TAVR (0.5 to 0.9 cm^2) and the ejection fraction decreased (64% to 62%). Interestingly though, even though the total coronary flow increased after TAVR (+21.5%), the total myocardial blood flow rate barely changed after the surgery (2.05 to 2.06 mL/min/g). This is likely due to the increase in the left ventricle mass index (77 to 93 g/m^2) which may be a by-product of the increase in left ventricle work (1.06 to 1.37 J).

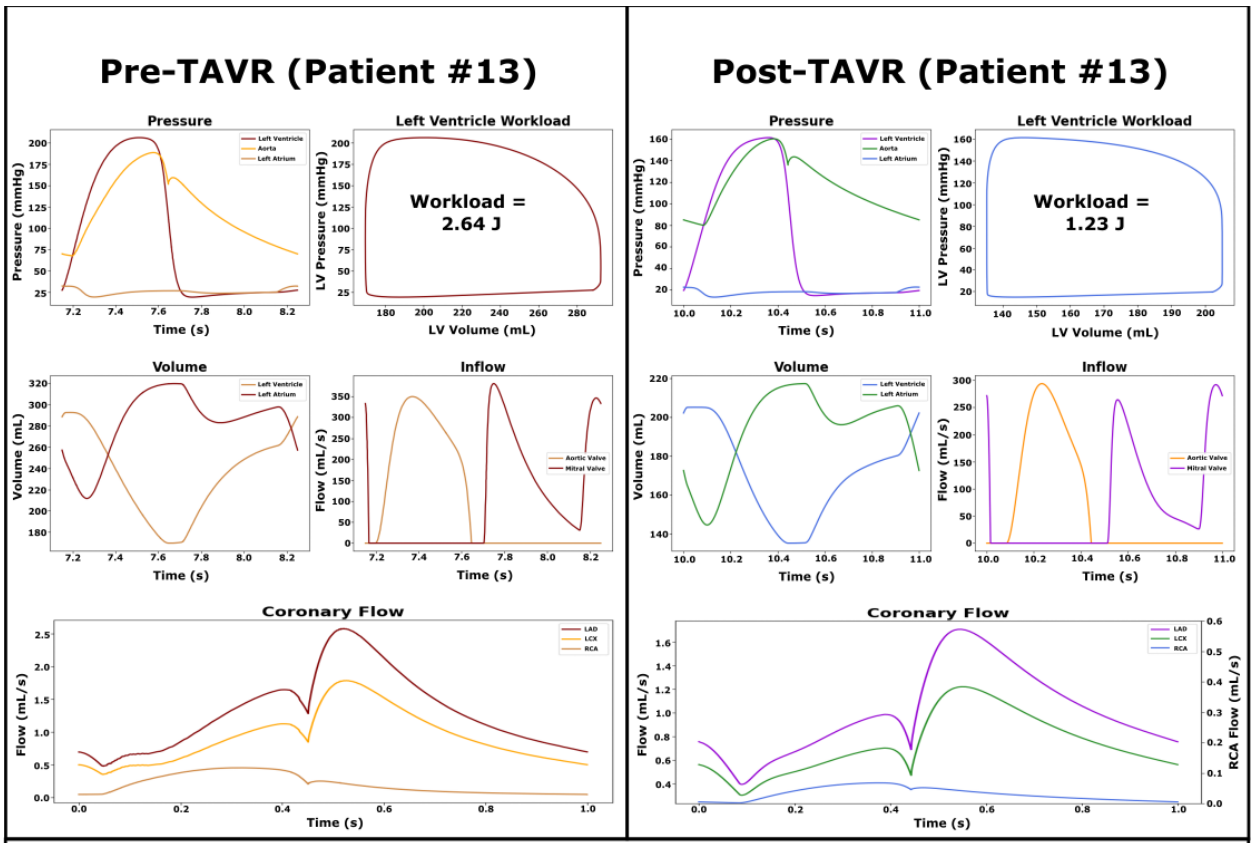

	Aortic Stenosis Severity	Aortic Valve Area (cm^2)	Max AV Velocity (m/s)	Ejection Fraction (%)	Cardiac Output (mL/s)	Resting Heart Rate (beats/min)	Mean Arterial Pressure (mmHg)	Maximum LV Pressure (mmHg)	Mean LAD Flowrate (mL/s)	Mean LCX Flowrate (mL/s)	Mean RCA Flowrate (mL/s)	Myocardial Blood Flow (mL/min/g)
Pre-TAVR	Severe	0.9	4.54	60	5497	55	115.8	205.9	1.29	0.92	0.21	2.42
Post-TAVR	-	1.04	3.13	64	3770	60	112.4	161.1	1.00	0.73	0.03	2.39

Figure 20: *Predicted cardiac and coronary hemodynamics (Patient #13). The plots on the left and right illustrate the pre-TAVR and post-TAVR data respectively. Before the intervention, this patient suffered from severe aortic stenosis. After TAVR, the mean pressure gradient, max aortic valve velocity, cardiac output, MAP, max LV pressure and myocardial blood flow all decreased while ejection fraction and resting heart rate increased.*

The examples illustrated by patients #18, #13 and #16 provide insight into the capabilities of the C3VM-LPM to compute patient specific cardiovascular data, including non-invasive insight into the hemodynamics in the coronary arteries. It also further highlights the patient specific nature of treating aortic stenosis and the resulting hemodynamics.

3.5. Discussion

As medicine becomes more patient centered, there is a strong motivation to create patient specific treatment approaches and design tools capable of capturing individual health data. The union between computational science, medical imaging, and cardiology has opened the doors to numerous new patient specific cardiovascular tools. “Cardiology is flow” [72] and providing

clinicians with a non-invasive window into coronary blood flow and global cardiovascular parameters can be advantageous in helping clinicians and cardiologists make treatment decisions [33, 73, 74]. Furthermore, the development of computationally efficient methods to non-invasively quantify blood flow may be useful in high volume clinical settings.

In this paper, we develop a novel LPM framework which utilizes non-invasive inputs to simulate blood flow waveforms in the main proximal coronary branches (LAD, LCX and RCA) as well as other global cardiovascular hemodynamic parameters. The model was then applied to 19 patients undergoing TAVR to examine the impact of the procedure on various cardiovascular metrics. The coronary flow results from the framework were compared with those from a patient specific 3D FSI model (n=19) and a model sensitivity analysis was conducted.

3.5.1 Coronary Blood Flow Increase or Decrease Varies in Patients After TAVR

The coronary waveforms from the lumped model for patients with and without aortic stenosis were very consistent with the waveforms reported in literature [57, 75, 70, 76]. For patients without aortic stenosis, a clear bi-phasic flow pattern was present with lower flow during systole and more flow occurring in diastole. In the presence of aortic stenosis, the blood flow during systole decreased considerably (in some cases resulting in zero or negative retrograde flow) and most of the blood flow was delivered to the coronaries in diastole. Garcia et al. [57], Hongo et al. [75] and others [70, 76] have observed very similar flow patterns in healthy and aortic stenosis cases.

After TAVR, the model yielded an increase in both the mean and peak flow rates during systole but a decrease during diastole. This trend has been observed in numerous other studies regarding the relationship between coronary flow and TAVR [70, 77, 78, 79]. In patients with aortic stenosis, systolic blood flow from the ventricle can be limited due to the obstruction caused by the stenotic valve, thus limiting coronary flow. Additionally, the elevated LV pressure enhances the impact of extravascular compression, further restricting systolic coronary flow. After TAVR, the increase in valve orifice area and reduction in ventricular pressure leads to increased blood flow during

systole, resulting in an increase in systolic coronary flow. Since aortic stenosis is a systolic phenomenon that impacts the opening rather than closing of the valve, TAVR has been shown to have a smaller impact on the diastolic phases and thus less impact on coronary flow during diastole [77, 78].

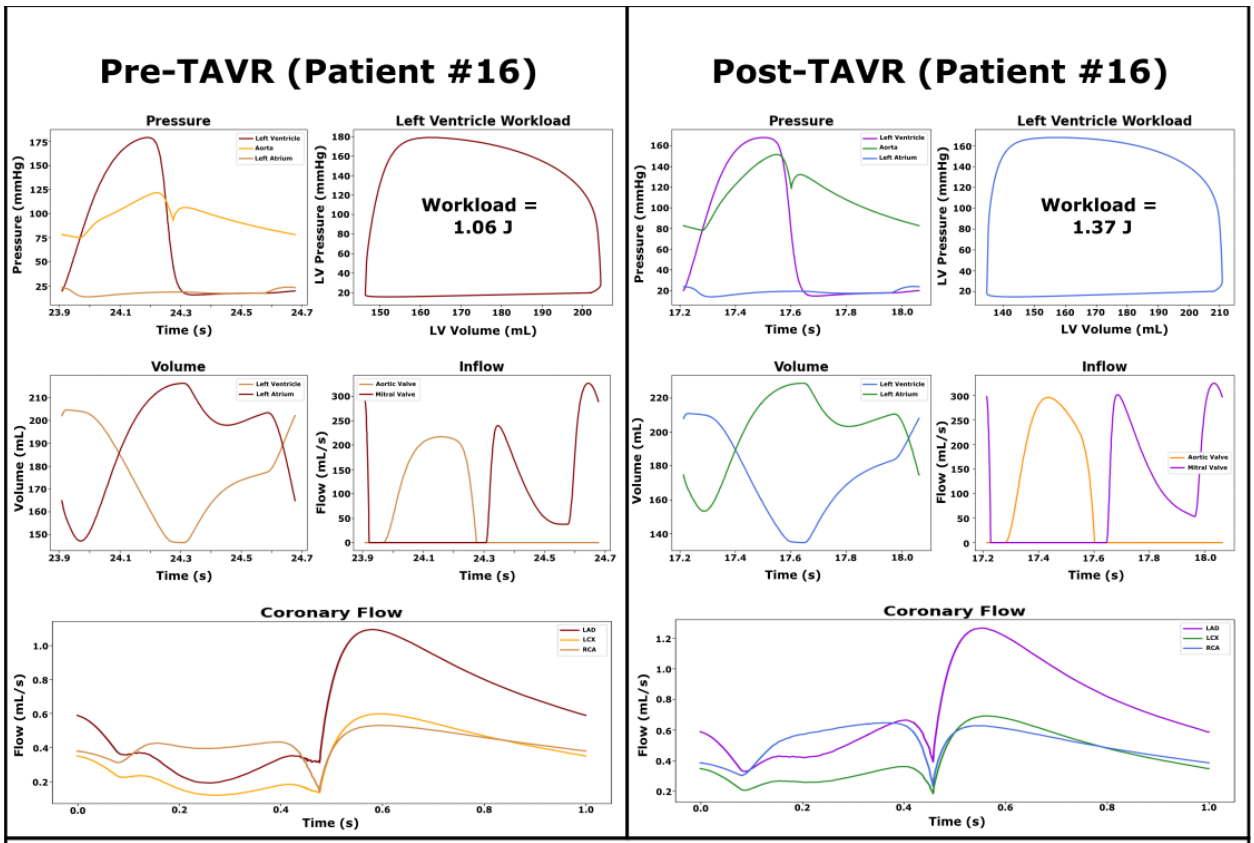

	Aortic Stenosis Severity	Aortic Valve Area (cm^2)	Max AV Velocity (m/s)	Ejection Fraction (%)	Cardiac Output (mL/s)	Resting Heart Rate (beats/min)	Mean Arterial Pressure (mmHg)	Maximum LV Pressure (mmHg)	Mean LAD Flowrate (mL/s)	Mean LCX Flowrate (mL/s)	Mean RCA Flowrate (mL/s)	Myocardial Blood Flow (mL/min/g)
Pre-TAVR	Severe	0.5	4.71	64	3849	78	94.7	178.8	0.59	0.34	0.42	2.05
Post-TAVR	-	0.9	3.17	62	4628	71	108.6	167.6	0.72	0.41	0.51	2.06

Figure 21*: Predicted cardiac and coronary hemodynamics (Patient #16). The plots on the left and right illustrate the pre-TAVR and post-TAVR data respectively. Before the intervention, this patient suffered from severe aortic stenosis. After TAVR, the mean pressure gradient, max aortic valve velocity, ejection fraction, resting heart rate and max LV pressure decreased while cardiac output and MAP increased. Coronary blood flow rate increased while the overall myocardial blood flow increased slightly after TAVR.*

This study demonstrated individual differences in terms of coronary blood flow increase or decrease for the full cardiac cycle after TAVR. This varying outcome has been previously noted, for instance, Ben-Dor et al. [70] found that of the 90 patients in their clinical study, only 48% had a ≥10% increase in their left main coronary flow velocity after TAVR. Relative reduction in coronary blood flow has been associated with various negative cardiovascular events including decreased ventricle contractile function, ventricular dysfunction and increased risk of ischemic events [80, 81]. Furthermore, moderate or prolonged reduction in coronary blood flow may lead to molecular and morphological changes in the myocardium and may worsen heart failure [80].

There is currently uncertainty around the optimal management and treatment of AS and coexisting CAD [82]. There is a current debate about whether CAD should be treated before AS, alongside the AS or after the AS [83, 18, 78]. Additionally, some preliminary research indicates that negative coronary events after TAVR may be driven by impaired coronary flow dynamics and coronary hypoperfusion related to the TAVR prosthesis [60]. Currently clinicians have relatively limited options to examine coronary flow hemodynamics in a rapid and non-invasive fashion [84]. By using frameworks like the one presented in this paper, clinicians may eventually be able understand, quantify, and predict adverse coronary related events surrounding TAVR that otherwise might be missed without this additional data and insight.

3.5.2 Global Hemodynamic Metrics Vary in Patients After TAVR

The increase or decrease in certain computed global hemodynamic parameters (LV workload, SBP, DBP and CO) varies from subject to subject after TAVR. LV workload for instance decreased in 10 patients while increasing for 9 subjects after TAVR. While the workload often decreases post-TAVR due to a reduction in afterload [28], this only occurred in a subset of our subjects. This observed increase in workload may be driven by the interplay of various cardiovascular factors such as the presence of mixed valvular disease including mitral valve regurgitation or post-TAVR complications such as paravalvular leakage (2 patients had mild and moderate to severe PVL respectively) [27]. In regard to blood pressure, according to our model SBP, DBP and MAP all increased in 68% of the subjects. Similarly, Perlman et al. [85] found that of 150 subjects who underwent TAVR, 51% had sustained increases in blood pressure after the procedure. Interestingly, in this study, subjects with increased blood pressure after TAVR had better a long-term prognosis and fewer adverse events after 30 days and 12 months [85]. While there are some disagreements regarding the benefits and drawbacks of increased blood pressure after TAVR, various studies have found that blood pressure increase or decrease after TAVR is highly dependant on the individual [67].

Unlike the other global metrics, aortic valve pressure gradient decreased in all but one subject after TAVR. Since implanting the new valve (and increasing the valve effective orifice area) is one of the main aims this procedure, it is expected that the valve pressure gradient would decrease after TAVR [28, 35]. In all, due to the highly interconnected and dynamic nature of cardiovascular system,

this patient specific variability in global hemodynamics can likely help explain why coronary blood flow increase or decrease after TAVR also varies.

3.5.3 Limitation of Current LPMs to Capture Coronary Blood Flow

While there exist some LPM frameworks developed for the coronary arteries [47, 48, 55, 86, 87, 88, 89] very few include patient specific coronary and cardiac segments. In work by Duanmu et al. [55], the authors use CT images to extract details of the coronary branches to tune the circuit elements but use generic heart functions as inputs to the coronary arteries. Li et al. [47] also used a similar approach but tuned the model parameters to match generic coronary artery flow patterns for a single patient. Calderan et al. [89] applied both an in-vivo model and lumped model to characterize the impact of TAVR on coronary artery flow but relied on semi-generic parameters and did not divide the blood flow into the 3 main coronary arteries. Currently, none of the existing pure LPM frameworks can simulate and examine the impact of TAVR on coronary blood flow in a patient specific manner.

In recent years, most of the developments related patient specific computational cardiology models have made use of 3D based modelling (computational fluid dynamics, FSI, Lattice-Boltzmann and others). These powerful models can provide detailed insight into parameters such as wall shear stress, multi-dimensional blood flow patterns, vortical structures and other key parameters. On the other end of the spectrum, LPM offers a simpler and computationally cheaper method to simulate a series of global cardiovascular metrics and flow/pressure waveforms. While LPM sacrifices the ability to compute many of the 3D based parameters, it reduces the computational time from hours or days to seconds and makes model automation easier.

3.6. Limitations

This study was performed and validated using 19 patients and showed strong agreement with both the pre- and post-TAVR results from the 3D FSI models. Numerous FSI models have been previously shown to accurately simulate blood flow in the cardiovascular system, including the coronary arteries [46, 56, 90, 91]. Furthermore, the cardiac LPM was previously designed to capture complex valvular, vascular, and ventricular diseases and has been previously validated against 49 patients with a wide range of diseases [35]. Nevertheless, future studies must consider validating the coronary flow waveforms from the model against invasive coronary catheter data.

As outlined in the analysis, the model is relatively sensitive to changes in coronary vessel cross sectional area, which is currently computed from 3D CT-based reconstructions. While a standard segmentation and reconstruction process is applied to all patients, it is currently done manually and is prone to a small degree of human error. This error could be reduced by using coronary CT angiography or standard angiography which produce higher quality coronary images.

The model is also sensitive to changes in mean arterial pressure, an input parameter currently obtained using a clinical grade sphygmomanometer. As coronary perfusion pressure (which is partially based on MAP) increases in healthy patients, the body naturally adjusts coronary resistance to help regulate the coronary blood flow rate [63]. Although it is not fully clear how this autoregulation is impacted by the presences of AS and CAD and only occurs for range of pressures, future models could be enhanced through the addition of patient specific control loops to further regulate the relationship between coronary pressure and flow.

Acknowledgments

This work was supported by NSERC Discovery Grant (RGPIN-2017-05349). NSERC (https://www.nserc-crsng.gc.ca/index_eng.asp) as the funders had no role in study design, data collection and analysis, decision to publish, or preparation of the manuscript.

Competing Interests

No authors report a conflict of interest and there are no relationships with industry for this work.

References

1. Bourantas, C. V. & Serruys, P. W. Evolution of Transcatheter Aortic Valve Replacement. *Circ. Res.* **114**, 1037–1051 (2014).
2. Carroll, J. D. *et al.* STS-ACC TVT Registry of Transcatheter Aortic Valve Replacement. *J. Am. Coll. Cardiol.* **76**, 2492–2516 (2020).
3. Elbaz-Greener, G. *et al.* Profiling Hospital Performance Based on Mortality After Transcatheter Aortic Valve Replacement in Ontario, Canada. *Circ. Cardiovasc. Qual. Outcomes* **11**, e004947 (2018).
4. Mach, M. *et al.* Vascular Complications in TAVR: Incidence, Clinical Impact, and Management. *J. Clin. Med.* **10**, 5046 (2021).
5. Ribeiro, H. B. *et al.* Coronary Obstruction Following Transcatheter Aortic Valve Implantation. *JACC Cardiovasc. Interv.* **6**, 452–461 (2013).
6. Mentias, A. *et al.* Incidence and Outcomes of Acute Coronary Syndrome After Transcatheter Aortic Valve Replacement. *JACC Cardiovasc. Interv.* **13**, 938–950 (2020).
7. Armijo, G., Nombela-Franco, L. & Tirado-Conte, G. Cerebrovascular Events After Transcatheter Aortic Valve Implantation. *Front. Cardiovasc. Med.* **5**, 104 (2018).
8. Eleid, M. Interventional management of paravalvular leak. *Heart* **104**, 1797–1802 (2018).
9. Feldman, D. R. *et al.* Comorbidity Burden and Adverse Outcomes After Transcatheter Aortic Valve Replacement. *J. Am. Heart Assoc.* **10**, e018978 (2021).
10. O'Sullivan, C. J. & Wenaweser, P. Optimizing clinical outcomes of transcatheter aortic valve implantation patients with comorbidities. *Expert Rev. Cardiovasc. Ther.* **13**, 1419–1432 (2015).
11. American Heart Association. *Cardiovascular Disease: A Costly Burden for America, Projections Through 2035*. (2017).
12. World Health Organization. Cardiovascular diseases (CVDs). *World Health Organization* https://www.who.int/news-room/fact-sheets/detail/cardiovascular-diseases-(cvds) (2017).
13. Nai Fovino, L. *et al.* Coronary Angiography After Transcatheter Aortic Valve Replacement (TAVR) to Evaluate the Risk of Coronary Access Impairment After TAVR-in-TAVR. *J. Am. Heart Assoc.* **9**, e016446 (2020).
14. Tarantini, G. & Nai Fovino, L. Coronary Access and TAVR-in-TAVR. *JACC Cardiovasc. Interv.* **13**, 2539–2541 (2020).
15. Adamson, P. D. & Newby, D. E. Non-invasive imaging of the coronary arteries. *Eur. Heart J.* **40**, 2444–2454 (2019).
16. Ciampi, Q. *et al.* Functional, Anatomical, and Prognostic Correlates of Coronary Flow Velocity Reserve During Stress Echocardiography. *J. Am. Coll. Cardiol.* **74**, 2278–2291 (2019).
17. Blanken, C. P. S. *et al.* Coronary Flow Assessment Using Accelerated 4D Flow MRI With Respiratory Motion Correction. *Front. Bioeng. Biotechnol.* **9**, 725833 (2021).
18. Faroux, L. *et al.* Coronary Artery Disease and Transcatheter Aortic Valve Replacement. *J. Am. Coll. Cardiol.* **74**, 362–372 (2019).
19. Khodaei, S. *et al.* Personalized intervention cardiology with transcatheter aortic valve replacement made possible with a non-invasive monitoring and diagnostic framework. *Sci. Rep.* **11**, 10888 (2021).
20. Khodaei, S. *et al.* Towards a non-invasive computational diagnostic framework for personalized cardiology of transcatheter aortic valve replacement in interactions with

complex valvular, ventricular and vascular disease. *Int. J. Mech. Sci.* **202–203**, 106506 (2021).
21. Primeaux, J., Salavitabar, A., Lu, J. C., Grifka, R. G. & Figueroa, C. A. Characterization of Post-Operative Hemodynamics Following the Norwood Procedure Using Population Data and Multi-Scale Modeling. *Front. Physiol.* **12**, 603040 (2021).
22. Ceballos, A., Prather, R., Divo, E., Kassab, A. J. & DeCampli, W. M. Patient-Specific Multi-Scale Model Analysis of Hemodynamics Following the Hybrid Norwood Procedure for Hypoplastic Left Heart Syndrome: Effects of Reverse Blalock–Taussig Shunt Diameter. *Cardiovasc. Eng. Technol.* **10**, 136–154 (2019).
23. Vardhan, M. *et al.* Non-invasive characterization of complex coronary lesions. *Sci. Rep.* **11**, 8145 (2021).
24. Mazzi, V. *et al.* Early Atherosclerotic Changes in Coronary Arteries are Associated with Endothelium Shear Stress Contraction/Expansion Variability. *Ann. Biomed. Eng.* **49**, 2606–2621 (2021).
25. Morris, P. D. *et al.* Computational fluid dynamics modelling in cardiovascular medicine. *Heart* **102**, 18–28 (2016).
26. Mittal, R. *et al.* Computational modeling of cardiac hemodynamics: Current status and future outlook. *J. Comput. Phys.* **305**, 1065–1082 (2016).
27. Keshavarz-Motamed, Z. *et al.* Mixed Valvular Disease Following Transcatheter Aortic Valve Replacement: Quantification and Systematic Differentiation Using Clinical Measurements and Image-Based Patient-Specific In Silico Modeling. *J. Am. Heart Assoc.* **9**, (2020).
28. Ben-Assa, E. *et al.* Ventricular stroke work and vascular impedance refine the characterization of patients with aortic stenosis. *Sci. Transl. Med.* **11**, eaaw0181 (2019).
29. Updegrove, A. *et al.* SimVascular: An Open Source Pipeline for Cardiovascular Simulation. *Ann. Biomed. Eng.* **45**, 525–541 (2017).
30. Arthurs, C. J. *et al.* CRIMSON: An open-source software framework for cardiovascular integrated modelling and simulation. *PLOS Comput. Biol.* **17**, e1008881 (2021).
31. Taylor, C. A., Fonte, T. A. & Min, J. K. Computational Fluid Dynamics Applied to Cardiac Computed Tomography for Noninvasive Quantification of Fractional Flow Reserve. *J. Am. Coll. Cardiol.* **61**, 2233–2241 (2013).
32. Driessen, R. S. *et al.* Comparison of Coronary Computed Tomography Angiography, Fractional Flow Reserve, and Perfusion Imaging for Ischemia Diagnosis. *J. Am. Coll. Cardiol.* **73**, 161–173 (2019).
33. Holmes, J. W. & Lumens, J. Clinical Applications of Patient-Specific Models: The Case for a Simple Approach. *J Cardiovasc. Transl. Res.* **11**, 71–79 (2018).
34. Garber, L., Khodaei, S. & Keshavarz-Motamed, Z. The Critical Role of Lumped Parameter Models in Patient-Specific Cardiovascular Simulations. *Arch. Comput. Methods Eng.* (2021) doi:10.1007/s11831-021-09685-5.
35. Keshavarz-Motamed, Z. A diagnostic, monitoring, and predictive tool for patients with complex valvular, vascular and ventricular diseases. *Sci. Rep.* **10**, 6905 (2020).
36. Keshavarz-Motamed, Z., Garcia, J., Pibarot, P., Larose, E. & Kadem, L. Modeling the impact of concomitant aortic stenosis and coarctation of the aorta on left ventricular workload. *J. Biomech.* **44**, 2817–2825 (2011).
37. Keshavarz-Motamed, Z., Edelman, E. R., Garcia, J., Dahdah, N. & Kadem, L. The role of aortic compliance in determination of coarctation severity: lumped parameter modeling, in vitro study and clinical evaluation. *J Biomech* **48**, 4229–4237 (2015).

38. Keshavarz-Motamed, Z. *et al.* Effect of coarctation of the aorta and bicuspid aortic valve on flow dynamics and turbulence in the aorta using particle image velocimetry. *Exp. Fluids* **55**, 1696 (2014).
39. Keshavarz-Motamed, Z. *et al.* A new approach for the evaluation of the severity of coarctation of the aorta using Doppler velocity index and effective orifice area: In vitro validation and clinical implications. *J. Biomech.* **45**, 1239–1245 (2012).
40. Benevento, E., Djebbari, A., Keshavarz-Motamed, Z., Cecere, R. & Kadem, L. Hemodynamic Changes following Aortic Valve Bypass: A Mathematical Approach. *PLOS ONE* **10**, e0123000 (2015).
41. Keshavarz-Motamed, Z. *et al.* Elimination of Transcoarctation Pressure Gradients Has No Impact on Left Ventricular Function or Aortic Shear Stress After Intervention in Patients With Mild Coarctation. *JACC Cardiovasc. Interv.* **9**, 1953–1965 (2016).
42. Sadeghi, R., Khodaei, S., Ganame, J. & Keshavarz-Motamed, Z. Towards non-invasive computational-mechanics and imaging-based diagnostic framework for personalized cardiology for coarctation. *Sci. Rep.* **10**, 9048 (2020).
43. Keshavarz-Motamed, Z. *et al.* Non-Invasive Determination of Left Ventricular Workload in Patients with Aortic Stenosis Using Magnetic Resonance Imaging and Doppler Echocardiography. *PLoS ONE* **9**, e86793 (2014).
44. Sadeghi, R. *et al.* Reducing Morbidity and Mortality in Patients With Coarctation Requires Systematic Differentiation of Impacts of Mixed Valvular Disease on Coarctation Hemodynamics. *J. Am. Heart Assoc.* **11**, e022664 (2022).
45. Mantero, S., Pietrabissa, R. & Fumero, R. The coronary bed and its role in the cardiovascular system: a review and an introductory single-branch model. *J. Biomed. Eng.* **14**, 109–116 (1992).
46. Kim, H. J. *et al.* Patient-Specific Modeling of Blood Flow and Pressure in Human Coronary Arteries. *Ann. Biomed. Eng.* **38**, 3195–3209 (2010).
47. Li, B., Wang, W., Mao, B. & Liu, Y. A Method to Personalize the Lumped Parameter Model of Coronary Artery. *Int. J. Comput. Methods* **16**, 1842004 (2019).
48. Mao, B. *et al.* Lumped parameter model based surgical planning for CABG. *Med. Nov. Technol. Devices* **2**, 100014 (2019).
49. Yin, M., Yazdani, A. & Karniadakis, G. E. One-dimensional modeling of fractional flow reserve in coronary artery disease: Uncertainty quantification and Bayesian optimization. *Comput. Methods Appl. Mech. Eng.* **353**, 66–85 (2019).
50. Tajeddini, F. *et al.* High precision invasive FFR, low-cost invasive iFR, or noninvasive CFR?: optimum assessment of coronary artery stenosis based on the patient-specific computational models. *Int. J. Numer. Methods Biomed. Eng.* **36**, (2020).
51. SimVascular Development Team. SimVascular Clinical Test Cases - Coronary Normal. *SimVascular* https://simvascular.github.io/clinicalCase3.html (2017).
52. Razminia, M. *et al.* Validation of a new formula for mean arterial pressure calculation: The new formula is superior to the standard formula. *Catheter. Cardiovasc. Interv.* **63**, 419–425 (2004).
53. Zhou, Y., Kassab, G. S. & Molloi, S. On the design of the coronary arterial tree: a generalization of Murray's law. *Phys. Med. Biol.* **44**, 2929–2945 (1999).
54. Sankaran, S. *et al.* Patient-Specific Multiscale Modeling of Blood Flow for Coronary Artery Bypass Graft Surgery. *Ann. Biomed. Eng.* **40**, 2228–2242 (2012).

55. Duanmu, Z., Yin, M., Fan, X., Yang, X. & Luo, X. A patient-specific lumped-parameter model of coronary circulation. *Sci. Rep.* **8**, 874 (2018).
56. Coogan, J. S., Humphrey, J. D. & Figueroa, C. A. Computational simulations of hemodynamic changes within thoracic, coronary, and cerebral arteries following early wall remodeling in response to distal aortic coarctation. *Biomech. Model. Mechanobiol.* **12**, 79–93 (2013).
57. Garcia, D. *et al.* Impairment of coronary flow reserve in aortic stenosis. *J. Appl. Physiol.* **106**, 113–121 (2009).
58. Ofili, E. O. *et al.* Differential characterization of blood flow, velocity, and vascular resistance between proximal and distal normal epicardial human coronary arteries: Analysis by intracoronary Doppler spectral flow velocity. *Am. Heart J.* **130**, 37–46 (1995).
59. Yushkevich, P. A. *et al.* User-guided 3D active contour segmentation of anatomical structures: Significantly improved efficiency and reliability. *NeuroImage* **31**, 1116–1128 (2006).
60. Faroux, L. *et al.* Coronary Artery Disease and Transcatheter Aortic Valve Replacement. *J. Am. Coll. Cardiol.* **74**, 362–372 (2019).
61. Weller, H. G., Tabor, G., Jasak, H. & Fureby, C. A tensorial approach to computational continuum mechanics using object-oriented techniques. *Comput. Phys.* **12**, 620 (1998).
62. Tuković, Ž., Karač, A., Cardiff, P., Jasak, H. & Ivanković, A. OpenFOAM Finite Volume Solver for Fluid-Solid Interaction. *Trans. FAMENA* **42**, 1–31 (2018).
63. Goodwill, A. G., Dick, G. M., Kiel, A. M. & Tune, J. D. Regulation of Coronary Blood Flow. in *Comprehensive Physiology* (ed. Terjung, R.) 321–382 (Wiley, 2017). doi:10.1002/cphy.c160016.
64. Benevento, E., Djebbari, A., Keshavarz-Motamed, Z., Cecere, R. & Kadem, L. Hemodynamic Changes following Aortic Valve Bypass: A Mathematical Approach. *PLOS ONE* **10**, e0123000 (2015).
65. Tran, J. S., Schiavazzi, D. E., Ramachandra, A. B., Kahn, A. M. & Marsden, A. L. Automated tuning for parameter identification and uncertainty quantification in multi-scale coronary simulations. *Comput. Fluids* **142**, 128–138 (2017).
66. Baumgartner, H. *et al.* Recommendations on the echocardiographic assessment of aortic valve stenosis: a focused update from the European Association of Cardiovascular Imaging and the American Society of Echocardiography. *Eur. Heart J. - Cardiovasc. Imaging* **18**, 254–275 (2017).
67. Yeoh, J. & MacCarthy, P. The Pressure Is On: Implications of Blood Pressure After Aortic Valve Replacement. *J. Am. Heart Assoc.* **8**, e014631 (2019).
68. Perlman, G. Y. *et al.* Post-Procedural Hypertension Following Transcatheter Aortic Valve Implantation. *JACC Cardiovasc. Interv.* **6**, 472–478 (2013).
69. Ramanathan, T. & Skinner, H. Coronary Blood Flow. *Contin. Educ. Anaesth. Crit. Care Pain* **5**, 61–64 (2005).
70. Ben-Dor, I. *et al.* Coronary Blood Flow in Patients With Severe Aortic Stenosis Before and After Transcatheter Aortic Valve Implantation. *Am. J. Cardiol.* **114**, 1264–1268 (2014).
71. Ramanathan, T. & Skinner, H. Coronary blood flow. *Contin. Educ. Anaesth. Crit. Care Pain* **5**, 61–64 (2005).
72. Richter, Y. & Edelman, E. R. Cardiology Is Flow. *Circulation* **113**, 2679–2682 (2006).
73. Gray, R. A. & Pathmanathan, P. Patient-Specific Cardiovascular Computational Modeling: Diversity of Personalization and Challenges. *J Cardiovasc. Transl. Res.* **11**, 80–88 (2018).

74. Niederer, S. A., Lumens, J. & Trayanova, N. A. Computational models in cardiology. *Nat. Rev. Cardiol.* **16**, 100–111 (2019).
75. Hongo, M. *et al.* Relation of phasic coronary flow velocity profile to clinical and hemodynamic characteristics of patients with aortic valve disease. *Circulation* **88**, 953–960 (1993).
76. Hozumi, T. *et al.* Noninvasive Assessment of Significant Left Anterior Descending Coronary Artery Stenosis by Coronary Flow Velocity Reserve With Transthoracic Color Doppler Echocardiography. *Circulation* **97**, 1557–1562 (1998).
77. Ahmad, Y. *et al.* Coronary Hemodynamics in Patients With Severe Aortic Stenosis and Coronary Artery Disease Undergoing Transcatheter Aortic Valve Replacement. *JACC Cardiovasc. Interv.* **11**, 2019–2031 (2018).
78. Vendrik, J. *et al.* Long-Term Effects of Transcatheter Aortic Valve Implantation on Coronary Hemodynamics in Patients With Concomitant Coronary Artery Disease and Severe Aortic Stenosis. *J. Am. Heart Assoc.* **9**, e015133 (2020).
79. Hildick-Smith, D. J. R. & Shapiro, L. M. Coronary flow reserve improves after aortic valve replacement for aortic stenosis: an adenosine transthoracic echocardiography study. *J. Am. Coll. Cardiol.* **36**, 1889–1896 (2000).
80. Heusch, G. Myocardial ischemia: lack of coronary blood flow, myocardial oxygen supply-demand imbalance, or what? *Am. J. Physiol.-Heart Circ. Physiol.* **316**, H1439–H1446 (2019).
81. McConkey, H. Z. R. *et al.* Coronary Microcirculation in Aortic Stenosis: A Physiological Hornets' Nest. *Circ. Cardiovasc. Interv.* **12**, e007547 (2019).
82. Cangemi, S. *et al.* Management of concomitant coronary artery disease and aortic valve stenosis in the era of transcatheter aortic valve treatment. *Mini-Invasive Surg.* (2022) doi:10.20517/2574-1225.2021.99.
83. Cavender, M. A. & Forrest, J. K. Planning for the Next Transcatheter Aortic Valve Replacement Starts Today. *Circ. Cardiovasc. Interv.* **13**, (2020).
84. Adamson, P. D. & Newby, D. E. Non-invasive imaging of the coronary arteries. *Eur. Heart J.* **40**, 2444–2454 (2019).
85. Perlman, G. Y. *et al.* Post-Procedural Hypertension Following Transcatheter Aortic Valve Implantation. *JACC Cardiovasc. Interv.* **6**, 472–478 (2013).
86. Maasrani, M. *et al.* Simulations of fluxes in diseased coronary network using an electrical model. in *The XIX International Conference on Electrical Machines - ICEM 2010* 1–6 (IEEE, 2010). doi:10.1109/ICELMACH.2010.5608460.
87. Mynard, J. P., Penny, D. J. & Smolich, J. J. Scalability and in vivo validation of a multiscale numerical model of the left coronary circulation. *Am. J. Physiol.-Heart Circ. Physiol.* **306**, H517–H528 (2014).
88. Pietrabissa, R., Mantero, S., Marotta, T. & Menicanti, L. A lumped parameter model to evaluate the fluid dynamics of different coronary bypasses. *Med. Eng. Phys.* **18**, 477–484 (1996).
89. Calderan, J., Mao, W., Sirois, E. & Sun, W. Development of an In Vitro Model to Characterize the Effects of Transcatheter Aortic Valve on Coronary Artery Flow: Thoughts and Progress. *Artif. Organs* **40**, 612–619 (2016).
90. Vardhan, M. *et al.* Non-invasive characterization of complex coronary lesions. *Sci. Rep.* **11**, 8145 (2021).

91. Zhong, L. *et al.* Application of Patient-Specific Computational Fluid Dynamics in Coronary and Intra-Cardiac Flow Simulations: Challenges and Opportunities. *Front. Physiol.* **9**, 742 (2018).
92. Mirramezani, M., Diamond, S. L., Litt, H. I. & Shadden, S. C. Reduced Order Models for Transstenotic Pressure Drop in the Coronary Arteries. *J. Biomech. Eng.* **141**, 031005 (2019).
93. Tanné, D., Kadem, L., Rieu, R. & Pibarot, P. Hemodynamic impact of mitral prosthesis-patient mismatch on pulmonary hypertension: an in silico study. *J Appl Physiol* **295**, 1916–1926 (2008).
94. Stergiopulos, N., Meister, J. J. & Westerhof, N. Determinants of stroke volume and systolic and diastolic aortic pressure. *Am. J. Physiol.-Heart Circ. Physiol.* **270**, H2050–H2059 (1996).
95. Mynard, J. P., Davidson, M. R., Penny, D. J. & Smolich, J. J. A simple, versatile valve model for use in lumped parameter and one-dimensional cardiovascular models. *Int. J. Numer. Methods Biomed. Eng.* **28**, 626–641 (2012).

Chapter 4: Conclusions and Future Directions

4.1 Conclusions

Cardiovascular lumped parameter modelling is a useful tool to rapidly generate patient-specific hemodynamic data. It utilizes a series of electronic circuits with tunable elements and an optimization algorithm to simulate blood flow waveforms in different cardiac and circulatory regions. Depending on the purpose and desired complexity of the model, additional circuit compartments, which represent cardiovascular components like valves or vessels, can be added or removed. While the outputs are not as detailed as other higher order modelling techniques, the results can be generated in a fraction of the time and require substantially less pre and post processing, making it a viable approach for real-world, high-volume clinics.

In this thesis, a patient-specific, non-invasive lumped parameter framework focusing primarily on the coronary arteries (LAD, LCX and RCA) was developed and validated on a series of patients undergoing TAVR (n=19). The model used only non-invasive clinical data as inputs: CT images, echocardiography data and cuff blood pressure. Blood flow and pressure waveforms were simulated in the coronary arteries alongside the left ventricle, aortic valve, left atrium, mitral valve, and aorta for each subject. Additional hemodynamic metrics such as left ventricle workload and myocardial blood flow rate were computed on a patient-specific basis.

To validate the model results, the diastolic coronary flow waveforms for each subject were compared with results from a patient specific 3D FSI model previously developed in the lab. Overall, there was strong qualitative and quantitative agreement with the FSI results during both pre- and post-TAVR. Numerous hemodynamic metrics were generated and tracked at both time points and compared for the 19 subjects. The clinical metrics that were directly tied to TAVR such as the aortic valve area and net pressure gradient across the aortic valve improve for almost all the subjects after the intervention. As for the hemodynamic data, there was substantial variability in terms of their increase or decrease post-TAVR. On average, LV workload and maximum LV pressure decreased while cardiac output, aortic pressure and resting heart rate increased. These individual variations in hemodynamic parameters helped contribute to variability in the coronary blood flow increase or decrease in the different vessels (LAD, LCX and RCA) and overall myocardial blood flow after the procedure. Some preliminary research

indicates that negative coronary events after TAVR may be partially driven by impaired or reduced coronary blood flow dynamics related to the TAVR prosthesis [16].

In conclusion, since there was large patient specific variability in hemodynamic changes after TAVR, having a non-invasive, patient-specific tool to rapidly quantify cardiac, circulatory and coronary data may eventually aid clinicians to better manage patient suffering from AS and CAD and improve the planning of the associated interventions.

4.2 Future Directions

With the newly developed C3VM lumped parameter framework, we can now simulate blood flow waveforms and hemodynamic metrics in the major cardiac chambers and vessels as well as the coronary arteries. In this work, a major focus is on examining the changes in metrics such as coronary blood flow rate (and myocardial blood flow) in the pre- and post-TAVR settings. Going forward, it would be interesting to see the relationship between these indices and longer-term clinical outcomes. While there is some research in this area [36, 37, 38], it is scarce and often does not focus directly on the coronary arteries. It would be interesting for instance to conduct a longitudinal study and collect non-invasive data from subjects at multiple time points pre- and post-TAVR. With this data, the C3VM model could be applied to see the relationships between the generated metrics like change in myocardial blood flow after TAVR and 6-month or 2-year mortality rate. This future research would be import since this could further highlight the validity of the model and emphasize its clinical utility.

With the enormous growth of machine learning (ML) over the past decade, it would also be interesting to combine the generated blood flow waveforms from the C3VM model with some ML algorithms to classify the severity of certain cardiovascular diseases (CAD severity for instance). A series of features could be extracted from the generated waveforms (such as mean flow, peak flow, flow derivates, etc.) or the waveforms could be transformed using signal processing techniques like fast Fourier transforms or continuous wavelet transforms to extract more complex features. If a large enough dataset was available, the features could be used in different ML algorithms (like logistic regression, random forest, or more complex neural network models) to attempt to classify the severity of a desired cardiovascular diseases.

Finally, future developments are needed to improve the framework for patients with complex cases of CAD. In Chapter 3, we outline that the model does not perform as well in cases where

patients have complex vessel geometry and CAD (ex. multi vessel CAD, highly tortuous vessels and LMCA CAD, etc.). Future developments in this area could include using different algorithms to better account for highly varying coronary vessel diameters or using different imaging modalities (such as CCTA) to better visualize the complex build-up of plaque in the arteries.

References

From Chapter 1 and Chapter 4

1. Zipes, D. P. *et al. Braunwald's Heart Disease: A Textbook of Cardiovascular Medicine Eleventh Edition*. (Elsevier, 2019).
2. World Health Organization. Cardiovascular diseases (CVDs). *World Health Organization* https://www.who.int/news-room/fact-sheets/detail/cardiovascular-diseases-(cvds) (2017).
3. Mensah, G. A., Roth, G. A. & Fuster, V. The Global Burden of Cardiovascular Diseases and Risk Factors. *J. Am. Coll. Cardiol.* **74**, 2529–2532 (2019).
4. Centers for Disease Control and Prevention. Heart Disease and Stroke. *National Center for Chronic Disease Prevention and Health Promotion (NCCDPHP)* https://www.cdc.gov/chronicdisease/resources/publications/factsheets/heart-disease-stroke.htm#:~:text=Leading%20risk%20factors%20for%20heart,unhealthy%20diet%2C%20and%20physical%20inactivity.
5. American Heart Association. What is Cardiovascular Disease? *www.heart.org* https://www.heart.org/en/health-topics/consumer-healthcare/what-is-cardiovascular-disease (2017).
6. de Azevedo Filho, A. F., Accorsi, T. A. & Ribeiro, H. B. Coronary Artery Disease in Patients with Aortic Stenosis and Transcatheter Aortic Valve Implantation: Implications for Management. *Eur. Cardiol. Rev.* **16**, e49 (2021).
7. Lindman, B. R. *et al.* Calcific aortic stenosis. *Nat. Rev. Dis. Primer* **2**, 16006 (2016).
8. Intermountain Healthcare. Aortic Valve Stenosis. *Heart Care - Aortic Valve Stenosis* https://intermountainhealthcare.org/services/heart-care/conditions/aortic-valve-stenosis/.
9. Clavel, M.-A. & Pibarot, P. A Decade of Revolutions in Calcific Aortic Stenosis. *Cardiol. Clin.* **38**, xiii–xiv (2020).
10. Carroll, J. D. *et al.* STS-ACC TVT Registry of Transcatheter Aortic Valve Replacement. *J. Am. Coll. Cardiol.* **76**, 2492–2516 (2020).
11. Grube, E. & Sinning, J.-M. The "Big Five" Complications After Transcatheter Aortic Valve Replacement. *JACC Cardiovasc. Interv.* **12**, 370–372 (2019).
12. American Heart Association. *Cardiovascular Disease: A Costly Burden for America, Projections Through 2035*. (2017).
13. Tsao, C. W. *et al.* Heart Disease and Stroke Statistics—2022 Update: A Report From the American Heart Association. *Circulation* **145**, (2022).
14. Serruys, P. W. *et al.* Percutaneous Coronary Intervention versus Coronary-Artery Bypass Grafting for Severe Coronary Artery Disease. *N. Engl. J. Med.* **360**, 961–972 (2009).
15. Mount Elizabeth Hospital. Coronary Artery Disease (CAD). https://www.mountelizabeth.com.sg/conditions-diseases/coronary-artery-disease/symptoms-causes.
16. Faroux, L. *et al.* Coronary Artery Disease and Transcatheter Aortic Valve Replacement. *J. Am. Coll. Cardiol.* **74**, 362–372 (2019).
17. Cavender, M. A. & Forrest, J. K. Planning for the Next Transcatheter Aortic Valve Replacement Starts Today. *Circ. Cardiovasc. Interv.* **13**, (2020).
18. Corrigan, F. E. *et al.* Imaging for Predicting, Detecting, and Managing Complications After Transcatheter Aortic Valve Replacement. *JACC Cardiovasc. Imaging* **12**, 904–920 (2019).
19. Ring, L. *et al.* Echocardiographic assessment of aortic stenosis: a practical guideline from the British Society of Echocardiography. *Echo Res. Pract.* **8**, G19–G59 (2021).

20. National Institute of Biomedical Imaging and Bioengineering (NIH). Computed Tomography (CT). *National Institute of Health* https://www.nibib.nih.gov/science-education/science-topics/computed-tomography-ct.
21. Blanke, P. *et al.* Computed Tomography Imaging in the Context of Transcatheter Aortic Valve Implantation (TAVI)/Transcatheter Aortic Valve Replacement (TAVR). *JACC Cardiovasc. Imaging* **12**, 1–24 (2019).
22. Gottumukkala, R. V., Kalra, M. K., Tabari, A., Otrakji, A. & Gee, M. S. Advanced CT Techniques for Decreasing Radiation Dose, Reducing Sedation Requirements, and Optimizing Image Quality in Children. *RadioGraphics* **39**, 709–726 (2019).
23. Patel, K. P. *et al.* Cardiac Computed Tomography: Application in Valvular Heart Disease. *Front. Cardiovasc. Med.* **9**, 849540 (2022).
24. National Institute of Biomedical Imaging and Bioengineering (NIH). Magnetic Resonance Imaging (MRI). *National Institute of Health* https://www.nibib.nih.gov/science-education/science-topics/magnetic-resonance-imaging-mri.
25. Azarine, A. *et al.* Four-dimensional Flow MRI: Principles and Cardiovascular Applications. *RadioGraphics* **39**, 632–648 (2019).
26. Kosova, E. & Ricciardi, M. Cardiac Catheterization. *J. Am. Med. Assoc.* **22**, 2344 (2017).
27. Omran, H. *et al.* Silent and apparent cerebral embolism after retrograde catheterisation of the aortic valve in valvular stenosis: a prospective, randomised study. *The Lancet* **361**, 1241–1246 (2003).
28. de Marvao, A., Dawes, T. J., Howard, J. P. & O'Regan, D. P. Artificial intelligence and the cardiologist: what you need to know for 2020. *Heart* **106**, 399–400 (2020).
29. Khodaei, S. *et al.* Personalized intervention cardiology with transcatheter aortic valve replacement made possible with a non-invasive monitoring and diagnostic framework. *Sci. Rep.* **11**, 10888 (2021).
30. Khodaei, S. *et al.* Towards a non-invasive computational diagnostic framework for personalized cardiology of transcatheter aortic valve replacement in interactions with complex valvular, ventricular and vascular disease. *Int. J. Mech. Sci.* **202–203**, 106506 (2021).
31. Keshavarz-Motamed, Z. A diagnostic, monitoring, and predictive tool for patients with complex valvular, vascular and ventricular diseases. *Sci. Rep.* **10**, 6905 (2020).
32. Tanné, D., Kadem, L., Rieu, R. & Pibarot, P. Hemodynamic impact of mitral prosthesis-patient mismatch on pulmonary hypertension: an in silico study. *J Appl Physiol* **295**, 1916–1926 (2008).
33. Keshavarz-Motamed, Z. *et al.* Elimination of Transcoarctation Pressure Gradients Has No Impact on Left Ventricular Function or Aortic Shear Stress After Intervention in Patients With Mild Coarctation. *JACC Cardiovasc. Interv.* **9**, 1953–1965 (2016).
34. Stergiopulos, N., Meister, J. J. & Westerhof, N. Determinants of stroke volume and systolic and diastolic aortic pressure. *Am. J. Physiol.-Heart Circ. Physiol.* **270**, H2050–H2059 (1996).
35. Mynard, J. P., Davidson, M. R., Penny, D. J. & Smolich, J. J. A simple, versatile valve model for use in lumped parameter and one-dimensional cardiovascular models. *Int. J. Numer. Methods Biomed. Eng.* **28**, 626–641 (2012).
36. Ben-Dor, I. *et al.* Coronary Blood Flow in Patients With Severe Aortic Stenosis Before and After Transcatheter Aortic Valve Implantation. *Am. J. Cardiol.* **114**, 1264–1268 (2014).

37. Ahmad, Y. *et al.* Coronary Hemodynamics in Patients With Severe Aortic Stenosis and Coronary Artery Disease Undergoing Transcatheter Aortic Valve Replacement. *JACC Cardiovasc. Interv.* **11**, 2019–2031 (2018).
38. Vendrik, J. *et al.* Long-Term Effects of Transcatheter Aortic Valve Implantation on Coronary Hemodynamics in Patients With Concomitant Coronary Artery Disease and Severe Aortic Stenosis. *J. Am. Heart Assoc.* **9**, e015133 (2020).